INTEGRATED EXPERIMENTAL AND THEORETICAL APPROACHES TOWARD UNDERSTANDING STRAIN-INDUCED CYTOSKELETAL REMODELING AND MECHANOTRANSDUCTION

A Dissertation

by

HUI-JU HSU

Submitted to the Office of Graduate Studies of
Texas A&M University
in partial fulfillment of the requirements for the degree of

DOCTOR OF PHILOSOPHY

August 2012

Major Subject: Biomedical Engineering

Integrated Experimental and Theoretical Approaches toward Understanding Strain-Induced Cytoskeletal Remodeling and Mechanotransduction

INTEGRATED EXPERIMENTAL AND THEORETICAL APPROACHES TOWARD UNDERSTANDING STRAIN-INDUCED CYTOSKELETAL REMODELING AND MECHANOTRANSDUCTION

A Dissertation

by

HUI-JU HSU

Submitted to the Office of Graduate Studies of
Texas A&M University
in partial fulfillment of the requirements for the degree of

DOCTOR OF PHILOSOPHY

Approved by:

Chair of Committee,	Roland R. Kaunas
Committee Members,	Emily Wilson
	James E. Moore, Jr.
	Wonmuk Hwang
Head of Department,	Gerard L. Cote

August 2012

Major Subject: Biomedical Engineering

ABSTRACT

Integrated Experimental and Theoretical Approaches toward Understanding Strain-Induced Cytoskeletal Remodeling and Mechanotransduction.

(August 2012)

Hui-Ju Hsu, B.S.; M.S., National Cheng Kung University;

M.S., Texas A&M University

Chair of Advisory Committee: Dr. Roland R. Kaunas

Actin stress fibers (SFs) are mechanosensitive structural elements that respond to applied strain to regulate cell morphology, signal transduction, and cell function. The purpose of this dissertation is to elucidate the effects of mechanical stretch on cell mechanobiology via the following three aims. First, a sarcomeric model of SFs was developed to describe the role of actomyosin crossbridge cycling in SF tension regulation and reorientation in response to various modes of stretch. Using model parameters extracted from literature, this model described the dependence of cyclic stretch-induced SF alignment on a two-dimensional (2-D) surface on positive perturbations in SF tension caused by the rate of lengthening, which was consistent with experimental findings. Second, the sarcomeric model was used to predict how stretch-induced pro-inflammatory mechanotransduction depends on the mode of strain application. Together with experimental data, the results indicated that stretch-induced stress fiber alignment, MAPK activations and downstream pro-inflammatory gene expressions are dependent on SF strain rate (and related changes in SF tension) rather than SF turnover. Third, to produce biocompatible materials that are both mechanically resilient under (physiological) load and also mechanosensitive, a novel hybrid engineered tissue was developed that transmits strain stimuli to cells residing in three-dimensional (3-D) collagen microspheres. However, the macroscopic stress is largely borne by a more resilient acellular polyethylene glycol diacrylate (PEGDA) hydrogel

supporting the microspheres. Careful analysis indicated that cell alignment occurs prior to significant collagen fibril alignment.

ACKNOWLEDGEMENTS

I am extremely grateful to my advisor, Professor Roland R. Kaunas, for his vital encouragement and guidance throughout my graduate studies and research. His patience and enthusiasm in research had motivated me. In addition, he was always accessible and willing to help me with my research.

In addition to my advisor, I would like to thank the rest of my committee members, Professors Emily Wilson, James E. Moore, Jr. and Wonmuk Hwang, for their time in reviewing this dissertation and for their thoughtful advice and feedback.

I also thank my fellow labmates, Abhishek Tondon, Candice Marie Haase, Julie Salazar, Andrea Locke, Sandhya Ramesh and Susan Vanderzyl for the experiment results that I used to compare with my simulations and for helping me with the experiments. They also inspire me in research through our interactions and discussions in the lab.

Last but not the least, my deepest gratitude goes to my family; most especially, my parents and Fiancé who spiritually supported me throughout my pursuit of a higher education.

TABLE OF CONTENTS

Page

Page

LIST OF FIGURES

Page

I. INTRODUCTION

I.A. Background

Vascular endothelial cells (ECs), forming a monolayer barrier in the lumen of arteries, are continuously subjected to the hemodynamic forces such as fluid shear stress and mechanical stretch (Gimbrone, 1999; Nerem, 1993). ECs can sense and respond to these mechanical factors through changes in intracellular signaling, gene expression, and protein synthesis to regulate cellular functions such as proliferation, apoptosis, migration and morphology (Haga et al., 2007; Wang and Thampatty, 2006). ECs dysfunction, such as enhanced EC turnover and inflammatory gene expression and reduced vasodilatory capacity, is emerging as a key component in the pathophysiology of cardiovascular abnormalities associated with atherosclerosis. Many of the risk factors for atherosclerosis, such as hyperglycemia in diabetes, hypertension, hypercholesterolemia/hyperlipidemia, and smoking are considered injurious to the endothelium (Kislinger et al., 2001; Paniagua et al., 2001; Sattar et al., 1998). Injury to ECs may facilitate the passage and deposition of lipids from the blood into the vessel wall. ECs respond to the damage by expressing proteins that recruit blood-borne monocytes that then migrate into the vessel wall, transform into macrophages, absorb lipids and transform into foam cells. The macrophages and injured ECs also produce chemical factors that increase the proliferation of smooth muscle cells and their migration into the intima. The accumulation of smooth muscle and foam cells in the intima forms the atheroma, which gradually narrows the artery and constricts blood flow to downstream tissues.

This dissertation follows the style of Cell.

Atherosclerotic lesions are primarily located at bifurcations and regions of curvature in arteries. The risk factors listed above would not be expected to lead to such localized atherogenesis. The hemodynamic environment at these locations is different from other locations in the arterial circulation. Specifically, fluid wall shear stress is low and oscillating, and tensile stretch in the wall is higher than in straight, unbranched arteries. These findings suggest a role for fluid shear stress and mechanical strain, acting on the endothelium, in the development of atherosclerosis (Giddens et al., 1993; Thubrikar and Robicsek, 1995). Interestingly, these are regions where ECs are not aligned in any particular direction. In contrast, straight, unbranched arterial segments are largely devoid of plaques and ECs are axially-oriented, i.e. perpendicular to the principal direction of cyclic stretch and parallel to the direction of flow. The lack of EC alignment at arterial branch points and curvatures leads to a relative high permeability to macromolecules which is associated with atherogenesis, suggesting that cell alignment is somehow important in maintaining an anti-atherogenic cell phenotype. The role of fluid forces in atherogenesis has received much more attention than has the effect of cyclic strain. This is somewhat surprising since pulse pressure, the driving force for cyclic stretching of the vessel wall, is highly correlated with cardiovascular disease. Therefore, the studies in this dissertation focus on elucidating the mechanism by which cyclic stretch of endothelial cells influences EC shape and function.

I.B. The Role of Integrins, Focal Adhesions, and Actin Cytoskeleton in Response to Mechanical Strain

Similar to arterial ECs in straight, unbranched arteries, cultured ECs subjected to periodic and directional strain become elongated and oriented in the direction perpendicular to the principal strain direction (Dartsch and Betz, 1989; Iba and Sumpio, 1991). The details of mechanotransduction from extracellular deformation to cell reorientation are not clear, however, it is clear that the actin cytoskeleton plays a major role.

The actin cytoskeleton is important in many aspects of cell functions, such as cell motility, cell division and intracellular transport. SFs are contractile bundles that form in response to myosin-dependent contractility and applied forces such as mechanical stretch. The elongation and orientation of cell shape actually follows the redistribution of SFs, which is inhibited by cytochalasin, suggesting that the reorientation of SFs is the essential mechanism in the strain-induced cell remodeling, but that of microtubules and intermediate filaments is not as important (Iba and Sumpio, 1991).

Integrins contained within focal adhesions are transmembrane proteins serving as receptors that mediate attachment between the intracellular actin cytoskeleton and the extracellular matrix (ECM). The integrin family consists of eighteen and eight subunits which form 24 different heterodimeric complexes. Various ECM proteins, including fibronectin, laminin, vitronectin, and collagen, are ligands for specific members of the integrin family (Chen et al., 1985). Integrins are indirectly linked to the actin cytoskeleton through a group of actin-associated proteins, including talin, vinculin and -actinin (Horwitz et al., 1986). Each of these anti-associated proteins has been identified at regions where actin stress fibers (SFs) terminate near the basal plasma membrane (i.e., sites of focal adhesions). Together, these studies suggest that integrins may function as mechanoreceptors as they are among the first cell-surface molecules to experience externally applied mechanical loads (Ingber, 1991; Shyy and Chien, 1997).

Focal adhesions are found at each end of SFs; therefore, this mechanical link of integrins, focal adhesion, and SFs is able to transmit the matrix forces into the cell and vice-versa. Focal adhesions are also found to orient perpendicular to the strain direction in ECs (Yano et al., 1997).

I.C. Modulation of Pro-inflammatory Signaling Pathways in Response to Mechanical Stimuli

ECs can transduce mechanical stimuli into biochemical signals to result in changes in the expression of a variety of genes by several signaling pathways. At very early stages of the disease, the ECs located at sites prone to atherosclerosis exhibit a pro-inflammatory phenotype characterized by high levels of expression of intracellular adhesion molecule (ICAM-1) (Nakashima et al., 1998), vascular adhesion molecule (VCAM-1) (Davies et al., 1993). The expressions of ICAM-1 and VCAM-1 on endothelial surface contribute to an increase in monocyte adhesion to the endothelium. The induction of these genes by mechanical stimuli has been shown to be regulated by AP-1 transcription factor, which is mediated by the MAPKs (Li et al., 1996; Liu et al., 2003; Wung et al., 1996). Members of the MAPK family include c-Jun NH_2-terminal kinase (JNK), extracellular signal-regulated kinase (ERK), and p38. The ERK signaling pathway is preferentially activated in response to growth factors and regulates cell proliferation and cell differentiation (Hoefen and Berk, 2002). JNK and p38 are thought to be the major regulators of pro-atherogenic inflammatory gene expression in ECs. Cyclic uniaxial stretch induces transient JNK activation that subsides as SFs align away from the direction of stretch, while cyclic equibiaxial stretch induces sustained JNK activation and SFs cannot align (Kaunas et al., 2006). A major goal of this dissertation was to study the mechanism by which strain-induced SF remodeling modulates the activation of MAPK in response to strain, which can then lead to changes in gene expression.

I.D. Outline of the Dissertation

I hypothesized that perturbations in SF tension induce the alignment of cells and their actin SFs, which serves to dampen the effects of stretch on pro-inflammatory mechanotransduction (**Fig. 1**). A major goal of this dissertation was to develop and experimentally test a mathematical model of stretch-induced SF remodeling based on a sarcomeric description of SFs and use this model to identify the role of myosin II in stretch-induced pro-inflammatory mechanotransduction. This hypothesis was tested via the following objectives. In **Section III**, I developed a simple, quantitative, sarcomeric model of SFs describing the role of actomyosin crossbridge cycling in SF tension regulation and reorientation in response to cyclic stretching. First, a dynamic mechanical model of an individual SF was developed. This was then coupled to a SF network model to describe the dependence of SF reorientation on the strain-rate of cyclic stretch. The model was tested and revised using data varying the lengthening vs. shortening rate of cyclic stretch. It predicted that SFs are much more responsive to the rate of lengthening than the rate of shortening during the stretch cycle due to positive perturbations in SF tension generated during lengthening.

In **Section IV**, guided by the SF model, I investigated the effect of the SF tension on the levels of phosphorylation of the MAPKs. Changes in ERK, JNK and p38 phosphorylations in response to different frequencies of stretch showed a similar dependence on strain rate as stretch-induced SF alignment. A step increase in equibiaxial stretch caused a transient increase in MAPK phosphorylation levels and releasing this stretch caused a transient decrease in MAPK phosphorylation levels. To further explore the role of SF tension on MAPK phosphorylation, ECs were treated with cytochalasin D to disrupt actin filaments and Y27632 to reduce actomyosin activity. ECs were also treated with jasplakinolide (10nM) to stabilize actin filaments. These experiments indicated that strain-induced MAPK activations are dependent on stretch-induced changes in SF strain rate (and related changes in SF tension) rather than SF turnover. The roles of FAK and matrix type (fibronectin vs. matrigel) on stretch-induced MAPK activations were also evaluated. The effect of the SF tension on the levels of pro-

inflammatory gene expressions, such as VCAM-1, ICAM 1 and fibronectin, were also be quantified by quantitative real time- polymerase chain reaction (qRT-PCR) following cyclic equibiaxial and uniaxial stretch of human aortic ECs (HAECs) at 1 Hz, and correlated with strain-induced SF alignment and JNK activations.

The studies above were performed with endothelial cells grown as 2-D monolayers. In **Section V**, studies of 3-D cell cultures were performed by using a hybrid tissue consisting of collagen-cell microspheres supported within a mechanically resilient PEGDA hydrogel. I hypothesized that although the PEGDA hydrogel bears most of the stress, the collagen domains are subjected to similar levels of strain as the PEGDA phase. To test this hypothesis, the strains developed within the cellular domains and surrounding PEGDA were directly measured. The effect of strain transmitted from the surroundings on cell alignment and collagen fiber orientation in collagen microspheres was also investigated and compared between the proposed hybrid tissues and pure collagen gels. These experiments demonstrated that cyclic uniaxial stretch induces cell reorientation and local collagen fiber alignment in a manner similar to that for stretching cells in pure collagen gels at similar strains.

II. METHODS AND MATERIALS

II.A. Cell Culture

Bovine aortic endothelial cells (Lonza), FAK-null (FAK -/-) and FAK-expressing (FAK +/+) mouse embryonic fibroblasts, and U2OS osteosarcoma cells (MarinPharm GmbH) were cultured in GIBCO DMEM (Invitrogen) supplemented with 10% fetal bovine serum, 2mM L-glutamine, 1mM sodium pyruvate and 1mM penicillin/streptomycin (Sigma) as described previously (Kaunas et al., 2006; Owen et al., 1999). Human aortic endothelial cells (Lonza) were cultured in EBM-2 (Lonza) supplemented with SingleQuots (Lonza) which consist of 2% fetal bovine serum. The cells were seeded onto the membranes, allowed to spread in complete media, and serum-starved overnight prior to stretching. Cell cultures and stretch experiments are performed in a humidified 5% CO_2-95% air incubator at 37°C.

II.B. Stretching Experiment

The cells were subjected to mechanical stretch using a custom-built device described previously (Hsu et al., 2009; Kaunas et al., 2006). Briefly, silicon rubber membranes (Specialty Manufacturing, Saginaw, MI) were mounted to polycarbonate chambers with O-ring and sterilized with UV radiation. After sterilization, the membrane was coated with 1 $\mu g/cm^2$ of fibronectin (Sigma) or 2.5 $\mu l/cm^2$ basement membrane (matrigel) overnight in the central 16 cm^2 region by the aid of a Teflon insert. Cells were seeding on the ECM-coated region of the membrane at ~50% confluence, cultured overnight to achieve confluence, and serum-starved 3 h prior to stretching. The stretching device was placed in humidified 5% CO_2-95% air incubator at 37°C and was capable of applying sinusoidally-varying stretch of different magnitudes (0-20%), frequencies (0.01-1 Hz), and patterns (e.g., pure uniaxial and equibiaxial) within the central region of the culture chamber.

Another stretch device was used for applying non-sinuoidal waveforms and for stretching 3-D hydrogels. This device consisted of two linear motors (Zaber, Canada)

that are used to stretch silicone rubber chambers (STREX, Japan). The entire stretch apparatus was mounted on the stainless steel stage (Gibraltar) of a Nikon FN1 upright microscope housed in a custom-made acrylic enclosure maintained at 37°C using a heat gun (Omega) regulated by a temperature controller (Omega).

II.C. Quantification of Stress Fiber and Collagen Fibril Organization

Cells were subjected to stretch, rinsed with PBS at 37°C, fixed in 4% paraformaldehyde (PFA) in PBS for 10 min at room temperature, and permeabilized with 0.5% Triton X-100 in PBS for 15 min. Actin filaments were then labeled with Alexa 488-phalloidin (Invitrogen) for 45 min at 1:200 dilution in PBS. Images were captured by a Nikon FN1 upright microscope and imaged with a Nikon C1 laser scanning confocal head with a 60X water-dipping objective illuminated with a 40-mW Argon ion laser (Melles Griot). The images were post-processed using a custom-made algorithm in MATLAB (the MathWorks, Natick, MA) to determine, circular variance or an order parameter based on a density distribution $g(\theta)$ of the SF or collagen fibril orientations (Hsu et al., 2009; Kaunas et al., 2006) was calculated for each individual cell (for non-confluent U2OS cells) or each image (for collagen fibrils) to characterize the dispersion in collagen fibrils or SF orientations.

$$\text{Circular Variance} = 1 - \frac{1}{N_{SF}}\sqrt{\left(\sum^{N_{SF}}(\sin\theta)\right)^2 + \left(\sum^{N_{SF}}(\cos\theta)\right)^2} \quad (1)$$

$$S = \langle \cos 2\theta \rangle = \int g(\theta) \cos 2\theta \, d\theta \quad (2)$$

where θ is the orientation of the SF and N_{SF} is the total number of SFs. The value of circular variance ranged between 1 and 0 for a random distribution and complete alignment, respectively. Values for S range from -1 to 1. Values of 0, 1 or -1 indicate the SFs are uniformly distributed in all directions, uniformly oriented parallel to the stretch direction, or uniformly oriented perpendicular to the stretch direction, respectively.

II.D. Immunoblotting

After a stretching experiment, cells were lysed in 400µl 2X Laemmli buffer (4% SDS, 20% glycerol, 10% 2-mercaptoethanol, 0.004% bromphenol blue and 0.125 M Tris HCl) and boiled for 5 min. Proteins were separated by 10% SDS-PAGE gel electrophoresis and transferred to polyvinylidene difluoride (PVDF) membranes. Membranes were blocked with 5% nonfat milk powder in TBS with 0.01% Tween-20 for 1 h and incubated with 1:1000 phosphorylation site-specific primary antibodies directioned against T183/Y185 JNK, T180/Y182 p38, or T202/Y204 ERK (Cell Signaling) at 4°C overnight or 1:5000 primary total JNK, total p38 or total ERK (Santa Cruz) at room temperature for 3 h. Blots were washed and incubated with 1:3000 horse radish peroxidase (HRP)-conjugated secondary goat anti-rabbit antibodies (Cell Signaling) for 1 h at room temperature. Membranes were then treated with ECL reagents (Pierce) and exposed to film (Denville Scientific). Membranes were reprobed after stripping with Restore western blot stripping buffer (Thermo Scientific).

II.E. Quantitative Polymerase Chain Reaction

Total RNA was prepared from stretched HAECs using TRIzol reagent (Invitrogen) and cDNA synthesized using the iScript cDNA Synthesis Kit (BioRad). To quantify the expression of mRNA in all experiments, qRT-PCR analysis (iCycler, BioRad) was performed on cDNA using fluorescent reporter probes to simultaneously quantify the mean starting quantity (threshold cycle) based on the standard curve, and gene expression determined as a ratio between the gene of interest and a housekeeping gene (2 -microglobulin).

II.F. Quantification and Statistical Analysis

Resultant protein bands were scanned and quantified using Image J software. Statistical differences between groups in the levels of phosphorylation were evaluated by ANOVA followed by Student-Newman-Keuls posthoc multi-comparison testing.

II.G. Collagen Hydrogel Preparation

Silicone rubber stretch chambers (STREX) were modified to include a circular well formed by adhering a silicone rubber sheet onto existing silicone rubber chamber. Collagen type I (4 μg/cm^2) was adsorbed onto the surface by flushing 500 ml of 0.3 mg/ml rat tail collagen type I (BD Biosciences) diluted in PBS into the well and then air dried. Collagen gel (3 mg/ml) was gelled within the collagen-coated well as described previously (Yeh et al., 2004). Briefly, reconstitution buffer was made with 2.2 g $NaHCO_3$ and 4.77 g HEPES in 100 mL 0.05 M NaOH and sterilized with a 0.22 mm filter. Seven parts of rat-tail collagen, type I (BD Biosciences, Bedford, MA) were mixed with two parts of 5X DMEM and one part buffer and neutralized with 1 M NaOH to pH 7.4. The gels that did not attach completely to the sides of the well were discarded.

II.H. Preparation of Collagen–U2OS Microspheres

U2OS cells resuspended with trypsin-EDTA were mixed with soluble collagen. Droplets of the collagen-cells mixtures were pipetted into culture dishes containing UV-irradiated parafilm covering the bottom of the dish to prevent adhesion of the droplets to the substratum after gelation. The collagen–U2OS mixtures underwent gelation when incubated at 37°C in a humidified atmosphere with 5% CO_2 for 30 min. The gelled droplets were then cultured in growth medium for 24 h prior, thus allowing the cells to spread and to contract the matrix.

II.I. Synthesis of PEGDA

PEGDA was prepared by combining 0.4 mmol/mL acryloyl chloride, 0.2 mmol/mL triethylamine, and 0.1 mmol/mL dry PEG (10 kDa; Fluka, Milwaukee, WI) in anhydrous dichloromethane under nitrogen overnight. The resulting PEGDA was then precipitated with ether, filtered, lyophilized, and stored under nitrogen at -20°C. PEGDA was analyzed by proton NMR (Avance 400 MHz; Bruker, Billerica, MA; solvent, N,N-dimethylformamide-d7) and only materials with a degree of acrylation >85% were used.

II.J. Microencapsulation

The collagen-U2OS microspheres were suspended in a solution of 10% (w/v) PEGDA in 3.6 mL PBS (pH7.4). Next, 40 μL/mL of 300 mg/mL 2,2-dimethoxy-2-phenylacetophenone in 1-vinyl-2-phenylacetophenone (photoinitiator) was added to the solution, which was then polymerized within a channel consisting of two 75×50 mm glass plates separated by 1.67 mm polycarbonate spacers and two strips of 0.61 mm porous hydrophilic polyethylene via exposure to a 10 mW/cm^2, 365 nm UV lamp for 2 min on each sides. PEGDA flows into the porous bars and, upon assembly, provides a means to mechanically couple the hydrogel to the motors of the uniaxial stretching platform. The glass plates were removed and the gel was allowed to swell in culture medium.

II.K. Three-Point Finite Strain Analysis

The strains fields produced by the device were determined by tracking the displacement of fluorescent beads in the hydrogel before and after stretch. The symmetric Lagragnian strain components E_{ll}, E_{l2} , and E_{22} are given by the definition (using Einstein's summation convention for repeated indices):

$$\mathrm{d}S^2 - \mathrm{d}S_0^2 = 2E_{\mathrm{ij}}\mathrm{d}a_{\mathrm{i}}\mathrm{d}a_{\mathrm{j}} \tag{3}$$

where dS and dS_0 are the deformed and undeformed lengths of a differential line element, and da_{i} are the coordinates of dS_0. Triads of beads in a focus plane in various locations

were selected to compute the symmetric Lagrangian strain tensor (E_{ij}) at each location. Three beads generated three equations determining the strain components, E_{ll} , E_{l2} , and E_{22}. The principal strains can then be obtained by solving the eigenvalue problem

$$(E_{ij} - E_{ij})v_i = 0 \tag{4}$$

where v_i is the direction vector. For nontrivial solution, the determinant

$$|E_{ij} - E_{ij}| = 0 \tag{5}$$

The solution of Eqn. 5 yields two real-valued principal strains, E_1 and E_2. The principal direction is determined by substituting the E_1 and E_2 into Eqn. 4 and solving for v_i. The relationship between the finite strains in the longitudinal (E_1) and lateral directions (E_2) and the Lagrangian strain tensor E_{11} and E_{22} (Fung, 1994) is

$$E_1 = \sqrt{1 + 2E_{11}} - 1 \tag{6}$$

$$E_2 = \sqrt{1 + 2E_{22}} - 1 \tag{7}$$

To determine shear, the change in the angle between the line segments which were originally approximately orthogonal was calculated using Eqn. 8.

$$\text{Deviation angle} = \theta_{\text{final}} - \theta_{\text{initial}} \tag{8}$$

II.L. Cell Shape Analysis

The GFP-actin image of a cell was thresholded to define the area *A* of the cell. The centroid of the cell $(\bar{x}, \bar{y})$ was then calculated, where

$$\bar{x} = \frac{1}{A}\int_A x\mathrm{d}A\,,\ \bar{y} = \frac{1}{A}\int_A y\mathrm{d}A \tag{9}$$

are the averages across the coordinates of the planes in the region *A*. The second moments of the region are defined as

$$I_x = \int_A (y-\bar{y})^2\,\mathrm{d}A,\ I_y = \int_A (x-\bar{x})^2\,\mathrm{d}A \tag{10}$$

and the moment of deviation, which is also named second moment of area, is

$$I_{xy} = \int_A (x-\bar{x})(y-\bar{y})\,\mathrm{d}A \tag{11}$$

Mohr's circle was then used to rotate the inertia tensor about the centroid to obtain the principal values of the moments of inertia,

$$I_{\text{major}} = \frac{1}{2}\left[I_x + I_y - \sqrt{\left(I_x - I_y\right)^2 + 4{I_{xy}}^2}\right],$$

$$I_{\text{minor}} = \frac{1}{2}\left[I_x + I_y + \sqrt{\left(I_x - I_y\right)^2 + 4{I_{xy}}^2}\right] \tag{12}$$

The ratio $I_{\text{minor}}/I_{\text{major}}$ is the Aspect Ratio for the cell, i.e. the extent of cell elongation. The orientation of the cell is taken as the angle of rotation , which is the angle between the axis of the original coordinate system and the principal axis of the cross section.

$$\alpha = -\frac{1}{2}\tan^{-1}\frac{2I_{xy}}{I_x - I_y} \tag{13}$$

III. DEVELOPMENT OF A SIMPLE QUANTITATIVE SARCOMERIC MODEL OF SFs DESCRIBING THE ROLE OF ACTOMYOSIN CROSSBRIDGE CYCLING IN SF TENSION REGULATION AND REORIENTATION IN RESPONSE TO CYCLIC STRETCHING*

III.A. Introduction

SF assembly is regulated by RhoA small GTPase through the activation of Rho kinase and mDia (Chrzanowska-Wodnicka and Burridge, 1996; Kaunas et al., 2005). Observations from several studies showed that stretch-induced SF reorientation at an oblique angle to the direction of stretch (Ahmed et al., 2010; Hayakawa et al., 2001). Previous studies reported that SFs rapidly disassemble upon loss of tension caused by reduced myosin activity or sudden cell shortening (Costa et al., 2002; Matsui et al., 2010). However, the molecular mechanism by which the actin cytoskeleton determines their specific response to particular changes in mechanical stretch remains unclear.

A sarcomeric model of SF has been developed based on the observations that SFs are destabilized when SF strain is perturbed from the homeostatic level, resulting in rapid SF disassembly and reassembly (Kaunas et al., 2011). As a result, SFs gradually accumulate in the direction of least matrix stretching (i.e., perpendicular to the direction of uniaxial stretch) to minimize perturbations in stress and/or strain. This theoretic model

---

successfully describes the frequency dependence of stretch-induced SF remodeling (Hsu et al., 2009; Lee et al., 2010). However, these experiments typically involved applying cyclic stretch waveforms in which the strain rate in a stretch cycle is proportional to stretch frequency. In this study, I hypothesized that the frequency dependence of cyclic stretch-induced SF reorganization may be more precisely defined as a sensitivity to strain rate rather than the frequency of stretching. The sarcomeric mechanical model of SF networks was tested and revised using data varying the lengthening vs. shortening rate of cyclic stretch to better understand the respective roles of strain rate and frequency on SF reorganization (Tondon et al., 2012).

III.B. Sarcomeric Model of Stress Fiber Networks

The model described below was executed numerically in Visual C++ (See Appendix B).

III.B.1. Introduction

SFs in non-muscle cells consist of bundles of actin filaments cross-linked mainly by -actinin and myosin II. Electron microscope images of microfilament bundles or SFs show the existence of a substructure of sites of myosin II location (electron-light regions) along SFs repeatedly alternate with sites of concentration of another contractile machinery, -actinin, (electron-dense regions). This finding indicates SF structure and contraction is similar to the organization of skeletal muscle sarcomeres (Langanger et al., 1986). Contractile tension generated in the sarcomere is due to sliding of bipolar myosin filaments running in opposite directions along adjacent actin filaments to result in overall shortening or lengthening of the SF during concentric and eccentric contractions, respectively.

Despite the similarity in sarcomeric structure, sarcomeres in SFs and myofibrils differ in many respects. Nonmuscle myosin II is important for SF disassembly in cell processes requiring actin cytoskeletal turnover, such as cell crawling (Wilson et al., 2010). In contrast, sarcomeres in myofibrils are very stable structures, which can be attributed to

additional supporting proteins (e.g. titin and nebulin) as well as the large number of myosin heads available for binding with actin filaments. Myosin filaments in SFs consists of 8-10 myosin proteins at each end of a filament, while those in myofibrils contain ~150 per half a myosin filament (Kovacs et al., 2007; Vicente-Manzanares et al., 2009). Therefore, the duty ratio for myosin filaments in SFs (i.e. the fraction of the time that the myosin domain spends attached to actin filaments) is reported to be only ~0.05, which is relatively low compared to that for myofibrils. Myosin with high duty ratios can maintain continuous attachment to their filaments and so can function on their own, while myosin with low duty ratios must oligomerize into large assemblies in order to produce continuous motility. Any decrease in the duty ratio, such as increasing myosin ATPase activity, could therefore lead to the detachment of a myosin filament from adjacent actin filaments.

Rapid crossbridge cycling, such as occurs during SF contraction, also lower the duty ratio. Studies using myosin II-coated beads indicate that at loads larger (or smaller) than the stall force, myosin-generated forward movement through transient detachment of actomyosin crossbridges is less (or greater) than backward slip, resulting in negative (or positive) velocities as in eccentric (or concentric) contractions of whole muscle. Thus, myosin sliding caused by either concentric or eccentric contractions is expected to reduce the duty ratio and hence decrease the stability of an SF due to fewer actomyosin cross-links. Consistent with this hypothesis, cyclic stretching of nonmuscle cells induces the gradual alignment of SFs in directions that minimize cyclic changes in SF length. The extent of SF alignment depends on the magnitude (Kaunas et al., 2005) and frequency (Hsu et al., 2009) of stretching.

The dynamic reorganization of SFs has been described with a phenomenological model of SF relaxation and turnover (Hsu et al., 2009). Further, analysis of SF behavior using a sarcomeric model demonstrated that the force-dependent rate of myosin movement along actin filaments provides a molecular mechanism for the relaxation of perturbations in SF tension in response to changes in SF length (Kaunas et al., 2011). In **Section III.B.6**, the sarcomeric model was modified to predict that stretch-induced

decreases in SF stability due to increased SF tension can describe the time-dependent alignment of SFs in response to different strain-rates.

III.B.2. Model of a Stress Fiber

The present mathematical model of an SF in nonmotile cells is based on a sarcomeric description of SFs. **Fig.2A** is a schematic representation of an individual SF that is firmly adhered to a surface at each end through transmembrane focal adhesion protein complexes in a nonmotile cell. SFs are composed of repeating units termed sarcomeres after the analogous muscle structures with a spatial periodicity, i.e., sarcomere length (l), ranging from 0.9 to 1.5 microns. These actin-myosin structures are bundled together in parallel so that there are 10 to 30 actin filaments along the cross-sectional midline of the SF. There would be roughly 100 to 700 filaments per sarcomere if assuming the SF cross-section is circular.

A minimal model for a SF must describe both the passive stiffness and the active contractile properties of the SF. To account for these properties, individual actomyosin subunits are described mechanically as two actin filament springs connected by a myosin filament (**Fig. 2B**) in view of the work by tracking the initial elastic recoil and subsequent myosin-mediated contractile shortening of individual sarcomere within severed SFs in living cells (Russell et al., 2009). The elastic-contractile model consisting of two springs connected by a myosin filament can describe the time-dependent response of intact SFs to changes in length.

The force-strain relationship for isolated SFs under rigor conditions is approximately linear at physiological strains (i.e. $F = K\varepsilon$ for ε<0.3) (Deguchi et al., 2006). As an initial approximation, the stiffness K of a sarcomere is assumed to be proportional to the number of actomyosin subunits N in the sarcomere, i.e. $K = kN$, where k represents the stiffness of each actomyosin subunit (**Fig. 2B**). Note that the level of tension in the SF (F) is equal to the force acting on (or, equivalently, generated by) the N actomyosin subunits acting in parallel in an SF cross-section (i.e., $f = F/N$). This stiffness is not attributed to any one component of the actomyosin subunit but represents the composite

stiffness of an average actomyosin subunit. Further, the SF is assumed to be composed of a series of identical sarcomeres where the strain ε in each sarcomere (and each actomyosin subunit) is equivalent to the strain in the entire SF. Noting that $\varepsilon = (l - l_{\mathrm{ref}})/l_{\mathrm{ref}}$, the force on each actomyosin subunit f is related to strain,

$$f = k\varepsilon = k\frac{(l - l_{\mathrm{ref}})}{l_{\mathrm{ref}}} \tag{14}$$

where l is the current length of the sarcomere and l_{ref} is the length (reference length) of the sarcomere if it were to suddenly elastically retract upon unloading (i.e., when $f = 0$). Movement of the myosin filament along the actin filament spring changes the value of l_{ref}, hence l_{ref} is a time-dependent variable. The regions of overhanging actin do not contribute to the reference length, as they are not under tension. Consequently, myosin movement along actin filaments at a shortening velocity v results in a change in the reference length as the amount of overhanging actin changes,

$$\frac{dl_{ref}}{dt} = -2v \tag{15}$$

where the factor of 2 comes from the additive shortening from each end of a myosin filament. To consider the role of myosin sliding on the time-dependent behavior of the sarcomeres, differentiation of Eqn. 14 and substitution of Eqn. 15 into the result gives

$$\frac{df}{dt} = \frac{k}{l_{ref}}\frac{dl}{dt} + \frac{2vkl}{{l_{ref}}^2} \tag{16}$$

The first term on the right side of Eqn. 16 represents the contribution of the elasticity of the sarcomere. The second term represents the rate that the sarcomere relaxes toward the stall force through myosin movement. The relative magnitude of these two terms determines the force generation in the SF. If the SF changes length much more quickly than myosin can respond, then the first term dominates and the SF behaves nearly elastically with a force that increases in proportion to the length. If the SF changes length slowly, then the second term would be roughly equal and opposite in magnitude to the first term, and the force would remain nearly constant.

The force-velocity relationship for skeletal muscle first reported in the classic work of A. V. Hill (1938) is illustrated schematically in **Fig. 2D**. The velocity of myosin movement depends on the force experienced by the myosin filament, and therefore, skeletal muscle's ability to shorten and lengthen against a load reflects the inherent load-dependence of the myosin molecular motor. A linearized form of the relationship between force (f) and myosin shortening velocity (v) is used to relate tension and shortening rate, $v = v_0/f_0(f_0 - f)$, where f_0 is defined as the stall force that is just sufficient to stop myosin movement, and v_0 is the velocity of shortening when the actomyosin subunit is completely unloaded. **Fig. 2D** also illustrated eccentric contraction (i.e. v<0 when f>f_0). Debold et al. reported a similar force-velocity relationship for skeletal muscle myosin that interacted with actin-coated microbeads in an optical trap such that only eight myosin head groups could interact with actin at a time. These authors demonstrated that the microbeads moved with a negative velocity when the applied force exceeded the stall force through a process involving slipping and reattachment of myosin heads. It suggested that myosin filaments in SFs containing 8-10 myosin molecules on each end of the myosin filament may also undergo lengthening via slipping and reattachment of myosin heads.

Large ventral SFs are anchored to the substrate at each end via focal adhesions. Consequently, myosin-generated contraction leads to the development of isometric tension or prestress (Polte et al., 2004) which extends SFs beyond their unloaded lengths (Deguchi et al., 2006; Lu et al., 2008). The level of SF pre-extension is maintained at a set point value with measured values ranging from 1.10 to 1.35 in a static condition (v=0). In this sarcomeric model, all newly assembled fibers are assumed uniformly prestretched to a magnitude $l/l_{ref} = 1 + \varepsilon = 1.10$ (Lu et al., 2008). According to the force-velocity relationship, the steady-state force on an actomyosin subunit is simply the stall force f_0 and the strain is $\varepsilon_0 = f_0/k$. Assuming that the cross-sectional area of an actomyosin subunit (A) remained unchanged under small strains, the model predicts that the SF maintains force per unit area, or stress, at a constant level equal to f_0/A. Given that the strain in an individual sarcomere is equal to that of the entire SF, the model

predicts that SF strain is also maintained constant at equilibrium. Thus, the model indicates that prestress and pre-extension are mutually related and are maintained by myosin force balances at the sarcomere level.

III.B.3. Model Parameters

Literature values for maximum myosin velocity v_0 ranged from 300 nm/s for nonmuscle myosin II in gliding assays to ~10 nm/s in intact SF sarcomeres. To our knowledge, the value for f_0 has not been reported for nonmuscle myosin II. However, based on each myosin minifilament containing 10 myosin molecules per side and a stall force for muscle myosin of 1.7 pN, it is reasonable to assume myosin stall force f_0 is 17 pN. Russell et al. (2009) estimated values of 1.21 and 0.085 μm for initial length and elastic retraction distance, respectively, for individual sarcomeres, which predicts an equilibrium prestrain of 0.076. This is roughly consistent with the value of ~0.10 reported by Lu group. Sanger et al. (1983) revealed sarcomere length along SFs in the range of 0.9 μm in epithelial cells and 1.5 μm in fibroblasts based on light and electron microscopic findings. The regression curve of force-strain relations for single SFs in the physiological strain range (ε<0.3) is nearly linear (Deguchi et al., 2006); therefore, according to the equation $F = K\varepsilon$, the value of SF spring constant K is about 49 pN. The model parameters and relevant literature values are summarized in Table 1.

Table 1 Model Parameters

Parameters	Meaning	Values	Literature values
f_0	Myosin stall force	17 pN	-
v_0	Maximum myosin velocity	0.03 μm/s	0.01-0.3 μm/s
L	Sarcomere length	1 μm	0.9 1.5 μm
K	SF spring constant	49 nN	49 nN
N	Actomyosin subunits per sarcomere	-	100-700
k	actomyosin subunits spring constant	170 pN	79-490 pN
N_{SF}	Number of SFs	1000	
Δt	Time increment	0.01 s	
α	SF disassembly parameter	0.00015 s^{-1}	
β	SF disassembly parameter	0.06	
γ	SF disassembly parameter	0.1 μm/s	

III.B.4. Cyclic Stretching of an Individual Stress Fiber

Numerical solutions to Eqns. 15 and 16 were derived with the values for the model parameters inferred from the literature (Table 1). The results were illustrated by the harmonic response of the model as a function of frequency (**Fig. 2C**). The time axis is scaled by the period of oscillation to facilitate comparisons between responses at different stretch frequencies. Eqn. 16 provides insight into the mechanisms determining the sensitivity to the frequency of cyclic stretch. At high frequencies, the first term on the right side of the equation is much larger than the second term; hence, the amplitude in force is proportional to the amplitude in substrate strain. The average force, however, does gradually decrease to f_0. The force amplitude decreases as frequency decreases because the second term becomes increasingly important. At very low frequencies, almost no force is generated by substrate stretching. In addition, there is an obvious phase shift as the stretch frequency decreases, which is indicative of a viscous-like effect caused by myosin sliding. Note that the force in the SF is simply $F = fN$. Thus, the tension in an SF composed of N actomyosin subunits in a cross-section follows the same pattern as that shown in **Fig. 2C**.

III.B.5. Turnover and Reorganization

Next we addressed the effects of myosin sliding on SF stability and the resulting reorganization of SF networks into a new steady-state organization upon application of cyclic stretch at different frequencies and patterns. Rapid crossbridge cycling, such as occurs during concentric loading, is predicted to lower the fraction of bound myosin heads, i.e., the duty ratio. As described by Howard (1997), the duty ratio is also equal to the ratio of the length of a power stroke and the distance between binding sites along the actin filament. Myosin binds to actin at sites ~36 nm apart, which is much larger than the myosin head working distance. Thus, each myosin head must wait until the actin filament has traveled some integer multiple of 36 nm before another binding event can occur. Further, myosin may miss some potential binding sites, depending on how quickly these sites pass by. Howard expressed the probability of myosin missing any

particular binding site increases as the velocity of actin passing the myosin head increases as $exp(-k_0\, x_0/v)$, where k_0 is the binding rate, and x_0 represents the width of the binding site "window". SFs are expected to be increasingly more unstable by decreasing the fraction of bound myosin heads as the velocity of myosin movement increases (Howard, 1997; Matsui et al., 2010). Eqn. 17 describes the probability of SF disassembly as a function of the magnitude of myosin velocity $|v|$ over a time interval Δt through a similar relationship:

$$P(\text{disassembly of the } i^{th} \text{ SF}) = \beta \cdot \exp(-\gamma/|v|) \quad (17)$$

where β and γ are model parameters. The numerical integrations were performed using a time increment Δt of 0.01 s. We found that decreasing Δt below 0.01 s did not significantly change the results of the simulations. The total number (N_{SF}) of SFs in the simulations was 1000. In test cases, we found that increasing N_{SF} reduced the noise in the circular variance curves, but the system response was otherwise identical. Myosin movement caused by either concentric or eccentric contraction (positive or negative velocity) is expected to reduce the duty ratio and hence decreases the stability of an SF due to fewer actomyosin cross-links. Disassembled SFs are assumed to provide the building material for the assembly of new SFs. Although SF assembly is expected to take seconds to minutes, in the present analysis, each disassembled SF is assumed to reassemble immediately. It is not clear how cyclic stretch determined the orientation of newly assembling fibers; hence, the newly assembled SF is oriented in a randomly chosen direction at an initial strain ε_0.

After model parameter optimization, the model provides a valuable tool to interpret the effect of stretch frequency on SF alignment (**Fig. 3**). At 0.01 Hz, the SF distribution is predicted to remains random at all time points because SF tension is maintained near f_0 (**Fig. 2C**, blue curve) at all times due to myosin sliding despite cyclic changes in fiber length. As the frequency increases from 0.01 to 1.0 Hz, the rate of myosin sliding is unable to keep up with the rate of matrix stretching (**Fig. 2C**, black curve). The ensuing perturbation in SF tension induces the disassembly of SFs oriented in the direction of

stretch. SF reassembly eventually results in the accumulation of SFs oriented perpendicular to the stretch direction since this is the most stable configuration (**Fig. 3**, red curve). At and above 1 Hz, the rate of change in sarcomere length is much faster than the velocity of myosin sliding; hence, the SF behaves nearly elastically. These simulation results compared well with experimentally measured values of circular variance of SF orientation distributions measured in endothelial cells subject to these same stretch conditions (**Fig. 4**) (Hsu et al., 2009).

III.B.6. Optimization of SF Model to Describe Unique Effects of SF Lengthening and Shortening

Typically, the strain rate in a stretch cycle is proportional to stretch frequency. I hypothesized that the frequency dependence of cyclic stretch-induced SF reorganization may be more precisely defined as a sensitivity to strain rate rather than the frequency of stretching. To test this hypothesis, cells were subjected to cyclic stretch at the same frequency (0.01Hz) for 12 hrs using two different waveforms – a triangle-stretch pattern (**Fig. 5A**) that provides the lowest strain rate and a square-stretch pattern (**Fig. 5C**) that provides very fast strain rates. Similar to results from using a sinusoidal-stretch pattern at this frequency, SFs did not become aligned in response to a triangle-stretch pattern of stretch at 0.01Hz (**Fig. 5B**). In contrast, a square-stretch pattern did result in significant alignment perpendicular to the stretch direction which is consistent with the hypothesis that SFs respond to the strain rate (**Fig. 5D**).

Cyclic stretch involves cyclic lengthening and shortening phases of the cell and its SFs, and the rates of these phases are of equal magnitude for triangle- and square-stretch. Eqn. 17 predicted that SFs are equally sensitive to the rates of lengthening and shortening. Wei et al. (2008) proposed a dynamic model of cyclic stretch-induced SF orientation in which SF growth is predicted to be greatest in the direction with the smallest shortening rate. To address the question of whether cells can discriminate between lengthening and shortening rates, our lab recently tested the effects of applying stretch patterns in which the rates of lengthening and shortening are unequal (**Fig. 6A**

and **6D**). Asymmetric strain waveforms were applied using the same fast strain rate as used for square-stretch, but with a slow rate of strain in the opposite phase of the cycle. Hereafter, these asymmetric waveforms are referred to as fast-lengthening-stretch and fast-shortening-stretch. Fast-lengthening-stretch at 0.01(**Fig. 6B**) and 0.1 Hz (**Fig. 6C**) resulted in comparable SF alignments to that caused by 0.01 (**Fig. 5D**) and 0.1Hz square-stretch, respectively. In contrast, fast-shortening-stretch resulted in no SF alignment at 0.01 Hz (**Fig. 6E**) and very little alignment at 0.1Hz (**Fig. 6F**).

These new results indicated a need to modify Eqn. 17 so that the probability of SF disassembly is greater under conditions of fast stretching than fast shortening. Bell (1978) showed that the rate constant for dissociation (k_{off}) of a protein-protein interaction increases when a force is applied, i.e. $k_{off} = k_{off}^0 \exp\left(\frac{f}{f_B}\right)$, where $k_{off}^0$is the value of k_{off} when f = 0 and f_β is a scaling factor. Assuming that the likelihood of SF dissociation followed a similar dependence on force, Eqn. 17 can be modified as

$$P(\text{disassembly of the } i^{th} \text{ SF}) = \alpha \cdot \exp(f/f_B) \cdot \quad t + \beta \cdot \exp(-\gamma/|v|) \qquad (18)$$

where the first term on the right hand side represents load-dependent breaking of bonds holding actin filaments together within the SF and the second term represents the decrease in fraction of bound myosin heads (i.e., the duty ratio) in a SF as actomyosin sliding velocity increases.

Fig. 7 illustrated the relationship between SF tension and the probability of SF disassembly. At low tension, myosin shortening increased the probability of SF disassembly (**Fig. 7**, red line). As tension approached the stall force, myosin shortening and the probability of SF disassembly decreased. Above the stall force, force-induced SF disassembly rose rapidly (**Fig. 7**, blue line). The summation of these effects was to make the SF more sensitive to high tension ($f > f_0$; caused by fast lengthening) than to low tension ($f < f_0$; caused by fast shortening).

The model was solved using my custom-written C++ code (Hsu et al., 2010) with modifications to incorporate Eqns. 14, 15 and 18. The initial conditions were that the

orientations of the population of the N_{SF} SFs are taken to be randomly distributed with each SF having an initial strain ε_0. This initial strain represented the pre-elongation caused by cell contractility. Further changes in SF strain occurred through deformation of the underlying matrix. The temporal pattern of matrix deformation was described as a series of incremental stretches taken over time increments Δt. Changes in substrate strain were applied in the x-direction with the strain in the y-direction dependent on the Poisson ratio of the substrate ($-\varepsilon_y/\varepsilon_x$). The dispersion in a SF orientation distribution can be summarized with a circular variance statistic (Eqn. 1), where 1 and 0 for a random distribution and complete alignment, respectively. As previously described (Hsu et al., 2009), the model parameters providing the best model fitting for the experiment data was determined by minimizing a root-mean sum-of-the-squares of the error between measured circular variances and those predicted by the model. Simulations were performed of 10% cyclic uniaxial stretch ($\varepsilon_x = 0.10, \varepsilon_y = 0$) using the various strain patterns at 0.01, 0.1 and 1 Hz, with the model parameters optimized to fit the experimental data (**Fig. 5 and 6**).

Fig. 8 showed comparisons in the angular histograms measured from the experiments and those generated from solving the model under identical stretching waveforms at 0.01 and 0.1 Hz. Fast-lengthening-stretch at 0.01 and 0.1 Hz resulted in comparable SF alignments to that caused by 0.01 and 0.1Hz square-stretch, respectively. In contrast, fast-shortening-stretch resulted in no SF alignment at 0.01 Hz and very little alignment at 0.1Hz, similar to that caused by triangle- stretch. The model was also used to predict how the population-average SF tension f varies over the first several cycles of stretch until achieving a dynamic steady-state response for each condition (**Fig. 9**). At 0.01 Hz, triangle-stretch generated an imperceptible perturbation in tension (amplitude of $0.02f_0$) since the strain rate is very small (**Fig. 9A**). The amplitude in tension perturbation did become apparent ($0.15f_0$) at 0.1 Hz. At both 0.01 and 0.1 Hz, the rapid lengthening rates in square-stretch generated a rapid rise in tension that decays back to f_0 within 5 s during the first half of the stretch cycle, followed by a rapid drop in tension that decayed back to f_0 within 5 s during the latter half of the cycle. The response to fast-lengthening-

stretch at 0.01 and 0.1 Hz (**Fig. 9B**) closely resembled the response to the first half of the cycle for square-stretch, with a rapid rise in tension occurring at the beginning of each cycle. The response to fast-shortening-stretch at 0.01 and 0.1 Hz mirrored the response to fast-lengthening-stretch, with a rapid fall in tension occurring at the end of each cycle. At 0.1 Hz, the asymmetric waveforms did not result in tension returning to f_0 during the periods of slow strain since the strain rate was sufficiently high to cause a small perturbation in tension. At 1 Hz, the responses took 5 s to reach steady-state and all the waveforms generated comparably large positive perturbations in tension ($>f_0$) since the SFs did not have enough time between cycles to relax (**Fig. 9A** and **9B**). Since these perturbations were of comparable size, each of the waveforms tested were predicted to result in a similar extent of SF alignment at 1 Hz. In summary, the model predicted that stretch waveforms with fast lengthening rates generate SF tension values greater than the stall force (f_0), while fast shortening reduced the tension below f_0. In turn, SFs became more likely to disassemble parallel to the direction of stretch for stretch waveforms involving rapid lengthening. Therefore, the model was able to predict SF orientation distributions similar to that observed in the experiments (cf. **Fig. 8**) and also predicts that the SFs were induced to reorganize in response to positive perturbations in SF tension.

III.C. Discussion

Individual cells tend to maintain intracellular strain (Lu et al., 2008) and stiffness (Wang et al., 2002) at a particular level. Mizutani et al. (2004) demonstrated that cell stiffness gradually relaxes following an initial rapid increase in stiffness caused by cell stretching. They attributed this tensional homeostasis to SFs, but did not propose a specific mechanism by which tensional regulation occurs. The level of tension in SFs within intact cells undergoing cyclic stretching has not been measured; however, time-dependent changes in SF tension can be predicted using theoretical models. In this **s**ection, tension regulation in individual SFs was analyzed using a sarcomeric model based on the Hill-type force-velocity relationship for myosin sliding. This model predicts that prestrain and prestress are generated by the steady-state balance between

myosin filaments and elastic resistance to stretching of the actomyosin subunits. Further, the model explains how SFs can regulate tension through two different mechanisms that become important under different situations. Under conditions when the rate of strain is low, such as during cyclic stretching at low stretch frequencies, myosin sliding quickly readjusts the reference length of the SF so as to quickly re-establish tensional homeostasis. Under conditions when the SF is subject to high rates of strain, such as during cyclic stretching at high stretch frequencies, myosin sliding is much slower than the rate of change in sarcomere length, and the SF behaves elastically. Here, the SFs must orient away from the direction of stretch in order to minimize perturbations in tension. This realignment process occurs as a consequence of the asymmetric increase in the rate of disassembly of SFs undergoing high rates of change in length, resulting in the accumulation of SFs in orientations that avoid changes in length. Thus, both relaxation and reorientation are important mechanisms that cells use to maintain SF tension at a preferred level, and myosin II plays an important role in each of these activities.

Previous studies have reported that cyclic stretch induces cell and SF alignment, with the extent of alignment dependent on stretch amplitude, frequency and spatial pattern (Jungbauer et al., 2008; Kaunas et al., 2006; Wang et al., 2001c). However, there is a need to examine the effects of the shape of the temporal waveform on stretch-induced SF reorganization. The experimental results clearly demonstrate that SFs are more sensitive to strain rate than stretch frequency per se by subjecting cells to triangle- versus square-stretch waveform. By applying asymmetric waveforms, SFs are more response to the rate of lengthening than the rate of shortening during the stretch cycle. A sarcomeric model with modification on the probability of SF disassembly can explain that SFs are more unstable in response to positive perturbation in tension.

The time-dependent mechanical properties of functional SFs have been estimated by severing SFs within intact cells and tracking their rate of recoil (Colombelli et al., 2009; Kumar et al., 2006; Russell et al., 2009). Mechanical models were proposed to interpret the measurements from these experiments where individual sarcomeres were modeled as either springs in parallel with a contractile element and a dashpot (Colombelli et al.,

2009; Stachowiak and O'Shaughnessy, 2009) or a spring in series with a contractile element (Russell et al., 2009). A spring in parallel with a contractile element would not be fully unloaded at low strain rates, leading to asymmetric increases in tension of SFs in the direction of stretch even at very low stretch frequencies. This is inconsistent with previous experimental results that SFs do not respond to stretching at 0.01 Hz (Hsu et al., 2009). However, a spring in series with a contractile element would remain at equilibrium at low strain rates. It is very similar to this model of an actomyosin subunit; however, in this model, the elastic and contractile elements are not treated as separate elements of an actomyosin subunit. Instead, myosin sliding acts to change the reference length of the elastic element so that strain changes without a change in the current length of the element (i.e., the actomyosin subunit). Na et al. (2007) modeled actin cytoskeletal remodeling in response to cyclic equibiaxial strain based solely on SF turnover, but their model cannot account for SF realignment or strain-rate dependence. De et al (2007) modeled stretch-induced cell alignment by treating whole cells as force dipoles. Similar to the current model, they proposed that cells try to maintain a mechanical variable at a set point level, but in their model the variable was the level of stress or strain in the adjacent elastic matrix. Although their model also predicts frequency-dependent alignment, it is not clear that their model is capable of predicting the effects of asymmetric waveforms. The model developed by Wei et al. (2008) predicts that actin is more likely to depolymerize in directions of rapid shortening, resulting in frequency-dependent SF alignment perpendicular to the direction of stretch. Their model is not consistent with our observation that SFs are not induced to align in response to rapid shortening. The present model seeks to provide insight into the role of myosin II, which has been predicted mediating both SF relaxation and turnover. Each of these phenomena contributes to SF adaptation to cyclic stretch, with SF relaxation being important at low strain rates and SF turnover becoming important as strain rate increases, especially in fast lengthening rates.

This sarcomeric model implicates actomyosin crossbridge cycling as the source for the apparent viscoelastic behavior of SFs. This mechanism is supported by direct

measurements of SF sarcomere shortening after SF severing (Russell et al., 2009). However, we cannot rule out other potential mechanisms that may also contribute to SF relaxation. Cytoskeletal fluidization has been proposed as a mechanism for stress dissipation in stretched cells (Trepat et al., 2007). However, previous studies have not observed the fluidization of SFs in cells expressing GFP-actin subject to 0.01 Hz cyclic stretch (Hsu et al., 2010; Lee et al., 2010). Myosin light chain and α-actinin turnover rates are reported to be in the range of 1-3 min in U2OS cells. Thus, the unbinding of stressed SF proteins followed by their rebinding in an unstressed configuration may relieve the overall stress in the SF. It is likely that sarcomere mechanics and SF protein turnover each play a role, and future studies using techniques such as fluorescence recovery after photobleaching of fluorescently labeled SFs subject to cyclic stretch will need to be performed to assess the role of SF protein turnover in SF relaxation.

Several simplifying assumptions were used to maintain the mathematical transparency of the current model without sacrificing physiological relevance. Sarcomere dimensions and actomyosin subunit force-velocity relationships are assumed to be uniform throughout an SF. There is evidence, however, that the contractile response of sarcomeres can vary along the length of an SF (Peterson et al., 2004). There is also some variance in sarcomere contraction distance in freely shortening SFs (Russell et al., 2009). Another limitation to this model is that it lacks sensitivity to biochemical inputs. In particular, it does not directly address regulation of myosin activity by signaling via myosin light chain kinases. The increase in elastic modulus and phase angle reported by Wakatsuki et al (2000) in response to stimulation with fetal calf serum suggests that increased myosin activation will increase both stall force and myosin shortening velocity. There is a need for more direct measurement of the effect of myosin activation on the force-velocity relationship of SFs or sarcomeres. The turnover of SFs does not include a description of SF assembly kinetics. Instead, SFs simply reassemble immediately after disassembling. The rebuilding of focal adhesions is not considered in the present study. Recently, Lee et al. (2010) demonstrated that cyclic stretch-induced SF reorientation did not require the turnover or sliding of associated focal adhesions.

Finally, this model does not capture the details of the complex process by which SFs reassemble during reorientation. Nonetheless, the present model captures many of the salient features of stretch-induced SF reorganization using rules motivated by the effects of actomyosin interactions.

IV. THE EFFECT OF THE SF TENSION ON THE LEVELS OF PHOSPHORYLATION OF THE MAPKs AND DOWNSTREAM PRO-INFLAMMATORY GENE EXPRESSION*

IV.A. Introduction

Cytoskeletal tension enables cells to adhere, spread, contract, and migrate. In adherent, non-muscle cells such as ECs and fibroblasts, tension is a result of actomyosin SFs generating forces that are resisted by cell-matrix adhesions. Stretching the matrix upon which cells adhere perturbs the cell-matrix traction forces and cells respond by actively re-establishing the pre-existing level of force (Brown et al., 1998; Gavara et al., 2008). Fiber tension extends SFs beyond their unloaded lengths and cells maintain fiber strain at an optimal level that depends on actomyosin activity (Lu et al., 2008). Sudden large (>20%) increases or decreases in matrix strain result in rapid SF disassembly and reassembly (Costa et al., 2002; Lu et al., 2008; Nekouzadeh et al., 2008), suggesting that perturbing fiber strain from the optimal level increases the rate of SF turnover.

In **Section III**, when cyclically stretched at frequencies at or above 1 Hz, cells and their SFs tend to orient away from the direction of stretch, but remain randomly oriented when subjected to stretch at low frequencies (Hsu et al., 2009; Jungbauer et al., 2008). Theoretical analyses indicate that the frequency dependence of stretch-induced SF alignment is a result of the competition between the rate of change in fiber tension due to

---

the applied strain and the rate of active fiber relaxation caused by myosin sliding (De et al., 2007; Hsu et al., 2009). At low stretch frequencies, perturbations in tension are predicted to relax quickly so that fiber tension remains constant despite cyclic changes in fiber length. At high stretch frequencies, the SFs cannot relax quickly enough to dampen the changes in fiber tension; hence, the SFs are expected to undergo a rapid increase in turnover. Over time, the levels of SF turnover and cytoskeletal tension are predicted to decrease as SFs accumulate in the direction generating the lowest stress or strain.

In arteries, ECs and their SFs are oriented perpendicular to the principal direction of cyclic circumferential stretching and parallel to the direction of blood flow (Nerem et al., 1981). The lack of EC alignment at arterial branch points and curvatures is associated with atherogenesis, suggesting that cell alignment is somehow important in maintaining an anti-atherogenic cell phenotype (Pradhan and Sumpio, 2004). Inhibition of any of the MAPKs attenuates activation of the AP-1 transcription element, but does not affect stretch-induced cell alignment (Kito et al., 2000). Although JNK does not appear to regulate stretch-induced cell alignment, SF alignment perpendicular to the direction of cyclic stretch results in suppression of stretch-induced JNK activation in bovine aortic ECs (BAECs) (Kaunas et al., 2006). Previous work showed that cytochalasin D greatly diminishes the number and size of SFs and the basal level of JNK activity in ECs (Kaunas et al., 2006), which may be due to decreased cytoskeletal tension. JNK and ERK activations are quantitatively related to tension in rat skeletal muscle preparations subjected to stretch (Martineau and Gardiner, 2001). These studies suggest that the time course of cyclic stretch-induced MAPK activations may be regulated by temporal changes in cytoskeletal tension as SFs align perpendicular to the direction of stretch. However, Katsumi et al. (2005) reported that JNK activation in response to stretch requires the formation of new integrin–matrix bonds. This study provides new experimental and theoretical insight into the roles of stretch-induced changes in SF tension and turnover in the activation of these MAPKs.

Focal adhesion kinase is recruited to focal adhesions in response to mechanical outside-in signaling to activate integrins, results in activation of downstream signaling

molecules, such as Rho GTPase, leading to cytoskeletal contraction (Tilghman and Parsons, 2008). Wang and colleagues (2001a) provided evidence that FAK is a force sensor since FAK-expressing mouse embryonic fibroblasts (MEFs) redirect their migration in response to local changes in matrix tension, while FAK-null MEFs do not. The level of FAK phosphorylation transiently increases in response to cyclic stretch in ECs (Naruse et al., 1998) and fibroblasts (Sai et al., 1999). FAK is reportedly required to stretch-induced MAPKs (Aikawa et al., 2002; Nadruz et al., 2005; Wang et al., 2001b), as well as stretch-induced cell alignment (Naruse et al., 1998; Petzold et al., 2009). However, FAK is not always required for EC mechanotransduction (Petzold et al., 2009). FAK activation may also occur downstream of SF formation (Gilmore and Romer, 1996). In this study, I used FAK-null MEFs to investigate the role of FAK in cell alignment and MAPK activations.

Strain-induced inflammatory gene expressions, such as ICAM-1 (Sung et al., 2007), VCAM-1 (Sung et al., 2007), fibronectin (Gruden et al., 2000), and matrix metalloprotein-2 (MMP-2) (Grote et al., 2003; Haseneen et al., 2003), have been reported to be modulated by MAPK signaling pathways (Gruden et al., 2000; Hu et al., 2008; Ishida et al., 1999; Milkiewicz et al., 2007). Previous results have also shown that the time course of JNK activation by cyclic stretch is dependent on the directionality of the stretch applied (Kaunas et al., 2006). This study also investigates the role of SF alignment induced by cyclic stretch in reducing stretch-induced inflammatory gene expression via MAPK signaling pathways.

How ECs respond to complex ECM in vivo is currently unclear. However, it has been shown that many cell responses to strain depend on the specific ECM to which cells are adhered. Static biaxial stretch of cardiac fibroblasts transiently activates ERK2 and JNK1 signaling pathways in an ECM-specific manner, but does not affect p38 signaling pathway (MacKenna et al., 1998). Activation of ERK2 only appeared in fibroblasts plated on fibronectin; activation of JNK1 appeared on fibronectin, vitronectin, or laminin; and no activation of these MAPKs appeared on collagen. In vascular smooth muscle cells, cyclic strain stimulated mitogenesis on collagen, fibronectin or vitronectin via

integrin $_{v}$ $_{5}$ and $_{3}$, but not on elastin or laminin (Wilson et al., 1995). Cyclic strain of smooth muscle cells (SMCs) increased apoptosis on collagen I mediated by $_{1}$-integrin–Rac–p38-p53 signaling pathways, but not on elastin, laminin, and pronectin (Wernig et al., 2003). Stretch-induced MAPK activations were inhibited in intestinal epithelial cells on a fibronectin substrate, but activated on collagen I, collagen IV, and laminin (Zhang et al., 2003a; Zhang et al., 2003b). Moreover, it has also been shown that shear stress leads to transient inactivation of Rho via matrix-specific binding with integrin $_{v}$ $_{3}$ (Tzima et al., 2001). Shear stress-induced activation of NF-κB occurs on fibronectin or fibrinogen matrix, but not in endothelial cells plated on collagen or laminin (Orr et al., 2005). These data taken together suggest that specific extracellular matrix proteins, including fibronectin and collagen, are involved in the cellular detection of mechanical forces. In the current study, the ability of matrix protein to modulate stretch-induced mechanotransduction and SF reorganization has been investigated.

Previous studies have reported the dependence of gene expression on the directionality of stretch. In mesenchymal stem cells, cyclic equiaxial strain downregulated the expression levels of contractile marker proteins, while cyclic uniaxial strain transiently upregulated their expression (Park et al., 2004). In adult rat cardiac fibroblasts, 3% surface area changes produced by uniaxial stretch resulted in 3-fold increase in fibronectin and collagen III mRNA expression, whereas the same area deformation produced by equibiaxial stretch caused only 1.5-fold increase in their expressions (Lee et al., 1999). The results of these studies support the idea that cells respond distinctly to different patterns of stretch in regulating gene induction.

IV.B. Results

IV.B.1. Cyclic Stretch Increases MAPK Phosphorylation Levels in a Strain Rate-dependent Manner

It has been shown that stretch-induced MAPK activations are regulated by the frequency of stretch (Hosokawa et al., 2002; Qu et al., 2007). However, the detail mechanism is not clear. As demonstrated in **Section III.B**, stretch-induced SF alignment depended on the frequency of stretch. The theoretical model predicted that SF turnover rate and tension depend on the frequency of matrix stretching as well (cf. **Fig. 2D**). Based on these works, it is reasonable to hypothesize that MAPK activation shows a similar dependence on stretch frequency as stretch-induced SF alignment. To test this hypothesis, BAECs were subjected to 30 minutes of 10% cyclic uniaxial and equibiaxial stretch at frequencies of 0.01, 0.1 and 1 Hz and the levels of JNK, ERK and p38 phosphorylation were quantified (**Fig. 10**). Stretching at 1Hz resulted in significant increases in the activities of each MAPK relative to static controls. Further, the extent of activation of each MAPK decreased as the frequency of stretch decreased to 0.01 Hz. Thus, JNK, ERK and p38 phosphorylation levels increased monotonically with strain rate in BAECs subjected to either uniaxial or equibiaxial stretch.

IV.B.2. Transient Changes in Fiber Strain Rate Induce Transient Changes in JNK and ERK Phophorylation Levels

The model developed in **Section III** predicted that both SF turnover rate and tension perturbations decrease as cyclic stretch frequency decreases (cf. **Fig. 2D**). These two responses are decoupled with step stretch, however. A 10% step increase stretch is predicted to result in an elastic increase in SF tension that quickly decays back to f_0 (**Fig. 11**). Later, releasing matrix stretch is then predicted to cause an elastic decrease in SF tension that also quickly decays back to f_0 (**Fig. 11**). Motivated by the predictions of SF relaxation, we hypothesized that a step increase in equibiaxial stretch would cause a transient increase in MAPK phosphorylation levels and releasing this stretch would

cause a transient decrease in MAPK phosphorylation levels. First, BAECs were subjected to 10% step equibiaxial stretch and measured changes in the levels of phosphorylated MAPKs. The levels of phosphorylation of JNK and ERK significantly increased at 0.15 hours and then subsided after 1 to 2 hours, while a small, not statistically significant, increase in the average levels of p38 phosphorylation was observed (**Fig. 11C-E**). Next, BAECs were subjected to a 10% step equibiaxial stretch, 12-hour hold, and stretch release maneuver (c.f., **Fig. 11A**) and quantified the levels of phosphorylation of the MAPKs over time. Releasing the 10% step equibiaxial stretch after a 12-hour hold resulted in a transient decrease in the levels of JNK and ERK phosphorylation, reaching a minimum at 0.5 hours, and returning to near baseline levels after 4 hours (**Fig. 11F and 11G**). The step stretch-release maneuver did not result in a significant change in p38 phosphorylation, however (**Fig. 11H**). It is not clear why the level of JNK phosphorylation did not fully return to the baseline level, however the difference was not statistically significant. Thus, a transient increase in the rate of strain caused a transient increase in JNK and ERK phosphorylation, while a transient decrease in the rate of strain caused a transient decrease in JNK and ERK phosphorylations.

To assess the effects of stretch on SF turnover, we subjected U2OS osteosarcoma cells expressing GFP-actin to step and cyclic changes in equibiaxial stretch. Neither a step stretch nor a step stretch-and-release (cf. **Fig. 11A**) resulted in obvious SF turnover (Hsu et al., 2010). Cyclic stretch at 1Hz, but not 0.01Hz, caused the cell to retract lamellipodia, but there were little obvious changes to central SFs (Hsu et al., 2010). Together, these results suggest that MAPK activation is dependent on stretch-induced changes in SF strain rate (and related changes in SF tension) rather than SF turnover.

IV.B.3. Stress Fiber Inhibitors Decrease JNK and ERK Phosphorylation Levels

To further explore the relative roles of SF tension and turnover on MAPK phosphorylation, SF contractile function was disrupted by treating BAECs with cytochalasin D (50nM) to disrupt actin filaments or Y27632 to reduce actomyosin activity (Hsu et al., 2010). Cytochalasin D and Y27632 significantly reduced the phosphorylation levels of JNK and ERK, but not p38, suggesting that JNK and ERK phosphorylation levels are regulated by cytoskeletal tension. Treating BAECs with jasplakinolide (10nM) to stabilize actin filaments, which is expected to maintain SF integrity in bovine ECs without significantly changing basal cell contractile tone (Goeckeler et al., 2008) , caused an increase in the level of JNK phosphorylation without significantly affecting p38 and ERK. These results are consistent with JNK and ERK phosphorylation levels being regulated by cytoskeletal tension since inhibitors that disrupt SF stability or contractility decrease JNK and ERK phosphorylation levels. Further, these results provide additional evidence that MAPK activities are not associated with SF turnover.

IV.B.4. FAK Is Not Required for Stretch-induced Changes in MAPK Phosphorylation in MEFs

There is also substantial evidence indicating that FAK is required for stretch-induced MAPK activations (Aikawa et al., 2002; Nadruz et al., 2005; Wang et al., 2001b). The role of FAK in regulating stretch-induced MAPK phosphorylation was evaluated using normal and knockout FAK MEFs subjected to 0.5 and 6 hours of 10% cyclic uniaxial stretch at 1 Hz. The levels of phosphorylated MAPKs were each transiently increased after 30 min of cyclic stretch in both FAK-null and FAK-expressing MEFs, indicating that FAK is not necessary for stretch-induced MAPK activations. While the absolute levels of phosphorylated MAPKs was higher in the FAK-null MEFs (**Fig. 13**, upper blots), this was attributed to higher levels of total JNK, ERK and p38 expression (**Fig. 13**, lower blots). Thus, FAK is not necessary for stretch-induced activation of JNK, p38 and ERK.

IV.B.5. Effect of Integrin-Matrix Proteins on Stretch-Induced MAPK Signaling Pathways

Several studies have reported that stretch-induced MAPKs activations are regulated by specific extracellular matrix proteins (MacKenna et al., 1998; Wernig et al., 2002; Wilson et al., 1995; Zhang et al., 2003a; Zhang et al., 2003b). Therefore, we hypothesized that stretch-induced mechanotransduction depends on what kind of ECM the cells are plated on. To test this hypothesis, HAECs or BAECs were seeded on fibronectin- or matrigel-coated silicone membranes followed by 10%, 1Hz cyclic uniaxial or equibiaxial stretch, respectively, and the levels of JNK, ERK and p38 phosphorylation were quantified, as well as the levels of ICAM-1 protein expression. Cyclic stretch resulted in significant increases in the activition of JNK and ERK on fibronectin, but not on matrigel (**Fig. 14**). Further, an increase in the protein expression of ICAM-1 was also observed on fibronectin versus matrigel; however the increase was not statistically significant relative to static controls (data not shown). These results suggest that specific extracellular matrix proteins are involved in the cellular detection of mechanical forces.

IV.B.6. Stretch-Induced Gene Expressions Correlate with Stress Fiber Tension

Previous studies supported the idea that cells respond distinctly to different patterns of stretch in regulating gene induction (Lee et al., 1999; Park et al., 2004). To test this hypothesis, HAECs were seeded onto stretch chambers with fibronectin-coated silicone rubber bottoms and subjected to 10%, 1Hz cyclic equibiaxial and uniaxial strain for the time period of 0, 4 and 8 h. After stretching, HAECs were lysed with TRIzol and changes in the expression of various genes were quantified by qRT-PCR. Our results showed that cyclic uniaxial stretch resulted in a transient increase in VCAM-1 and ICAM-1 by 4 h that subsided to basal level by 8 h (**Fig. 15A-B**, gray columns). However, equibiaxial stretch resulted in larger and more prolonged elevation of VCAM-1 and ICAM-1 (**Fig. 15A-B**, black columns). Both cyclic uniaxial and equibiaxial stretch caused sustained upregulation of fibronectin and MMP-2 mRNA; however, cyclic

equibiaxial stretch induced a significantly higher induction of fibronectin at 8 h compared to cyclic uniaxial stretch and a non-significantly higher induction of MMP-2 (**Fig. 15C-D**). The levels of eNOS mRNA were somewhat upregulated by cyclic stretch (**Fig. 15E**), however this was not statistically significant. As expected, there was no obvious change in VE-cadherin expression caused by cyclic stretch for either stretch pattern (**Fig. 15F**). These results suggest that mechanical stimuli which regulate cytoskeletal alignment are associated with increased expression of the genes encoding VCAM-1, ICAM-1, fibronectin, and MMP-2, but not eNOS and VE-cadherin.

IV.C. Discussion

It is becoming increasingly clear that cytoskeletal tension plays a major role in maintaining normal cell function, and that loss of 'tensional homeostasis' promotes disease progression, including fibrosis, cancer and atherosclerosis (Butcher et al., 2009). While stretching SFs increase their tension (Deguchi et al., 2006), SFs display viscoelastic properties (Kumar et al., 2006) that allow relaxation of perturbations in tension. Dynamic changes in cytoskeletal structure, mechanical properties, and intracellular signaling all depend on the spatio-temporal pattern of externally applied forces as well as active responses within the cell. Theoretical modeling developed in **Section III** provides a valuable tool to make sense of this complex system. The present study, which was designed and interpreted using a simple sarcomeric model of SF dynamics and mechanics, supports the hypothesis that stretch-induced mechanotransduction via the MAPK pathways are regulated by perturbations in SF tension. Importantly, the model illustrates a mechanism by which SFs respond to perturbations in cytoskeletal tension through tension relaxation and SF reorientation to re-establish tensional homeostasis. The results of this study indicate that this model provides a useful framework for exploring the mechanisms by which cytoskeletal tension and remodeling modulate stretch-induced mechanotransduction.

Gavara and colleagues (2008) reported that cell-matrix traction forces increase in response to a step increase in equibiaxial stretch, but later, after the stretch is released,

traction forces drop below baseline levels and gradually return toward baseline levels over a period of ten minutes. These authors attributed the changes in traction forces to changes in actin cytoskeletal tension. Assuming that fiber stretch is proportional to average traction force, the predictions of this study (**Fig. 11A**) are consistent with the changes in traction force caused by stretch and release measured by Gavara and colleagues (2008), with a time constant on the order of several minutes. This is a much larger value for the time constant than the value ~ 0.5 sec found to describe the frequency dependence of cyclic stretch-induced SF alignment (**Fig. 3**). For the case of a step change in stretch, a value for τ determined from experimental measurements is likely to be more accurate than the one extracted from the model parameter fitting to cyclic stretch data. Regardless of the discrepancy in the value for τ, the model predicts full SF relaxation within minutes.

Step equibiaxial stretch-induced JNK activation in fibroblasts has been reported to require the formation of new integrin-matrix bonds (Katsumi et al., 2005). SF assembly also requires the formation of new integrin-matrix bonds. In this study, we also tested if stretch-induced JNK and ERK activations by stretch may be related with SF reorganization. The results showed that neither a 10% step equibiaxial stretch nor a 10% equibiaxial step stretch-and-release (cf. **Fig. 11A**) resulted in significant SF disassembly and reassembly (Hsu et al., 2010). Cyclic equibiaxial stretch at 1Hz, but not 0.01Hz, caused the cell to retract lamellipodia, but there were little obvious changes to central SFs (Hsu et al., 2010). Together, these results suggest that MAPK activation is dependent on stretch-induced changes in SF strain rate (and related changes in SF tension) rather than SF turnover.

In vivo, fibronectin deposition into the ECM correlates with areas of inflammatory gene expression, suggesting transition to a fibronectin matrix may regulate early atherogenesis (Orr et al., 2005). Our results in **Section IV.B.5** support the role of fibronectin in a pro-inflammatory phenotype characterized by resulting in a higher activation of JNK and ERK as well as a higher protein expression of ICAM-1 in response to hemodynamic forces (**Fig. 15**). This indicates that subendothelial ECM with

high deposition of fibronectin might affect pro-inflammatory mechanotranduction to promote atherosclerosis. Further, there is a reactivation at 8 h, which is consistent with the time course for JNK phosphorylation in response to wall shear stress by Hahn et al (2011). This reactivation implies that there may be another delayed mechanotransduction pathway distinct from the initial activation of these MAPKs at the earlier time point. Stretching experiment with extending time frames may offer more detail about the stretch-induced signaling pathway.

Since the activation of JNK induced by mechanical stimuli has been reported to mediate the expression of several genes, including ICAM-1, regulated by the AP-1 transcription factor (Cheng et al., 1996), it indicates that changes in ICAM-1 expression could take longer to occur than the changes in JNK phosphorylation. This is consistent with our observation in **Section IV.B.5** that cyclic uniaxial stretch resulted in a transient increase in ICAM-1 gene expression at 4 h that subsided to basal level at 8 h.

V. MECHANOBIOLOGY OF CELLULAR MICRO-ENVIRONMENTS WITHIN ENGINEERED TISSUES

V.A. Introduction

Our knowledge about the role of cell behavior in tissue formation, function, and pathology is derived primarily from studies on planar two-dimensional (2-D) cell culture substrates. While this approach has produced many important conceptual advances, cells grown on stiff 2-D substrates, such as polystyrene, are considerably different in their morphology, cell-cell and cell-matrix interactions, migration, proliferation, signaling, and cytoskeletal function from cells grown in more physiological 3-D environments made of reconstituted ECM proteins such as collagen I (Abbott, 2003; Birgersdotter et al., 2005; Cukierman et al., 2001; Griffith and Swartz, 2006; Haga et al., 2007; Thie et al., 1991). In vitro 3-D cell culture systems fulfill a need for reductionist approaches toward studying cell-matrix interactions in tissues. Thus, it is important to select a biocompatible 3-D microenvironment that mimics native tissue and provides appropriate mechanical cues for studies of cell behaviors.

Fibroblasts and SMC in 3-D collagen matrices have been shown to elongate in parallel with the predominant alignment of collagen fibrils in the direction of stretch (Brown et al., 1998; Kanda et al., 1993; Pang et al., 2011). These authors attributed the co-alignment of the cells and collagen fibrils to so-called ‘contact guidance’, a phenomenon in which cells tend to orient parallel to topological structures that they are in contact with such as matrix fibrils. However, our lab has recently observed that U2OS cells cultured on the surface of collagen matrices can align parallel to matrix stretch without fibril alignment. This discrepancy suggests that contact guidance might be more important in a 3-D than a 2-D environment.

Poly(ethylene glycol) diacrylate (PEGDA) hydrogels are cross-linked by photoinitiator under sufficiently mild conditions to enable high cell viability after encapsulation within a 3-D PEGDA network (Nguyen and West, 2002). PEGDA hydrogels are immunoprotective, biocompatible, and mechanically resilient supporting

scaffold which makes them attractive for systematic exploration of cell response to specific alterations in extracellular microenvironment properties. Decreasing the molecular weight and/or increasing concentration of PEGDA increase the elastic modulus (Al-Nasassrah et al., 1998; Gunn et al., 2005; Padmavathi and Chatterji, 1996). The ability to tune the mechanical properties of PEGDA hydrogels allows us to study cell response to substrate rigidity, which may play an important role in the pathogenesis of disease states (Nemir et al., 2010). However, isolated cells suspended in PEGDA are unable to remodel the surrounding PEGDA matrix; hence they are incapable of elongating and reorienting in response to stretch.

Collagen is often used in tissue engineering and many biomedical applications, including skin replacement, bone substitutes, artificial blood vessels and valves, drug delivery system and basic matrices for cell culture systems, since it is biocompatible and its stiffness can be tuned (Lee et al., 2001). Collagen is the most prevalent protein in the body, and so the response of cells to the mechanical properties of collagen has been of great interest. Collagen tissue is often reconstituted from soluble collagen that is allowed to gel into a fibrillar matrix. Previous studies observed that simply increasing the stiffness of the collagen matrix by increasing the concentration or enhancing fibril crosslinking of collagen, without altering the integrin recognition or binding of 1, can result in increased fibroblast and tumor cell migration and signaling (Grinnell, 2003). However, the use of reconstituted collagen as a tissue scaffold is limited by its weak mechanical properties as compared to inorganic polymers such as PEGDA.

Cells mechanically remodel the nearby ECM, which plays a critical role in tissue engineering, wound healing, embryonic development, and many disease states (Abercrombie et al., 1956; Enever et al., 2002; Weinberg and Bell, 1986). Stevenson et al. (2010) proposed that rather than sensing average properties of the ECM, cells sense mechanical properties in their local pericellular environment. Motivated by this concept, we developed a hybrid tissue consisting of cell-populated collagen microspheres suspended in an acellular PEGDA hydrogel. The bulk matrix (PEGDA) bears the majority of applied mechanical loads while supporting the more fragile collagen

microspheres. The microspheres still deform with the bulk matrix, which is expected to induce mechanotransduction in the resident cells and the reciprocal remodeling of the cell and matrix architectures. Therefore, we hypothesized that this hybrid tissue can bear the comparable levels of stress as does pure PEGDA, while the reduced stress transmitted to the cellular microenvironment is sufficient to induce the same cell and collagen remodeling as occurs in pure collagen matrices subjected to comparable levels of strain (but much less stress).

V.B. Results

V.B.1. Strain Field Transmission

To quantify the strains in the collagen microspheres and the surrounding hydrogel, fluorescent beads (0.2 μm Fluospheres, Molecular Probes) were mixed into the hydrogel and collagen-U2OS solution prior to assembly to serve as fiducial markers with different colors used in each phase. 2-D strains in the focus plane were quantified using three-point finite strain analysis (Barbee et al., 1994) as described in **Section II**.

We quantified the deformation of pure collagen matrices (3.5 mg/ml) for comparison to the deformation of hybrid constructs using strains ranging from 0.025 to 0.125 (i.e., 2.5 to 12.5% stretch). In the pure collagen matrices, only 65% of the applied strain was transmitted (**Fig. 16A**). In contrast, the normal strains developed inside the microspheres and in the surrounded PEGDA hydrogel were essentially equal to the nominal strain (**Fig. 16A**). These results demonstrate strain continuity between collagen microspheres and the surrounding hydrogel. The relatively low normal strain measured in the pure collagen gel was due to the manner in which it was stretched. The collagen gel only adhered to the bottom of the stretching chamber, thus the strain was only applied from the bottom of collagen gel resulting in 65% of the applied strain (**Fig. 17**). In addition, the lateral strain caused by the Poisson effect in the microspheres was slightly smaller than that in PEGDA hydrogel, and practically no deviation angle ($\theta_{\text{final}} - \theta_{\text{initial}}$) in the focus plane

(xy plane), a measurement of shear strain (Eqn. 8), was observed in hybrid tissue compared to in pure collagen gels.

V.B.2. Quantify the Effect of Applied Strains on Cell Morphology and Alignment within 3-D Collagen Gels

We encapsulated GFP-actin-expressing U2OS cells in pure 3-D collagen matrices and subjected them to 6 hours of 10% cyclic uniaxial stretch at 1Hz. The whole collagen-cell gel was then fixed for 30 minutes. Maximum intensity projection of confocal image stacks followed by cell shape analysis (see **Section II**) was used to quantify cell elongation (aspect ratio) and orientation. Some cells did not appear to elongate and orient in the focal plane (aspect ratio < 2), hence these cells were excluded from our measurements of the distribution of cell orientations generated in response to stretch. Confocal reflectance microscopy was used to image the collagen fibril organization immediately surrounding the cells inside the hydrogel. The order parameter, ($\langle \cos 2\theta \rangle$) used to quantify the dispersion in cell and collagen fibril orientations was calculated using Eqn. 2 (**Section II**). The results indicated that (1) both U2OS cells and collagen fibers are significantly aligned in the direction of cyclic uniaxial stretch after 6 hr of cyclic stretch (**Fig. 18B** and **18D**); and (2) collagen fibers ($\langle \cos 2\theta \rangle = 0.22$) are less strongly oriented toward the direction of stretch than are the cells ($\langle \cos 2\theta \rangle = 0.51$) (**Fig. 18E**). The results are somewhat, but not entirely, consistent with the co-alignment of the cells and collagen fibrils in the direction of stretch reported by others (Brown et al., 1998; Pang et al., 2011). The correlation between cell and collagen fibers alignment was not high (**Fig. 18F**). Together, these results indicate that stretch-induced cell alignment takes place without obvious alignment of the surrounding collagen fibrils.

V.B.3. Quantify the Effects of Applied Strains on Cell Morphology and Alignment within the Hybrid Constructs

Section V.B.1 demonstrated a continuous transmission of strain from the surrounding hydrogel into the microspheres. This hybrid construct allows us to study the effect of local forces transduced from the macro-level to pericellular environments on cell alignment and collagen fiber orientation. We mixed cells with collagen and then encapsulated collagen-cell microspheres into PEGDA hydrogel (see **Section II.** Preparation of Collagen–U2OS Microspheres and Microencapsulation). This hybrid tissue was allowed to swell in DMEM growth medium overnight before applying mechanical stretch. We used the same stretching device that has been used for stretching pure collagen gels, but porous polyethylene strips were used to provide strong attachment points for the motor arms (**Fig. 19**). Collagen fibril and cell orientation distributions were then quantified within individual spheroids induced by cell contractility and uniaxial stretching at 6hr at frequencies of 1 and 0.01 Hz as we have done previously for pure collagen gels in **Section V.B.2**. At least five microspheres per sample for three experiments were analyzed. Similar to the pure collagen gel, the values of order parameter (Eqn. 2) indicated that cells in the center of the spheroidal collagen domains are significantly elongated parallel with the predominant alignment of collagen fibrils which align along the direction of matrix stretch at 1Hz, but not at 0.01 Hz. Also, cells ($\langle \cos 2\theta \rangle = 0.52$) aligned to a greater extent than the surrounding collagen fibrils ($\langle \cos 2\theta \rangle = 0.18$) at 1Hz, but not at 0.01 Hz (**Fig. 20E**). These results suggest that cell alignment occurs prior to significant collagen fibril alignment and both cell and collagen fibril orientations are dependent on strain rate. Interestingly, at 1Hz cells near the surface of collagen spheroids were elongated along the collagen-PEGDA interface (**Fig. 21A-F**). Of note, not all cells followed this trend (**Fig. 21C**). These results suggest that cells may sense and respond to the relatively stiff PEGDA near the interface. Therefore, cells seem to primarily respond through contact guidance at the interface, but respond primarily to the stretch signal in the region far away from the interface.

V.C. Discussion

Our hybrid construct is a novel approach that can facilitate the generation of engineered tissues for fundamental investigation of cell mechanobiology in a 3-D environment. The construct consists of a load-bearing acellular hydrogel supporting collagen microspheres containing cells that sense and respond to strains transmitted from the surroundings. Cells and collagen fibrils in the microspheres aligned parallel to the direction of stretch in a manner similar to that observed in pure collagen gels. This composite-material approach will allow systematic manipulation of the chemical, mechanical and geometrical properties of the cellular micro-environment for optimal cell function, as well as control over the global material properties of the hybrid tissue. We can then expand upon this research to the focused development of engineered tissues having specific functions (e.g. gene expression profiles, differentiated phenotype) meant for replacement of specific tissues.

Local geometric features such as the shape of the cellular niche have seen to affect cell organization, proliferation, and differentiation under static culture conditions (Kilian et al., 2010; Ruiz and Chen, 2008). Mechanical cues are then transduced into intercellular signals that regulate gene expression, and ultimately cell function. Kurpinsky and colleagues (2006) used elastomeric membranes with parallel microgrooves to simulate the vascular cell alignment and investigate the anisotropic mechanical sensing by mesenchymal stem cells (MSCs). They found that cells cultured on micropatterned poly(dimethyl siloxane) (PDMS) membranes with parallel microgrooves under static culture conditions aligned with these grooves via contact guidance (Thakar et al., 2003) and micropatterned guidance helped maintain MSC alignment with the axis of stretch during cyclic uniaxial stretch (Kurpinski et al., 2006). In contrast, stress fibers in C2C12 skeletal myoblasts seeded on fibronectin lines with different orientations relative to the stretch direction all aligned oblique to the stretch direction when 7%, 0.5Hz cyclic uniaxial stretch is applied, suggesting that actin fiber organization is dominantly controlled by anisotropic strain (Ahmed et al., 2010). These opposing results were obtained from cells on a 2-D culture surface, which may due to

differences in how the cells were spatially constrained. Our results reveal that U2OS cells in the center of microdomains embedded in a gel under stretched conditions align toward the direction of stretch depending on strain rate, while cells near the boundary align tangent to the sphere-PEG interface regardless of applied strain (**Fig. 21**). Buxboim and colleagues estimated the distance that cells can feel into soft matrices by measuring cell spreading area on soft brain-like gels of varying thickness that are affixed to a rigid substrate (Buxboim et al., 2010). On thick gels, the cells did not spread well. They observed that cell spreading area increases as gel thickness decreased below a threshold value which cells begin to respond to the rigidity of the underlying rigid glass substrate. These results suggest that cells near the collagen-PEGDA interface may spread along the interface due to the relatively high local effective rigidity of PEGDA.

Contact guidance is a term describing the correlation between cell alignment and the orientation of collagen fibrils. Our results showed that there is a general trend that both cells and collagen fibrils aligned parallel to the direction of stretch, but that there is only little correlation at the level of individual cells. Yoshigi et al. (2003) stretched cells which are cultured on a collagen-coated silicone membrane and found no topographical changes in collagen fibrils. Recent experiments performed in our laboratory have shown that U2OS cells cultured on the surface of collagen matrices can align parallel to matrix stretch without fibril alignment (data not published yet). Together, these results indicate that contact guidance is not a strong driving force for cell alignment. In addition, the detail mechanism by which contact guidance occurs is not clear. Tranquillo group referred contact guidance to cell aligning with aligned fibrils and therefore exerting traction in the direction of aligned fibrils (Girton et al., 2002). Wang et al. found out that cells oriented along the longitudinal direction of microgrooved silicone membranes lead to the production of aligned collagenous matrix (Wang et al., 2003). Mudera et al. (2000) subjected cells, which are originally aligned along the fibronectin strands in 3-D collagen gel, to a perpendicular uniaxial stretch and observed sustain upregulated expressions of matrix metalloproteinases MMP-1, -2, and -3 even after most of the cells had realigned parallel to the applied mechanical load. Nguyen et al. (2009) demonstrated

that a combination of cell seeding and cyclic stretch can remodel and reorient collagen fibrils in bioscaffolds. Together, these studies indicate that cells align toward to the direction of stretch via contact guidance. Of note, this cell/fibril co-alignment requires several hours to occur. Our data suggests that cells react foremost to external mechanical cues without significant co-alignment of collagen fibrils. A possible concept to reconcile these two views of contact guidance is shown in **Fig. 22**. Specifically, cell alignment occurs initially without substantial collagen fibril alignment. Aligned cells then exert traction forces and produce MMPs to remodel and align the matrix. The aligned matrix then serves to reinforce cell alignment in the parallel direction. Here, collagen fiber alignment caused by the cells creates an anisotropic mechanical environment; therefore, cell might sense the anisotropic mechanical properties of the matrix and orient itself accordingly. This orientation might explain why cells have been found to align to a greater extent with respect to external strain than the surrounding collagen fibrils.

Previous studies have shown that cells in free-floating collagen matrices contract the matrix and tend to undergo apoptosis, while cells in collagen matrix with constrained boundaries are proliferative, more responsive to growth factors, and exhibit a relatively elongated morphology (Lin et al., 1998). The Kameoka group at TAMU recently developed a microfluidic platform for high throughput generation of cell-populated collagen microspheres (Mehrotra et al., 2008; Xu et al., 2005). In their device, the collagen microspheres are floating inside growth medium in the end of fabrication, which might increase apoptosis in contractile cells. In contrast, I fabricated collagen microspheres by dropping the mixture of collagen and cells onto the surface of parafilm, which may provide sufficient adhesion for cells inside collagen to be able to generate contractile forces that inhibit apoptotic signals (see **Section II.** Preparation of Collagen–U2OS Microspheres). This idea will require additional characterization to validate.

In **Section V.B.2**, subjecting U2OS osteosarcoma cells stably transfected with GFP-actin to 6 hours of 10% cyclic uniaxial stretch at 1Hz on 3-D collagen matrices induced cell alignment towards the direction of stretch. In contrast, U2OS cells stretched on relatively stiff silicone rubber coated with a molecular layer of collagen align

perpendicular to the direction of stretch (Lee et al., 2010; Tondon et al., 2012), which is consistent with our previous results using endothelial cells in **Section III.B.5** (Hsu et al., 2009). Given that collagen fibrils co-aligned with the cells in the microspheres, it is possible that contact guidance plays a significant role. It is also possible that cells in soft materials respond to stretch differently than cells on stiffer materials. The sarcomeric model developed in **Section III** provides some insight into this stiffness dependence of stretch-induced SF remodeling by considering the interaction between stretch and ECM stiffness to regulate stress fiber tension. In a soft matrix, SFs are suppressed due to the lack of contracting force in the matrix to generate tension. Stretching is predicted to increase the stability of SFs in the direction of applied loads by increasing SF tension toward the optimal value.

VI. GENERAL CONCLUSION

Many cells in vivo, ECs in particular, are continuously subjected to cyclic stretch and apparently adapt to this stretching through both structural and biochemical changes (Kaunas et al., 2006). It is becoming increasingly clear that cytoskeletal tension plays a significant role in maintaining normal cell function through modulation of intracellular signaling and gene expressions. Loss of "tensional homeostasis" promotes disease progression, including fibrosis, cancer and atherosclerosis (Butcher et al., 2009). The theoretical model developed in **Section III** provides a framework for incorporating molecular details of myosin II behavior into mechanical models of SF networks (**Fig. 1**). A sarcomeric description of SFs is particularly useful for understanding the molecular mechanism (e.g. role of actomyosin interactions) by which cells regulate intracellular tension. This model indicates that strain-rate dependent of SF relaxation and reorientation acts as negative feedback in maintaining not only mechanical homeostasis of the cytoskeleton, but also downstream pro-inflammatory mechanotransduction, which is studied in **Section IV**. A hybrid tissue developed in **Section V** provides a biocompatible 3-D microenvironment that mimics native tissue and provides appropriate mechanical cues for studies of cell behavior. Given that cyclic stretch induces cytoskeleton alignment, MAPK activation, and gene expression in many cell types, I expect that the results of this study to be of general relevance to many adherent cells. I wish to emphasize that the present results provide guidance toward the development of more realistic mathematical descriptions of SF remodeling and mechanotransduction to shed light on the complex interplay of intra- and extracellular forces in regulating cell shape and function. Further, the role of cytoskeletal remodeling in stretch-induced activation of other intracellular signaling pathways and their functional consequences will need to be determined in future studies. Nonetheless, the results of this study indicate that this project will provide a useful tool for exploring the mechanisms by which cytoskeletal tension and remodeling modulate stretch-induced mechanotransduction.

REFERENCES

Abbott, A. (2003). Cell culture: Biology's new dimension. Nature *424*, 870-872.

Abercrombie, M., Flint, M.H., and James, D.W. (1956). Wound contraction in relation to collagen formation in scorbutic guinea-pigs. J Embryol Exp Morph *4*, 167-175.

Ahmed, W.W., Kural, M.H., and Saif, T.A. (2010). A novel platform for in situ investigation of cells and tissues under mechanical strain. Acta Biomaterialia *6*, 2979-2990.

Aikawa, R., Nagai, T., Kudoh, S., Zou, Y., Tanaka, M., Tamura, M., Akazawa, H., Takano, H., Nagai, R., and Komuro, I. (2002). Integrins play a critical role in mechanical stress-induced p38 MAPK activation. Hypertension *39*, 233-238.

Al-Nasassrah, M.A., Podczeck, F., and Newton, J.M. (1998). The effect of an increase in chain length on the mechanical properties of polyethylene glycols. Eur J Pharm Biopharm *46*, 31-38.

Barbee, K.A., Macarak, E.J., and Thibault, L.E. (1994). Strain-measurements in cultured vascular smooth-muscle cells subjected to mechanical deformation. Ann Biomed Eng *22*, 14-22.

Bell, G.I. (1978). Models for the specific adhesion of cells to cells. Science *200*, 618-627.

Birgersdotter, A., Sandberg, R., and Ernberg, I. (2005). Gene expression perturbation in vitro - A growing case for three-dimensional (3D) culture systems. Semin Cancer Biol *15*, 405-412.

Brown, R.A., Prajapati, R., McGrouther, D.A., Yannas, I.V., and Eastwood, M. (1998). Tensional homeostasis in dermal fibroblasts: mechanical responses to mechanical loading in three-dimensional substrates. J Cell Physiol *175*, 323-332.

Butcher, D.T., Alliston, T., and Weaver, V.M. (2009). A tense situation: forcing tumour progression. Nature Reviews Cancer *9*, 108-122.

Buxboim, A., Rajagopal, K., Brown, A.E.X., and Discher, D.E. (2010). How deeply cells feel: methods for thin gels. J Phys-Condens Mat *22*.

Chen, W.T., Hasegawa, E., Hasegawa, T., Weinstock, C., and Yamada, K.M. (1985). Development of cell surface linkage complexes in cultured fibroblasts. J Cell Biol *100*, 1103-1114.

Cheng, J.J., Wung, B.S., Chao, Y.J., and Wang, D.L. (1996). Cyclic strain enhances adhesion of monocytes to endothelial cells by increasing intercellular adhesion molecule-1 expression. Hypertension *28*, 386-391.

Chrzanowska-Wodnicka, M., and Burridge, K. (1996). Rho-stimulated contractility drives the formation of stress fibers and focal adhesions. J Cell Biol *133*, 1403-1415.

Colombelli, J., Besser, A., Kress, H., Reynaud, E.G., Girard, P., Caussinus, E., Haselmann, U., Small, J.V., Schwarz, U.S., and Stelzer, E.H. (2009). Mechanosensing in actin stress fibers revealed by a close correlation between force and protein localization. J Cell Sci *122*, 1665-1679.

Costa, K.D., Hucker, W.J., and Yin, F.C. (2002). Buckling of actin stress fibers: a new wrinkle in the cytoskeletal tapestry. Cell Motil Cytoskeleton *52*, 266-274.

Cukierman, E., Pankov, R., Stevens, D.R., and Yamada, K.M. (2001). Taking cell-matrix adhesions to the third dimension. Science *294*, 1708-1712.

Dartsch, P.C., and Betz, E. (1989). Response of cultured endothelial cells to mechanical stimulation. Basic Res Cardiol *84*, 268-281.

Davies, M.J., Gordon, J.L., Gearing, A.J., Pigott, R., Woolf, N., Katz, D., and Kyriakopoulos, A. (1993). The expression of the adhesion molecules ICAM-1, VCAM-1, PECAM, and E-selectin in human atherosclerosis. J Pathol *171*, 223-229.

De, R., Zemel, A., and Safran, S.A. (2007). Dynamics of cell orientation. Nature Physics *3*, 655-659.

Deguchi, S., Ohashi, T., and Sato, M. (2006). Tensile properties of single stress fibers isolated from cultured vascular smooth muscle cells. Journal of Biomechanics *39*, 2603-2610.

Enever, P.A., Shreiber, D.I., and Tranquillo, R.T. (2002). A novel implantable collagen gel assay for fibroblast traction and proliferation during wound healing. J Surg Res *105*, 160-172.

Gavara, N., Roca-Cusachs, P., Sunyer, R., Farre, R., and Navajas, D. (2008). Mapping cell-matrix stresses during stretch reveals inelastic reorganization of the cytoskeleton. Biophys J *95*, 464-471.

Giddens, D.P., Zarins, C.K., and Glagov, S. (1993). The role of fluid mechanics in the localization and detection of atherosclerosis. J Biomech Eng *115*, 588-594.

Gilmore, A.P., and Romer, L.H. (1996). Inhibition of focal adhesion kinase (FAK) signaling in focal adhesions decreases cell motility and proliferation. Mol Biol Cell *7*, 1209-1224.

Gimbrone, M.A., Jr. (1999). Vascular endothelium, hemodynamic forces, and atherogenesis. Am J Pathol *155*, 1-5.

Girton, T.S., Barocas, V.H., and Tranquillo, R.T. (2002). Confined compression of a tissue-equivalent: collagen fibril and cell alignment in response to anisotropic strain. J Biomech Eng *124*, 568-575.

Goeckeler, Z.M., Bridgman, P.C., and Wysolmerski, R.B. (2008). Nonmuscle myosin II is responsible for maintaining endothelial cell basal tone and stress fiber integrity. Am J Physiol-Cell Ph *295*, C994-C1006.

Griffith, L.G., and Swartz, M.A. (2006). Capturing complex 3D tissue physiology in vitro. Nat Rev Mol Cell Biol *7*, 211-224.

Grinnell, F. (2003). Fibroblast biology in three-dimensional collagen matrices. Trends Cell Biol *13*, 264-269.

Grote, K., Flach, I., Luchtefeld, M., Akin, E., Holland, S.M., Drexler, H., and Schieffer, B. (2003). Mechanical stretch enhances mRNA expression and proenzyme release of matrix metalloproteinase-2 (MMP-2) via NAD(P)H oxidase-derived reactive oxygen species. Circulation Research *92*, e80-86.

Gruden, G., Zonca, S., Hayward, A., Thomas, S., Maestrini, S., Gnudi, L., and Viberti, G. (2000). Mechanical stretch-induced fibronectin and transforming growth factor-beta 1 production in human mesangial cells is p38 mitogen-activated protein kinase-dependent. Diabetes *49*, 655-661.

Gunn, J.W., Turner, S.D., and Mann, B.K. (2005). Adhesive and mechanical properties of hydrogels influence neurite extension. J Biomed Mater Res A *72*, 91-97.

Haga, J.H., Li, Y.S.J., and Chien, S. (2007). Molecular basis of the effects of mechanical stretch on vascular smooth muscle cells. Journal of Biomechanics *40*, 947-960.

Hahn, C., Wang, C., Orr, A.W., Coon, B.G., and Schwartz, M.A. (2011). JNK2 promotes endothelial cell alignment under flow. PLoS One *6*, e24338.

Haseneen, N.A., Vaday, G.G., Zucker, S., and Foda, H.D. (2003). Mechanical stretch induces MMP-2 release and activation in lung endothelium: role of EMMPRIN. Am J Physiol Lung Cell Mol Physiol *284*, L541-547.

Hayakawa, K., Sato, N., and Obinata, T. (2001). Dynamic reorientation of cultured cells and stress fibers under mechanical stress from periodic stretching. Experimental Cell Research *268*, 104-114.

Hill, A.V. (1938). The heat of shortening and the dynamic constants of muscle. Proceedings of the Royal Society of London Series B-Biological Sciences *126*, 136-195.

Hoefen, R.J., and Berk, B.C. (2002). The role of MAP kinases in endothelial activation. Vascul Pharmacol *38*, 271-273.

Horwitz, A., Duggan, K., Buck, C., Beckerle, M.C., and Burridge, K. (1986). Interaction of plasma membrane fibronectin receptor with talin--a transmembrane linkage. Nature *320*, 531-533.

Hosokawa, H., Aiuchi, S., Kambe, T., Hagiwara, Y., and Kubo, T. (2002). Mechanical stretch-induced mitogen-activated protein kinase activation is mediated via angiotensin and endothelin systems in vascular smooth muscle cells. Biol Pharm Bull *25*, 1588-1592.

Howard, J. (1997). Molecular motors: structural adaptations to cellular functions. Nature *389*, 561-567.

Hsu, H.J., Lee, C.F., and Kaunas, R. (2009). A dynamic stochastic model of frequency-dependent stress fiber alignment induced by cyclic stretch. PLoS One *4*, e4853.

Hsu, H.J., Lee, C.F., Locke, A., Vanderzyl, S.Q., and Kaunas, R. (2010). Stretch-induced stress fiber remodeling and the activations of JNK and ERK depend on mechanical strain rate, but not FAK. PLoS One *5*.

Hu, X.B., Zhang, Y.Y., Cheng, D.Y., Ding, Y., Yang, D.M., Jiang, F., Zhou, C., Ying, B.W., and Wen, F.Q. (2008). Mechanical stress upregulates intercellular adhesion molecule-1 in pulmonary epithelial cells. Respiration *76*, 344-350.

Iba, T., and Sumpio, B.E. (1991). Morphological response of human endothelial cells subjected to cyclic strain in vitro. Microvasc Res *42*, 245-254.

Ingber, D. (1991). Integrins as mechanochemical transducers. Curr Opin Cell Biol *3*, 841-848.

Ishida, T., Haneda, M., Maeda, S., Koya, D., and Kikkawa, R. (1999). Stretch-induced overproduction of fibronectin in mesangial cells is mediated by the activation of mitogen-activated protein kinase. Diabetes *48*, 595-602.

Jungbauer, S., Gao, H., Spatz, J.P., and Kemkemer, R. (2008). Two characteristic regimes in frequency-dependent dynamic reorientation of fibroblasts on cyclically stretched substrates. Biophysical Journal *95*, 3470-3478.

Kanda, K., Matsuda, T., and Oka, T. (1993). Mechanical stress induced cellular orientation and phenotypic modulation of 3-D cultured smooth muscle cells. ASAIO J *39*, M686-690.

Katsumi, A., Naoe, T., Matsushita, T., Kaibuchi, K., and Schwartz, M.A. (2005). Integrin activation and matrix binding mediate cellular responses to mechanical stretch. J Biol Chem *280*, 16546-16549.

Kaunas, R., Hsu, H.J., and Deguchi, S. (2011). Sarcomeric model of stretch-induced stress fiber reorganization. Cell Health and cytoskeleton *3*, 13-22.

Kaunas, R., Nguyen, P., Usami, S., and Chien, S. (2005). Cooperative effects of Rho and mechanical stretch on stress fiber organization. Proc Natl Acad Sci U S A *102*, 15895-15900.

Kaunas, R., Usami, S., and Chien, S. (2006). Regulation of stretch-induced JNK activation by stress fiber orientation. Cell Signal *18*, 1924-1931.

Kilian, K.A., Bugarija, B., Lahn, B.T., and Mrksich, M. (2010). Geometric cues for directing the differentiation of mesenchymal stem cells. Proc Natl Acad Sci U S A *107*, 4872-4877.

Kislinger, T., Tanji, N., Wendt, T., Qu, W., Lu, Y., Ferran, L.J., Jr., Taguchi, A., Olson, K., Bucciarelli, L., Goova, M.*, et al.* (2001). Receptor for advanced glycation end products mediates inflammation and enhanced expression of tissue factor in vasculature of diabetic apolipoprotein E-null mice. Arterioscler Thromb Vasc Biol *21*, 905-910.

Kito, H., Chen, E.L., Wang, X., Ikeda, M., Azuma, N., Nakajima, N., Gahtan, V., and Sumpio, B.E. (2000). Role of mitogen-activated protein kinases in pulmonary endothelial cells exposed to cyclic strain. J Appl Physiol *89*, 2391-2400.

Kovacs, M., Thirumurugan, K., Knight, P.J., and Sellers, J.R. (2007). Load-dependent mechanism of nonmuscle myosin 2. Proc Natl Acad Sci U S A *104*, 9994-9999.

Kumar, S., Maxwell, I.Z., Heisterkamp, A., Polte, T.R., Lele, T.P., Salanga, M., Mazur, E., and Ingber, D.E. (2006). Viscoelastic retraction of single living stress fibers and its impact on cell shape, cytoskeletal organization, and extracellular matrix mechanics. Biophysical Journal *90*, 3762-3773.

Kurpinski, K., Chu, J., Hashi, C., and Li, S. (2006). Anisotropic mechanosensing by mesenchymal stem cells. Proc Natl Acad Sci U S A *103*, 16095-16100.

Langanger, G., Moeremans, M., Daneels, G., Sobieszek, A., De Brabander, M., and De Mey, J. (1986). The molecular organization of myosin in stress fibers of cultured cells. J Cell Biol *102*, 200-209.

Lee, A.A., Delhaas, T., McCulloch, A.D., and Villarreal, F.J. (1999). Differential responses of adult cardiac fibroblasts to in vitro biaxial strain patterns. Journal of Molecular and Cellular Cardiology *31*, 1833-1843.

Lee, C.F., Haase, C., Deguchi, S., and Kaunas, R. (2010). Cyclic stretch-induced stress fiber dynamics - dependence on strain rate, Rho-kinase and MLCK. Biochem Biophys Res Commun *401*, 344-349.

Lee, C.H., Singla, A., and Lee, Y. (2001). Biomedical applications of collagen. Int J Pharm *221*, 1-22.

Li, Y.S., Shyy, J.Y., Li, S., Lee, J., Su, B., Karin, M., and Chien, S. (1996). The Ras-JNK pathway is involved in shear-induced gene expression. Mol Cell Biol *16*, 5947-5954.

Lin, Y.C., Ho, C.H., and Grinnell, F. (1998). Decreased PDGF receptor kinase activity in fibroblasts contracting stressed collagen matrices. Experimental Cell Research *240*, 377-387.

Liu, J.C., Chen, J.J., Chan, P., Cheng, C.F., and Cheng, T.H. (2003). Inhibition of cyclic strain-induced endothelin-1 gene expression by resveratrol. Hypertension *42*, 1198-1205.

Lu, L., Feng, Y., Hucker, W.J., Oswald, S.J., Longmore, G.D., and Yin, F.C. (2008). Actin stress fiber pre-extension in human aortic endothelial cells. Cell Motil Cytoskeleton *65*, 281-294.

MacKenna, D.A., Dolfi, F., Vuori, K., and Ruoslahti, E. (1998). Extracellular signal-regulated kinase and c-Jun NH2-terminal kinase activation by mechanical stretch is integrin-dependent and matrix-specific in rat cardiac fibroblasts. J Clin Invest *101*, 301-310.

Martineau, L.C., and Gardiner, P.F. (2001). Insight into skeletal muscle mechanotransduction: MAPK activation is quantitatively related to tension. J Appl Physiol *91*, 693-702.

Matsui, T.S., Ito, K., Kaunas, R., Sato, M., and Deguchi, S. (2010). Actin stress fibers are at a tipping point between conventional shortening and rapid disassembly at physiological levels of MgATP. Biochem Biophys Res Commun *395*, 301-306.

Mehrotra, R., Jing, N., and Kameoka, J. (2008). Monodispersed polygonal water droplets in microchannel. Appl Phys Lett *92*.

Milkiewicz, M., Mohammadzadeh, F., Ispanovic, E., Gee, E., and Haas, T.L. (2007). Static strain stimulates expression of matrix metalloproteinase-2 and VEGF in

microvascular endothelium via JNK- and ERK-dependent pathways. J Cell Biochem *100*, 750-761.

Mizutani, T., Haga, H., and Kawabata, K. (2004). Cellular stiffness response to external deformation: Tensional homeostasis in a single fibroblast. Cell Motility and the Cytoskeleton *59*, 242-248.

Mudera, V.C., Pleass, R., Eastwood, M., Tarnuzzer, R., Schultz, G., Khaw, P., McGrouther, D.A., and Brown, R.A. (2000). Molecular responses of human dermal fibroblasts to dual cues: contact guidance and mechanical load. Cell Motil Cytoskeleton *45*, 1-9.

Na, S., Meininger, G.A., and Humphrey, J.D. (2007). A theoretical model for F-actin remodeling in vascular smooth muscle cells subjected to cyclic stretch. J Theor Biol *246*, 87-99.

Nadruz, W., Jr., Corat, M.A., Marin, T.M., Guimaraes Pereira, G.A., and Franchini, K.G. (2005). Focal adhesion kinase mediates MEF2 and c-Jun activation by stretch: role in the activation of the cardiac hypertrophic genetic program. Cardiovasc Res *68*, 87-97.

Nakashima, Y., Raines, E.W., Plump, A.S., Breslow, J.L., and Ross, R. (1998). Upregulation of VCAM-1 and ICAM-1 at atherosclerosis-prone sites on the endothelium in the ApoE-deficient mouse. Arteriosclerosis Thrombosis and Vascular Biology *18*, 842-851.

Naruse, K., Yamada, T., Sai, X.R., Hamaguchi, M., and Sokabe, M. (1998). Pp125FAK is required for stretch dependent morphological response of endothelial cells. Oncogene *17*, 455-463.

Nekouzadeh, A., Pryse, K.M., Elson, E.L., and Genin, G.M. (2008). Stretch-activated force shedding, force recovery, and cytoskeletal remodeling in contractile fibroblasts. J Biomech *41*, 2964-2971.

Nemir, S., Hayenga, H.N., and West, J.L. (2010). PEGDA hydrogels with patterned elasticity: Novel tools for the study of cell response to substrate rigidity. Biotechnol Bioeng *105*, 636-644.

Nerem, R.M. (1993). Hemodynamics and the vascular endothelium. J Biomech Eng *115*, 510-514.

Nerem, R.M., Levesque, M.J., and Cornhill, J.F. (1981). Vascular endothelial morphology as an indicator of the pattern of blood flow. J Biomech Eng *103*, 172-176.

Nguyen, K.T., and West, J.L. (2002). Photopolymerizable hydrogels for tissue engineering applications. Biomaterials *23*, 4307-4314.

Nguyen, T.D., Liang, R., Woo, S.L.Y., Burton, S.D., Wu, C.F., Almarza, A., Sacks, M.S., and Abramowitch, S. (2009). Effects of cell seeding and cyclic stretch on the fiber remodeling in an extracellular matrix-derived bioscaffold. Tissue Eng Pt A *15*, 957-963.

Orr, A.W., Sanders, J.M., Bevard, M., Coleman, E., Sarembock, I.J., and Schwartz, M.A. (2005). The subendothelial extracellular matrix modulates NF-kappaB activation by flow: a potential role in atherosclerosis. J Cell Biol *169*, 191-202.

Owen, J.D., Ruest, P.J., Fry, D.W., and Hanks, S.K. (1999). Induced focal adhesion kinase (FAK) expression in FAK-null cells enhances cell spreading and migration requiring both auto- and activation loop phosphorylation sites and inhibits adhesion-dependent tyrosine phosphorylation of Pyk2. Mol Cell Biol *19*, 4806-4818.

Padmavathi, N.C., and Chatterji, P.R. (1996). Structural characteristics and swelling behavior of poly(ethylene glycol) diacrylate hydrogels. Macromolecules *29*, 1976-1979.

Pang, Y., Wang, X., Lee, D., and Greisler, H.P. (2011). Dynamic quantitative visualization of single cell alignment and migration and matrix remodeling in 3-D collagen hydrogels under mechanical force. Biomaterials *32*, 3776-3783.

Paniagua, O.A., Bryant, M.B., and Panza, J.A. (2001). Role of endothelial nitric oxide in shear stress-induced vasodilation of human microvasculature: diminished activity in hypertensive and hypercholesterolemic patients. Circulation *103*, 1752-1758.

Park, J.S., Chu, J.S.F., Cheng, C., Chen, F.Q., Chen, D., and Li, S. (2004). Differential effects of equiaxial and uniaxial strain on mesenchymal stem cells. Biotechnology and Bioengineering *88*, 359-368.

Peterson, L.J., Rajfur, Z., Maddox, A.S., Freel, C.D., Chen, Y., Edlund, M., Otey, C., and Burridge, K. (2004). Simultaneous stretching and contraction of stress fibers in vivo. Mol Biol Cell *15*, 3497-3508.

Petzold, T., Orr, A.W., Hahn, C., Jhaveri, K.A., Parsons, J.T., and Schwartz, M.A. (2009). Focal adhesion kinase modulates activation of NF-kappaB by flow in endothelial cells. Am J Physiol Cell Physiol *297*, C814-822.

Polte, T.R., Eichler, G.S., Wang, N., and Ingber, D.E. (2004). Extracellular matrix controls myosin light chain phosphorylation and cell contractility through modulation of cell shape and cytoskeletal prestress. Am J Physiol Cell Physiol *286*, C518-528.

Pradhan, S., and Sumpio, B. (2004). Molecular and biological effects of hemodynamics on vascular cells. Front Biosci *9*, 3276-3285.

Qu, M.J., Liu, B., Wang, H.Q., Yan, Z.Q., Shen, B.R., and Jiang, Z.L. (2007). Frequency-dependent phenotype modulation of vascular smooth muscle cells under cyclic mechanical strain. J Vasc Res *44*, 345-353.

Ruiz, S.A., and Chen, C.S. (2008). Emergence of patterned stem cell differentiation within multicellular structures. Stem Cells *26*, 2921-2927.

Russell, R.J., Xia, S.L., Dickinson, R.B., and Lele, T.P. (2009). Sarcomere mechanics in capillary endothelial cells. Biophysical Journal *97*, 1578-1585.

Sai, X., Naruse, K., and Sokabe, M. (1999). Activation of pp60(src) is critical for stretch-induced orienting response in fibroblasts. J Cell Sci *112 (Pt 9)*, 1365-1373.

Sanger, J.W., Sanger, J.M., and Jockusch, B.M. (1983). Differences in the stress fibers between fibroblasts and epithelial-cells. J Cell Biol *96*, 961-969.

Sattar, N., Petrie, J.R., and Jaap, A.J. (1998). The atherogenic lipoprotein phenotype and vascular endothelial dysfunction. Atherosclerosis *138*, 229-235.

Shyy, J.Y., and Chien, S. (1997). Role of integrins in cellular responses to mechanical stress and adhesion. Curr Opin Cell Biol *9*, 707-713.

Stachowiak, M.R., and O'Shaughnessy, B. (2009). Recoil after severing reveals stress fiber contraction mechanisms. Biophysical Journal *97*, 462-471.

Stevenson, M.D., Sieminski, A.L., McLeod, C.M., Byfield, F.J., Barocas, V.H., and Gooch, K.J. (2010). Pericellular conditions regulate extent of cell-mediated compaction of collagen gels. Biophys J *99*, 19-28.

Sung, H.J., Yee, A., Eskin, S.G., and McIntire, L.V. (2007). Cyclic strain and motion control produce opposite oxidative responses in two human endothelial cell types. Am J Physiol-Cell Ph *293*, C87-C94.

Thakar, R.G., Ho, F., Huang, N.F., Liepmann, D., and Li, S. (2003). Regulation of vascular smooth muscle cells by micropatterning. Biochem Biophys Res Commun *307*, 883-890.

Thie, M., Schlumberger, W., Semich, R., Rauterberg, J., and Robenek, H. (1991). Aortic smooth muscle cells in collagen lattice culture: effects on ultrastructure, proliferation and collagen synthesis. Eur J Cell Biol *55*, 295-304.

Thubrikar, M.J., and Robicsek, F. (1995). Pressure-induced arterial wall stress and atherosclerosis. Ann Thorac Surg *59*, 1594-1603.

Tilghman, R.W., and Parsons, J.T. (2008). Focal adhesion kinase as a regulator of cell tension in the progression of cancer. Semin Cancer Biol *18*, 45-52.

Tondon, A., Hsu, H.J., and Kaunas, R. (2012). Dependence of cyclic stretch-induced stress fiber reorientation on stretch waveform. J Biomech *45*, 728-735.

Trepat, X., Deng, L., An, S.S., Navajas, D., Tschumperlin, D.J., Gerthoffer, W.T., Butler, J.P., and Fredberg, J.J. (2007). Universal physical responses to stretch in the living cell. Nature *447*, 592-595.

Tzima, E., del Pozo, M.A., Shattil, S.J., Chien, S., and Schwartz, M.A. (2001). Activation of integrins in endothelial cells by fluid shear stress mediates Rho-dependent cytoskeletal alignment. Embo Journal *20*, 4639-4647.

Vicente-Manzanares, M., Ma, X.F., Adelstein, R.S., and Horwitz, A.R. (2009). Non-muscle myosin II takes centre stage in cell adhesion and migration. Nature Reviews Molecular Cell Biology *10*, 778-790.

Wakatsuki, T., Kolodney, M.S., Zahalak, G.I., and Elson, E.L. (2000). Cell mechanics studied by a reconstituted model tissue. Biophysical Journal *79*, 2353-2368.

Wang, H.B., Dembo, M., Hanks, S.K., and Wang, Y. (2001a). Focal adhesion kinase is involved in mechanosensing during fibroblast migration. Proc Natl Acad Sci U S A *98*, 11295-11300.

Wang, J.G., Miyazu, M., Matsushita, E., Sokabe, M., and Naruse, K. (2001b). Uniaxial cyclic stretch induces focal adhesion kinase (FAK) tyrosine phosphorylation followed by mitogen-activated protein kinase (MAPK) activation. Biochem Biophys Res Commun *288*, 356-361.

Wang, J.H., Goldschmidt-Clermont, P., Wille, J., and Yin, F.C. (2001c). Specificity of endothelial cell reorientation in response to cyclic mechanical stretching. J Biomech *34*, 1563-1572.

Wang, J.H., Jia, F., Gilbert, T.W., and Woo, S.L. (2003). Cell orientation determines the alignment of cell-produced collagenous matrix. J Biomech *36*, 97-102.

Wang, J.H.C., and Thampatty, B.P. (2006). An introductory review of cell mechanobiology. Biomechanics and Modeling in Mechanobiology *5*, 1-16.

Wang, N., Tolic-Norrelykke, I.M., Chen, J.X., Mijailovich, S.M., Butler, J.P., Fredberg, J.J., and Stamenovic, D. (2002). Cell prestress. I. Stiffness and prestress are closely associated in adherent contractile cells. Am J Physiol-Cell Ph *282*, C606-C616.

Wei, Z.S., Deshpande, V.S., McMeeking, R.M., and Evans, A.G. (2008). Analysis and interpretation of stress fiber organization in cells subject to cyclic stretch. Journal of Biomechanical Engineering-Transactions of the Asme *130*, -.

Weinberg, C.B., and Bell, E. (1986). A blood-vessel model constructed from collagen and cultured vascular cells. Science *231*, 397-400.

Wernig, F., Mayr, M., and Xu, Q.B. (2002). Mechanical stretch-induced apoptosis of vascular smooth muscle cells is p53-dependent and mediated by beta 1-integrin signal pathways. Circulation *106*, 241-241.

Wernig, F., Mayr, M., and Xu, Q.B. (2003). Mechanical stretch-induced apoptosis in smooth muscle cells is mediated by beta(1)-integrin signaling pathways. Hypertension *41*, 903-911.

Wilson, C.A., Tsuchida, M.A., Allen, G.M., Barnhart, E.L., Applegate, K.T., Yam, P.T., Ji, L., Keren, K., Danuser, G., and Theriot, J.A. (2010). Myosin II contributes to cell-scale actin network treadmilling through network disassembly. Nature *465*, 373-377.

Wilson, E., Sudhir, K., and Ives, H.E. (1995). Mechanical strain of rat vascular smooth-muscle cells is sensed by specific extracellular matrix/integrin interactions. Journal of Clinical Investigation *96*, 2364-2372.

Wung, B.S., Cheng, J.J., Chao, Y.J., Lin, J., Shyy, Y.J., and Wang, D.L. (1996). Cyclical strain increases monocyte chemotactic protein-1 secretion in human endothelial cells. Am J Physiol *270*, H1462-1468.

Xu, S., Nie, Z., Seo, M., Lewis, P., Kumacheva, E., Stone, H.A., Garstecki, P., Weibel, D.B., Gitlin, I., and Whitesides, G.M. (2005). Generation of monodisperse particles by using microfluidics: Control over size, shape, and composition (vol 44, pg 724, 2005). Angew Chem Int Edit *44*, 3799-3799.

Yano, Y., Geibel, J., and Sumpio, B.E. (1997). Cyclic strain induces reorganization of integrin alpha 5 beta 1 and alpha 2 beta 1 in human umbilical vein endothelial cells. J Cell Biochem *64*, 505-513.

Yeh, A.T., Kao, B.S., Jung, W.G., Chen, Z.P., Nelson, J.S., and Tromberg, B.J. (2004). Imaging wound healing using optical coherence tomography and multiphoton microscopy in an in vitro skin-equivalent tissue model. J Biomed Opt *9*, 248-253.

Yoshigi, M., Clark, E.B., and Yost, H.J. (2003). Quantification of stretch-induced cytoskeletal remodeling in vascular endothelial cells by image processing. Cytometry A *55*, 109-118.

Zhang, J., Li, W., Sanders, M.A., Sumpio, B.E., Panja, A., and Basson, M.D. (2003a). Regulation of the intestinal epithelial response to cyclic strain by extracellular matrix proteins. FASEB J *17*, 926-928.

Zhang, J., Li, W., Sumpio, B.E., and Basson, M.D. (2003b). Fibronectin blocks p38 and jnk activation by cyclic strain in Caco-2 cells. Biochem Biophys Res Commun *306*, 746-749.

APPENDIX A FIGURES

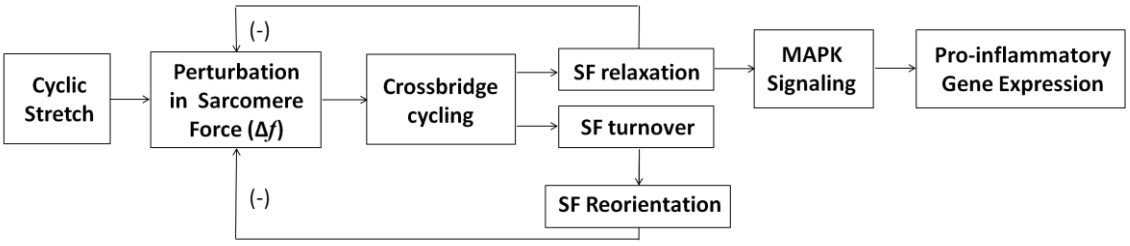

Figure 1. Diagram illustrating that cyclic stretching of SFs altered SF tension to result in pro-inflammatory gene expression mediated by the MAPK signaling proteins (JNK, ERK and p38). Compensatory SF relaxation and reorganization acted as a negative feedback on tension perturbations and downstream mechanotransduction.

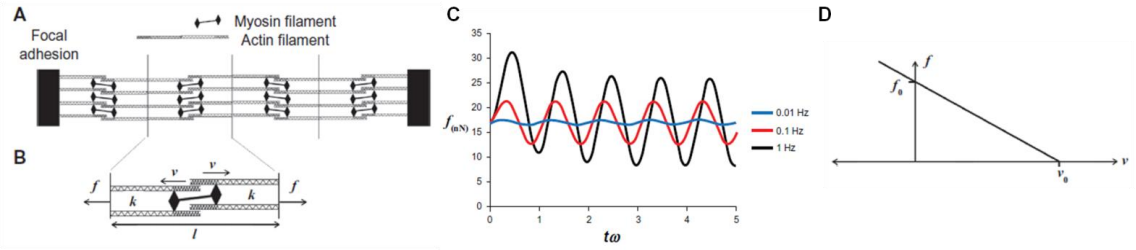

Figure 2. Mathematical model of a SF. (**A**) A stress fiber is composed of multiple sarcomeres in series. (**B**) Each sarcomere can be modeled as a myosin contractile unit with a variable-length spring at each end. (**C**) The model predicted that, in response to 10% cyclic stretch, a stress fiber acted nearly elastically at high frequency (1Hz, black curve), and became progressively more viscous at lower frequencies (0.1 Hz, red curve and 0.01 Hz,blue curve). (**D**) The velocity of shortening of the spring (v) depended on the force acting on myosin II.

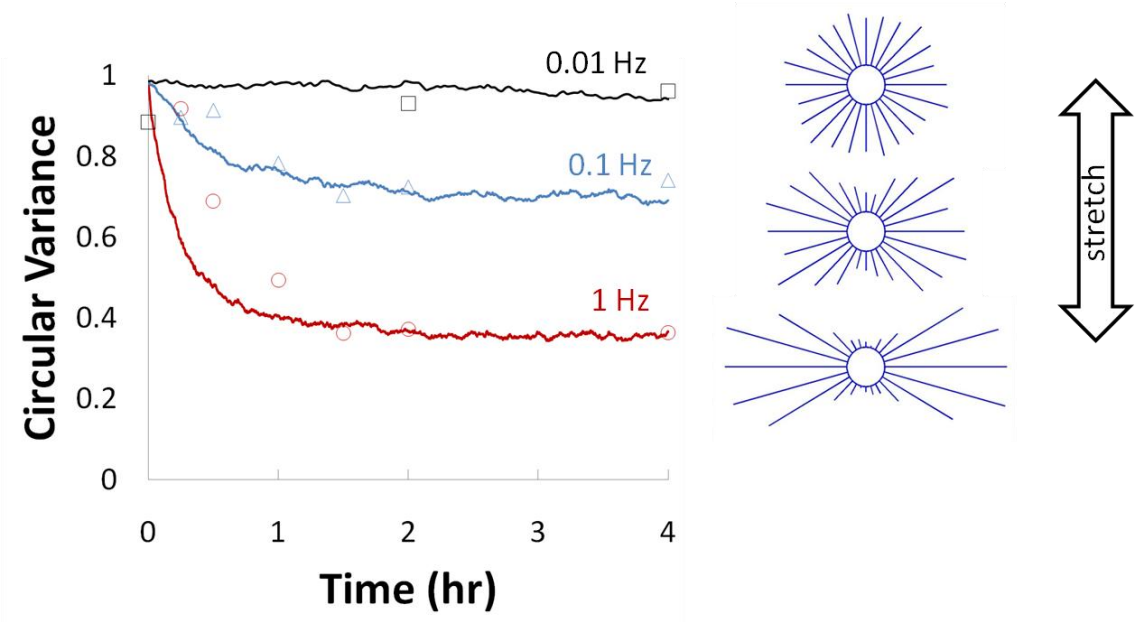

Figure 3. The time courses of stress fiber alignment in response to 10% cyclic uniaxial stretch at frequencies of 1 (red circles), 0.1 (blue triangles), and 0.01 Hz (black squares). Results from simulations using the optimized parameter values (= $5x10^{-7}$ s^{-1}, = $5x10^{-4}$, γ = 0.05 μm/s, and f_B = 3.0 pN) were illustrated for these conditions. The distributions of SF orientations were shown after 4 h of stretching.

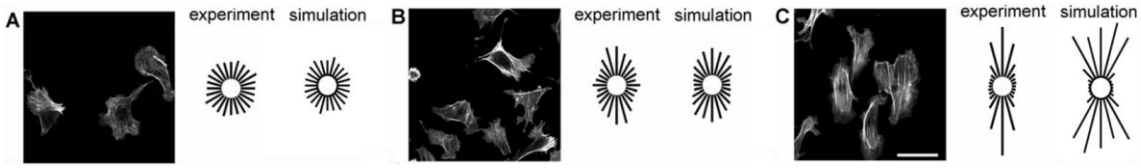

Figure 4. The extent of stress fiber alignment depended on the frequency of cyclic uniaxial stretch. Representative images were shown of sparsely seeded bovine aortic ECs that were subjected to 4 hr of 10% cyclic uniaxial stretch at frequencies of 1 (**A**), 0.1 (**B**), and 0.01 Hz (**C**). The distributions of stress fiber orientations were determined using an intensity gradient algorithm and the results from multiple cells (n = 50 cells) were summarized as angular histograms (direction of stretch is horizontal with respect to the page). Simulations of SF reorganization in response to 4 hr of 10% cyclic uniaxial stretch at frequencies of 1, 0.1 and 0.01 Hz were performed using the optimized parameter values and the angular histograms are shown for comparison to the experimental results. Bar, 50 mm.

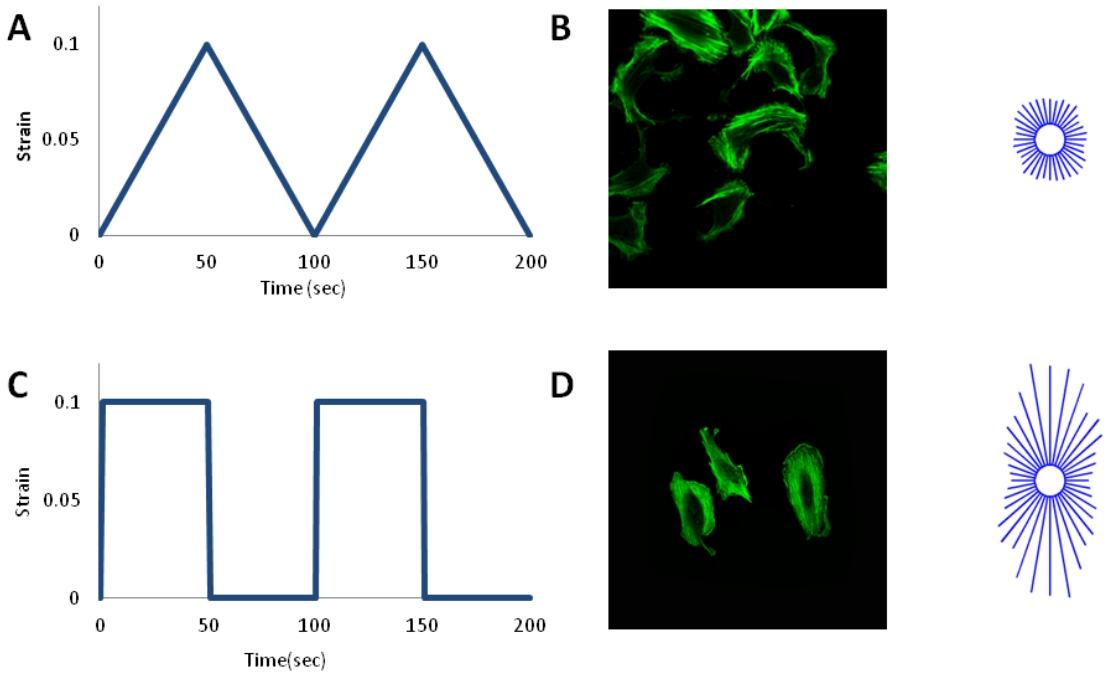

Figure 5. SF alignment in response to square-wave pattern, but not triangle-wave pattern. Illustrations of two cycles of symmetric wave strain pattern for 10% cyclic stretch at 0.01Hz with triangle-wave (**A**) and square-wave patterns (**C**). Representative images of sparsely seeded U2OS cells subjected to 12 hr of 10% uniaxial stretch with triangle-wave pattern (**B**) and square-wave pattern (**D**) at a frequency of 0.01Hz. The distributions of stress fiber orientations were determined using an intensity gradient algorithm and the results are summarized as angular histograms (direction of stretch is horizontal with respect to the page).

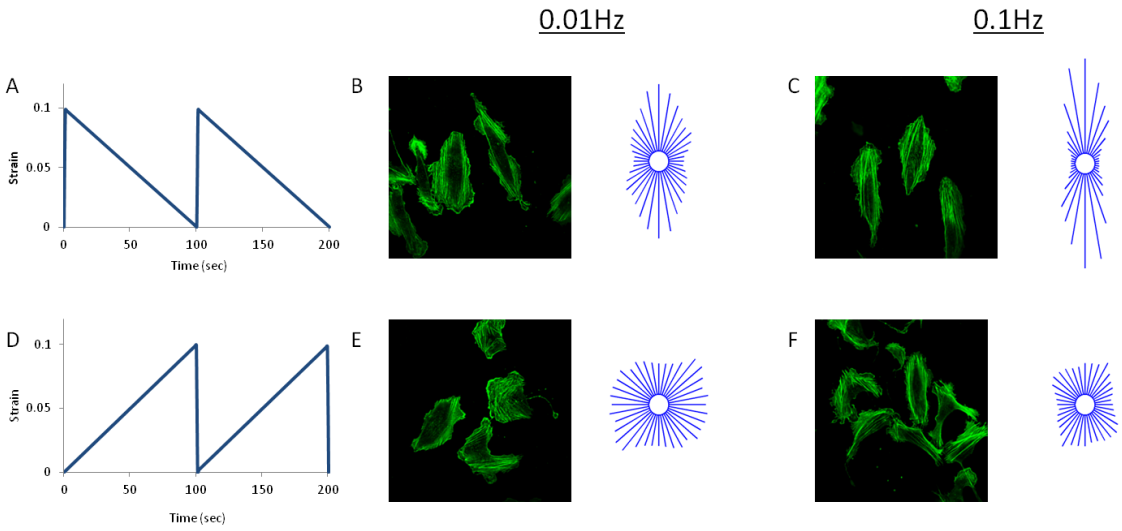

Figure 6. SF alignment in response to fast lengthening, but not fast shortening. Illustration of two cycles of asymmetric wave strain pattern for 10% cyclic stretch at 0.01Hz with fast stretching rate (**A**) and fast relaxation rate (**D**). Representative images of sparsely seeded U2OS cells subjected to 12 hr of 10% uniaxial stretch with fast stretching rate at a frequency of 0.01 (**B**) and 0.1 HZ (**C**), and with fast shortening rate at a frequency of 0.01 (**E**) and 0.1 HZ (**F**) The distributions of stress fiber orientations were determined using an intensity gradient algorithm and the results from multiple cells (n = 100 cells) were summarized as angular histograms (direction of stretch is horizontal with respect to the page).

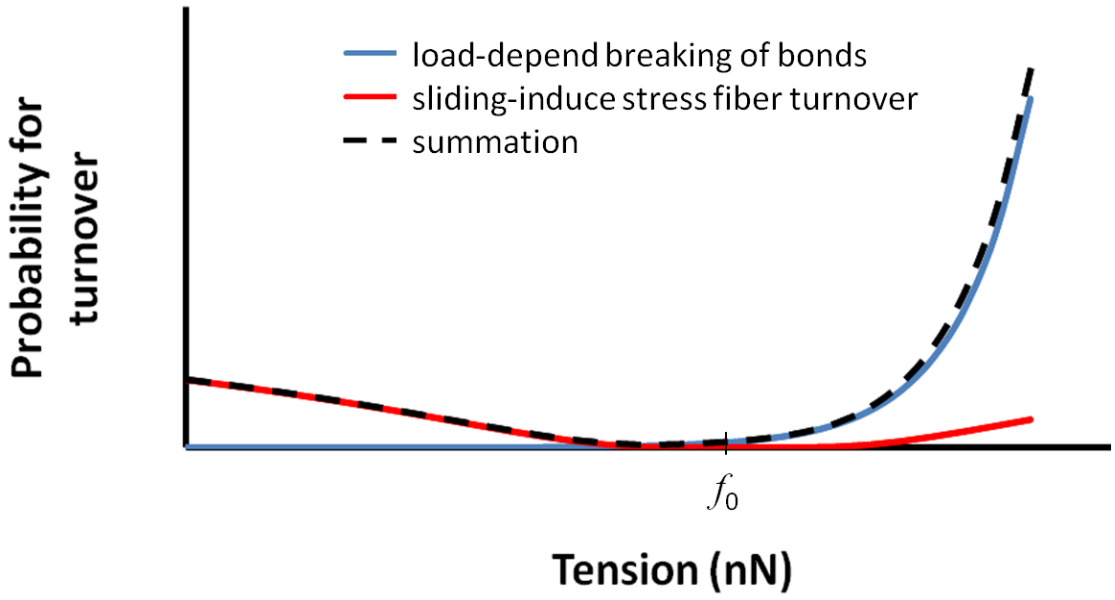

Figure 7. Predicted probability for stress fiber turnover resulted from fiber tension (solid blue), myosin sliding (solid red), and both (dash black).

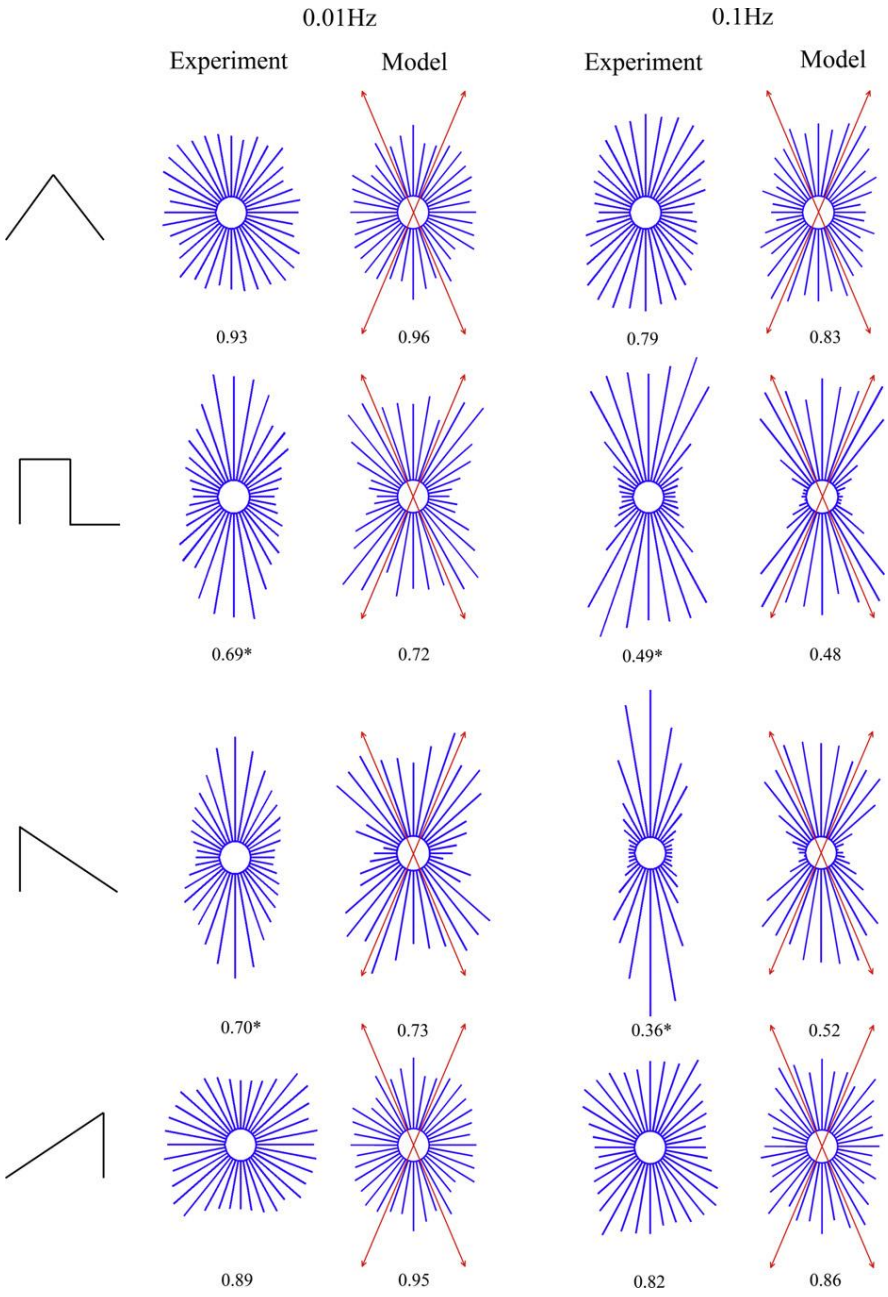

Figure 8. Comparisons of measured and simulated SF alignment distributions. Circular histograms depicting the experimentally measured and theoretically predicted SF distribution in cells subjected to 12 h of stretching using the various strain patterns. Red arrows indicated the preferred orientations ($\pm 67°$ relative to the direction of stretch) of SFs as predicted by the model.

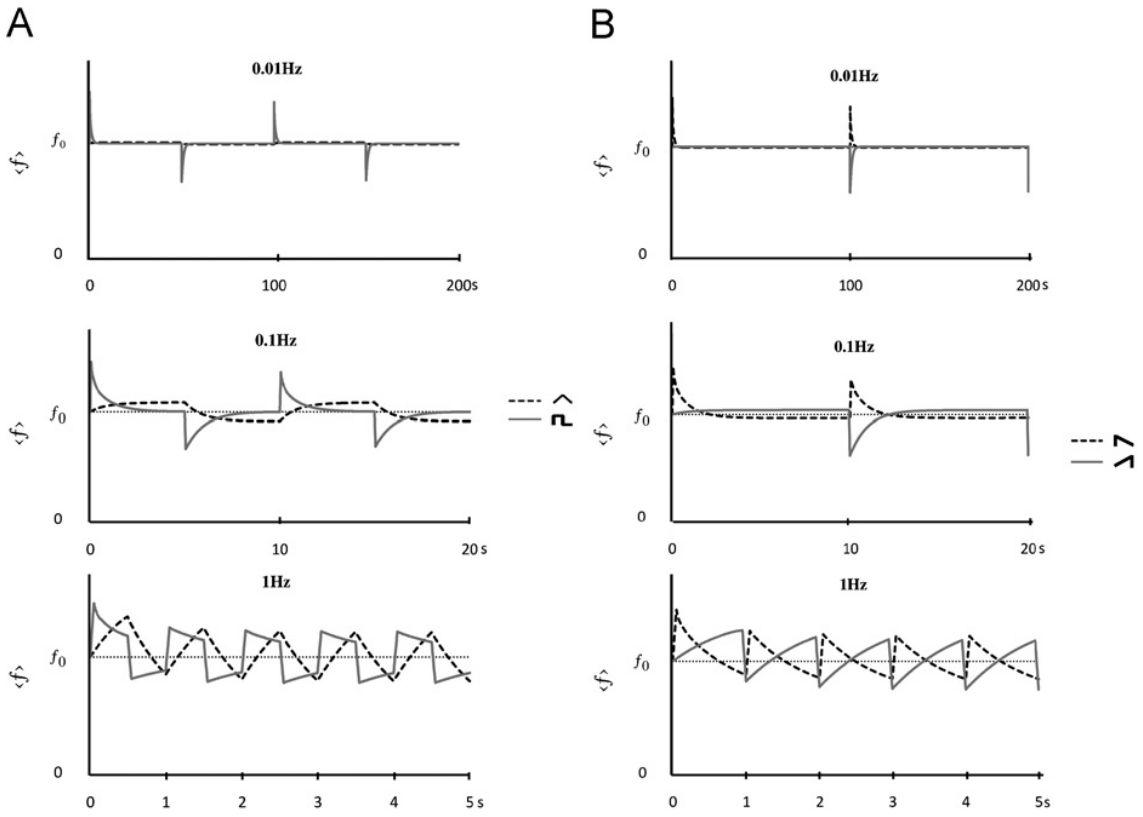

Figure 9. SF tension depended on waveform pattern and frequency. The model was used to predict population-average SF tension <*f*> for the first several cycles of stretch using the optimized model parameter values for triangle-and square-stretch (**A**) and for fast-lengthening-stretch and fast-shortening-stretch (**B**) at 0.01, 0.1, and 1Hz.

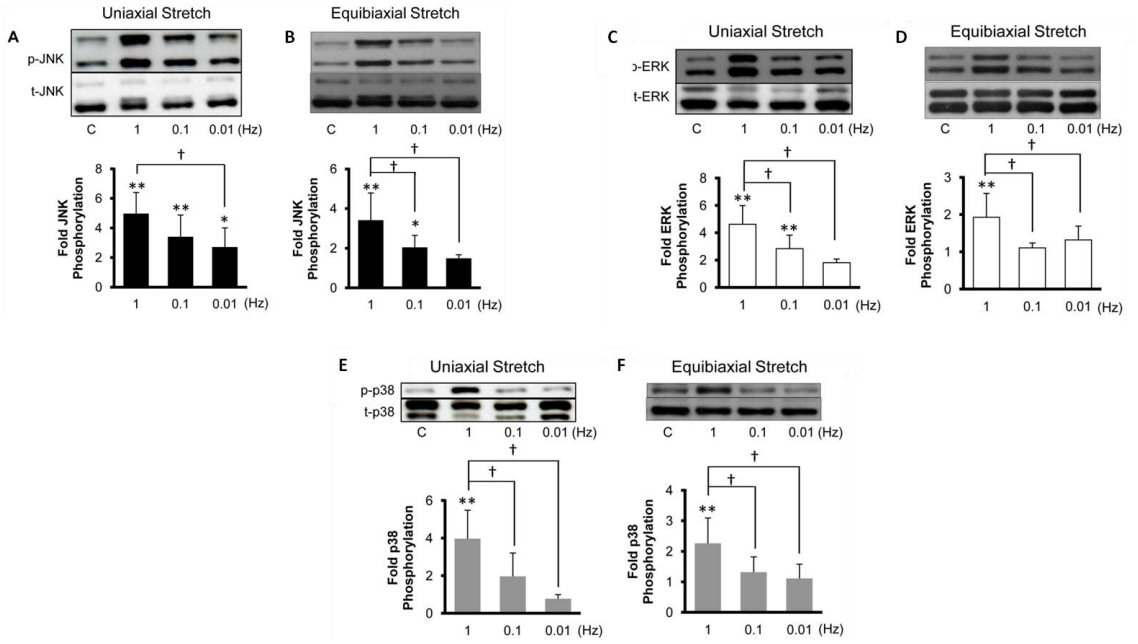

Figure 10. Representative Western blots of phospho-specific and total JNK (**A**, **B**), ERK (**C**, **D**) and p38 (**E**, **F**) were obtained from confluent BAECs kept as static controls or subjected to 10% cyclic uniaxial (**A**, **C**, **E**) or equibiaxial (**B**, **D**, **F**) stretch for 30 min at the indicated frequencies. The values (means±S.D.; n=6 for uniaxial and n=7 for equibiaxial) indicated the fold change in phosphorylation relative to the static control for each individual experiment. * and ** indicated significant difference from static controls (*P<0.05, **P<0.01). † indicates significant difference between groups stretched at different frequencies (P<0.05).

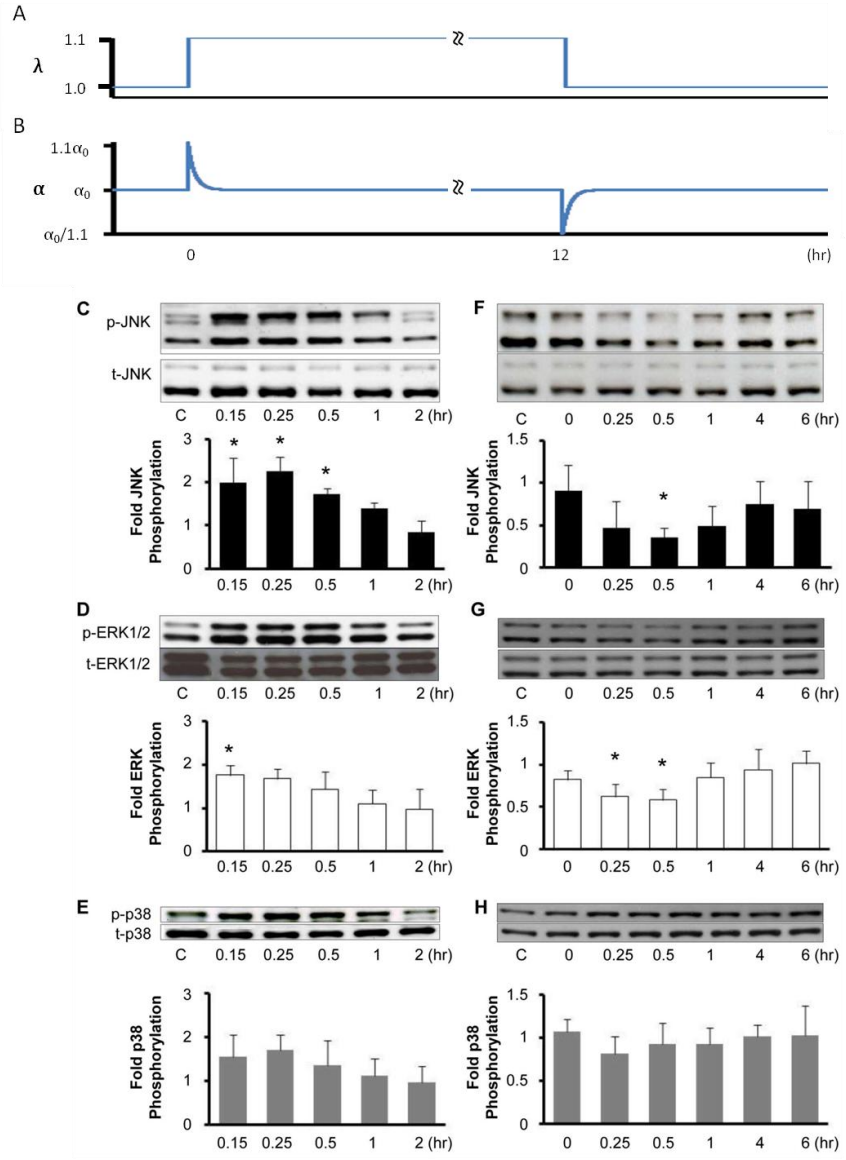

Figure 11. Transient changes in strain rate induced transient changes in the levels of JNK, ERK and p38 phosphorylation. Confluent BAECs were subjected to a stretch release maneuver consisting of 10% equibiaxial stretch λ, followed by the release of the stretch 12 hr later (**A**), which was predicted to generate a transient increase and subsequent transient decrease in fiber stretch α (**B**). Representative Western blots of phospho-specific and total JNK (**C, F**), ERK (**D, G**) and p38 (**E, H**) from cell lysates collected at the indicated times after the initial stretch (**C-E**) and subsequent stretch release (**F-H**). The values (means±S.D.; n = 4) indicated the fold change in phosphorylation relative to static controls for each individual experiment. * indicated significant difference from static control ($P<0.05$).

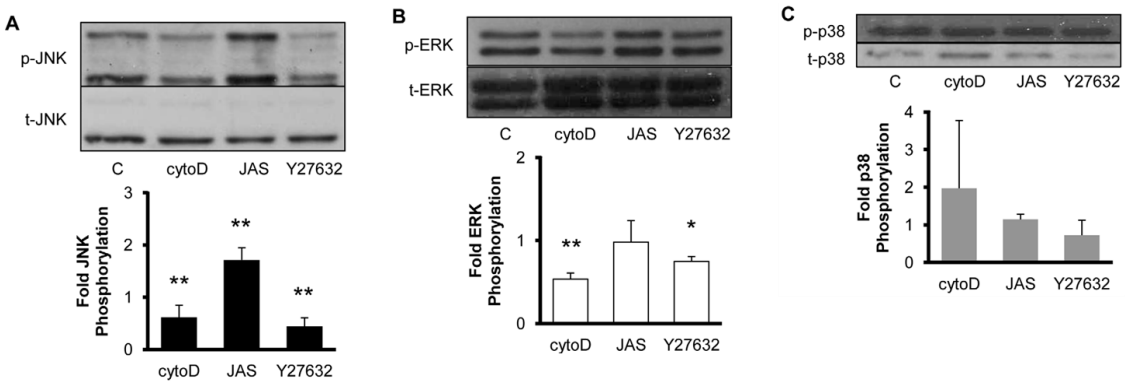

Figure 12. JNK and ERK phosphorylation was decreased by inhibitors of Rho kinase and actin polymerization. Representative Western blots were shown of phospho-specific and total JNK (**A**), ERK (**B**) and p38 (**C**) from cell lysates collected from confluent BAECs treated for 30 min with vehicle (0.1% DMSO; lane 1), 50 nM cytochalasin D, 10 nM jasplakinolide or 10 mM Y27632. Optical density measurements were quantified to determine relative amounts of phosphorylated MAPK normalized by the respective total MAPK. The values (means±S.D.; n = 4) indicated the fold change in phosphorylation relative to the DMSO-treated controls for each individual experiment. * and ** indicated significant difference from the control (*P<0.05, **P<0.01).

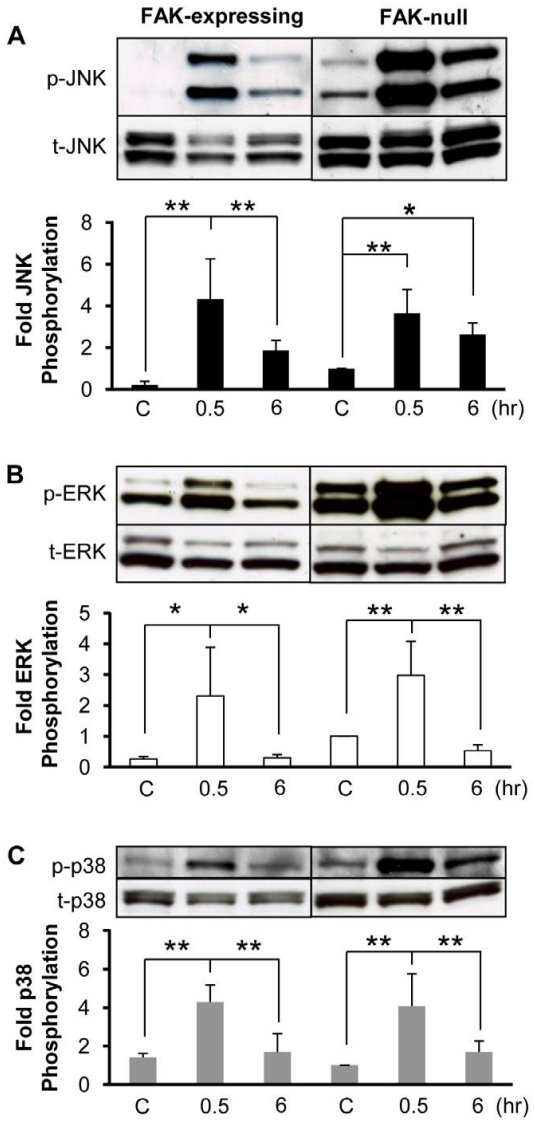

Figure 13. FAK is not necessary for stretch-induced increases in JNK, ERK and p38 phosphorylation. Representative immunoblots were shown from experiments in which confluent FAK-expressing and FAK-null MEFs are kept as static controls or subjected to 10% cyclic uniaxial stretch at 1 Hz for 0.5 and 6 hr. Immunoblot pairings for JNK (**A**), ERK (**B**) and p38 (**C**) for the FAK-expressing and FAK-null MEFs were taken from two locations on the same blot. Optical density measurements were quantified to determine relative amounts of phosphorylated MAPK normalized by the respective total MAPK. The values (means±S.D.; n = 4) indicated the fold change in phosphorylation relative to the FAK-null static control for each individual experiment. * and ** indicated significant difference between groups (*P<0.05, **P<0.01).

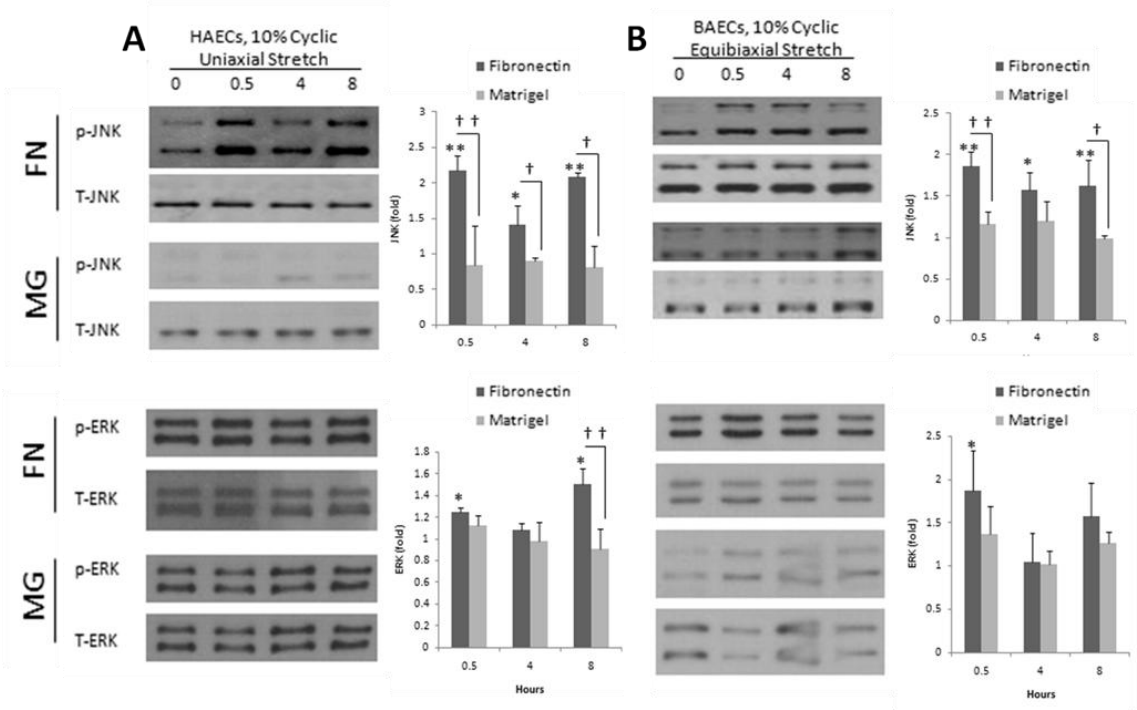

Figure 14. Fibronectin showed a significantly higher activation of JNK and ERK than matrigel for (**A**) HAECs and (**B**) BAECs. Values were means ± S.D. *P<0.05, **P<0.01 compared to static control. †P<0.05, ††P<0.01 matrigel compared to fibronectin at the specific time point. Representative blots for phosphor-JNK, phosphor-ERK, total-JNK and total ERK for fibronectin and matrigel were shown to the left.

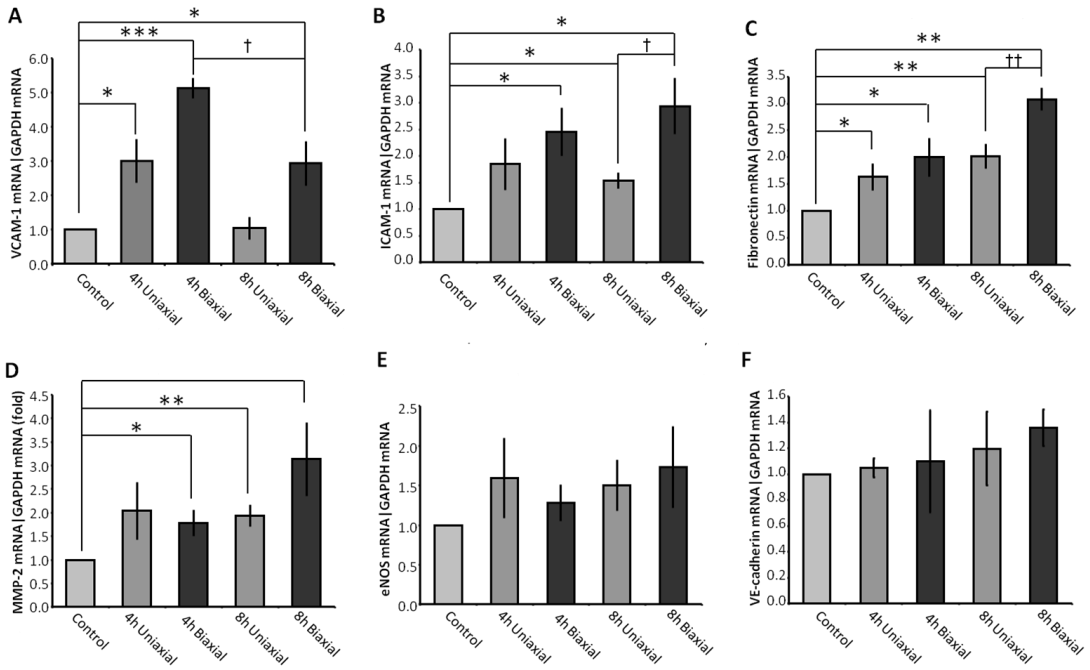

Figure 15. The effects of the direction of cyclic stretch on mRNA levels of VCAM-1(**A**), ICAM-1(**B**), fibronectin(**C**), MMP-2(**D**), eNOS(**E**), and VE-cadherin(**F**) in HAECs. *, **, and *** indicated significant difference from static controls (*P<0.05, **P<0.01, ***P<0.001). † and †† indicated significant difference between groups stretched at different frequencies (†P<0.05, ††P<0.01).

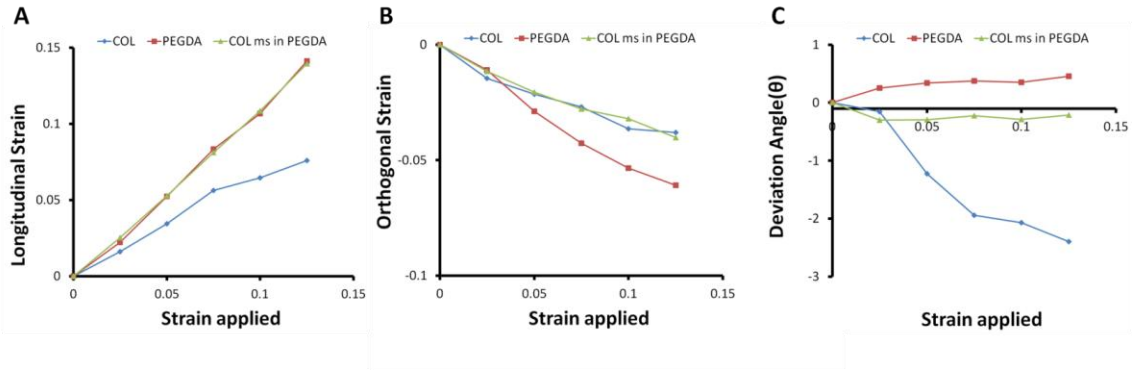

Figure 16. Strain field transmission. Fluorescent beads (0.2 μm Fluospheres, Molecular Probes) were mixed into the hydrogels and collagen-U2OS solution prior to assembly to serve as fiducial markers with different colors used in each phase. 2-D lateral (**A**) and orthogonal (**B**) strains and deviation angle (**C**) in the focus plane were quantified using 3-points analysis for pure collagen gel (blue), PEGDA hydrogel (red), and cellular domains surrounded by PEGDA (green).

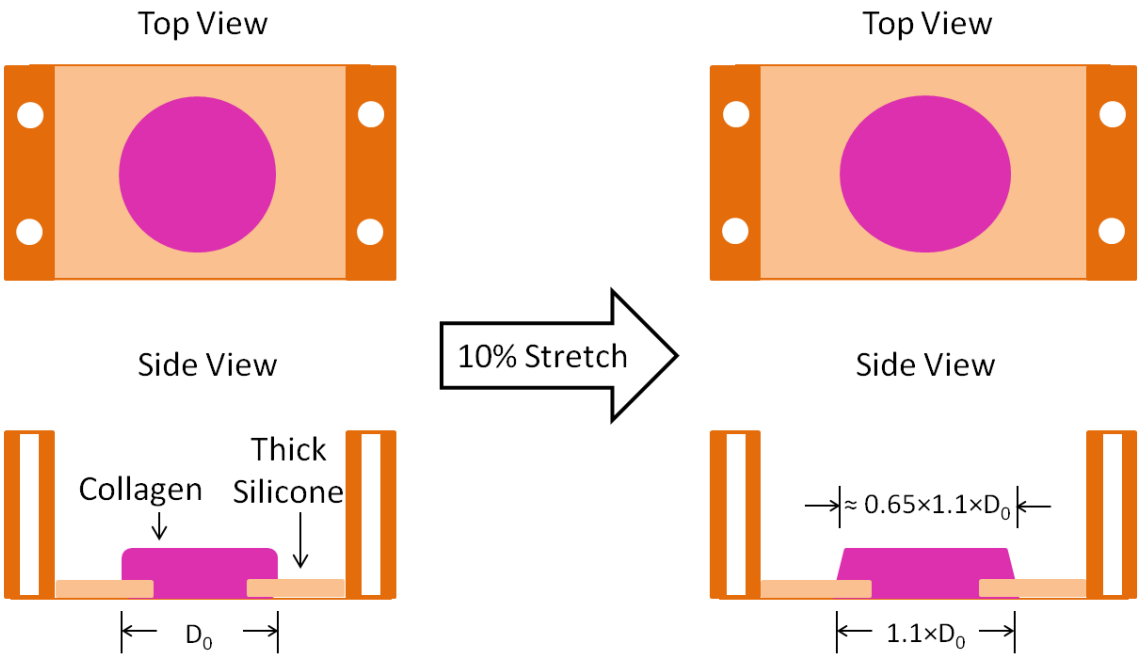

Figure 17. A diagram of pure collagen matrix (pink) which was confined into a circular footprint using a silicone rubber mold (yellow). After 10% stretch, shear strain (depicted by the angle θ in the xz-plane) was expected develop which decreases the strain in the x-direction near the top of the matrix.

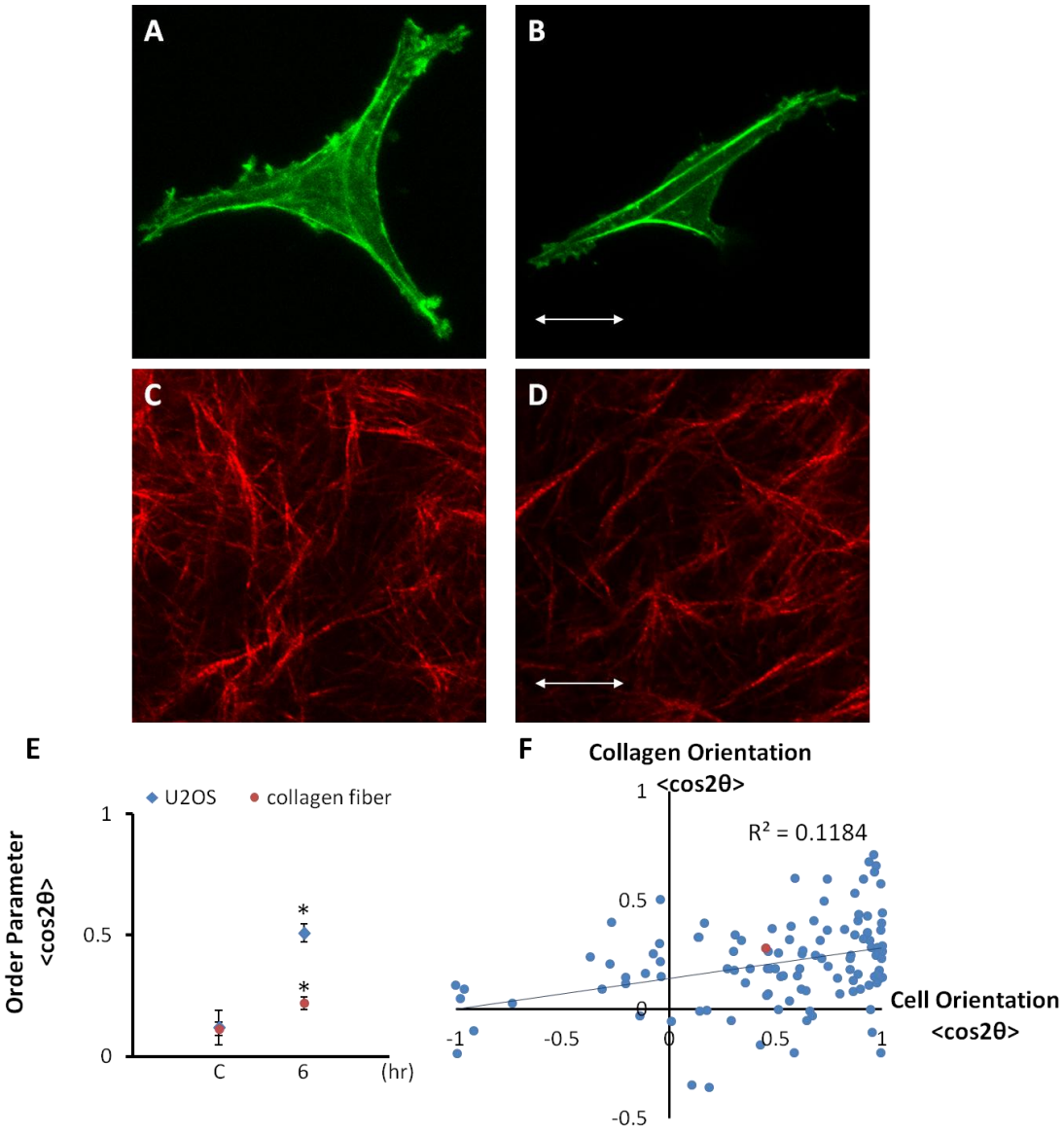

Figure 18. Cyclic stretch induced U2OS cells and collagen fibrils to align in the direction of stretch in pure collagen hydrogels. Representative images of U2OS cells (**A**, **B**) and collagen fibrils (**C**, **D**) subjected to 6 hours of 10% cyclic uniaxial stretch at a frequency 1 Hz in the direction indicated in (**B**) and (**D**) compared to static controls (**A**, **C**). (**E**) Order parameters were computed for each image to quantify the extent of cell (blue diamond) and collagen fibril (red circle) alignment and the results were summarized (mean ± S.D.; n = 25). * indicates significant difference from static control ($P<0.01$). (**F**) The orientations of cell and their surrounding collagen fibril in response to stretch were correlated for each image ($R^2=0.1184$). Red circle was the data for the representative image (**B**) and (**D**).

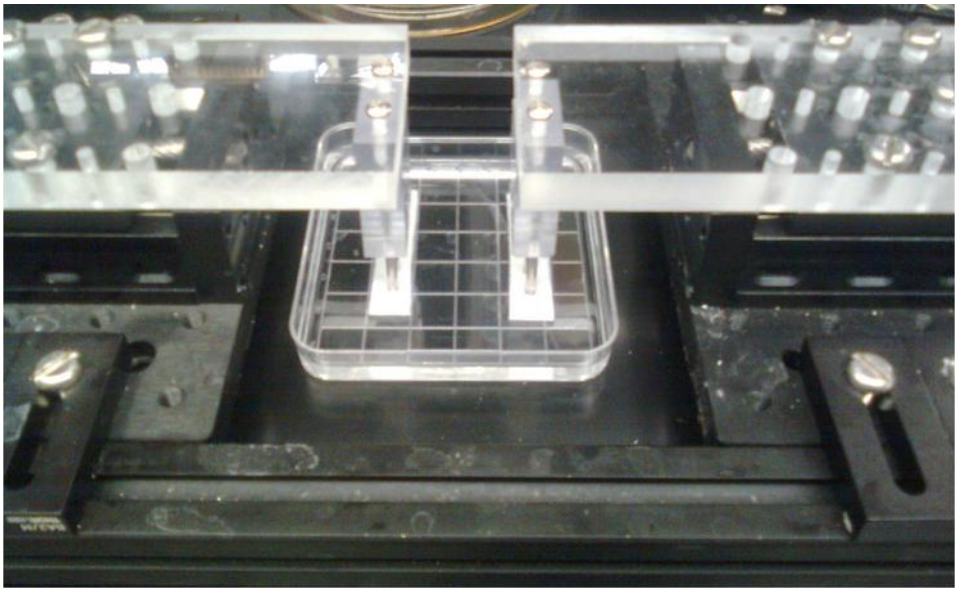

Figure 19. Experimental setting of the stretching device mounted under confocal microscope. Porous polyethelene strips (white) were used to provide a means to mechanically couple the PEGDA hydrogel (nearly invisible) to the motors of the uniaxial stretching platform.

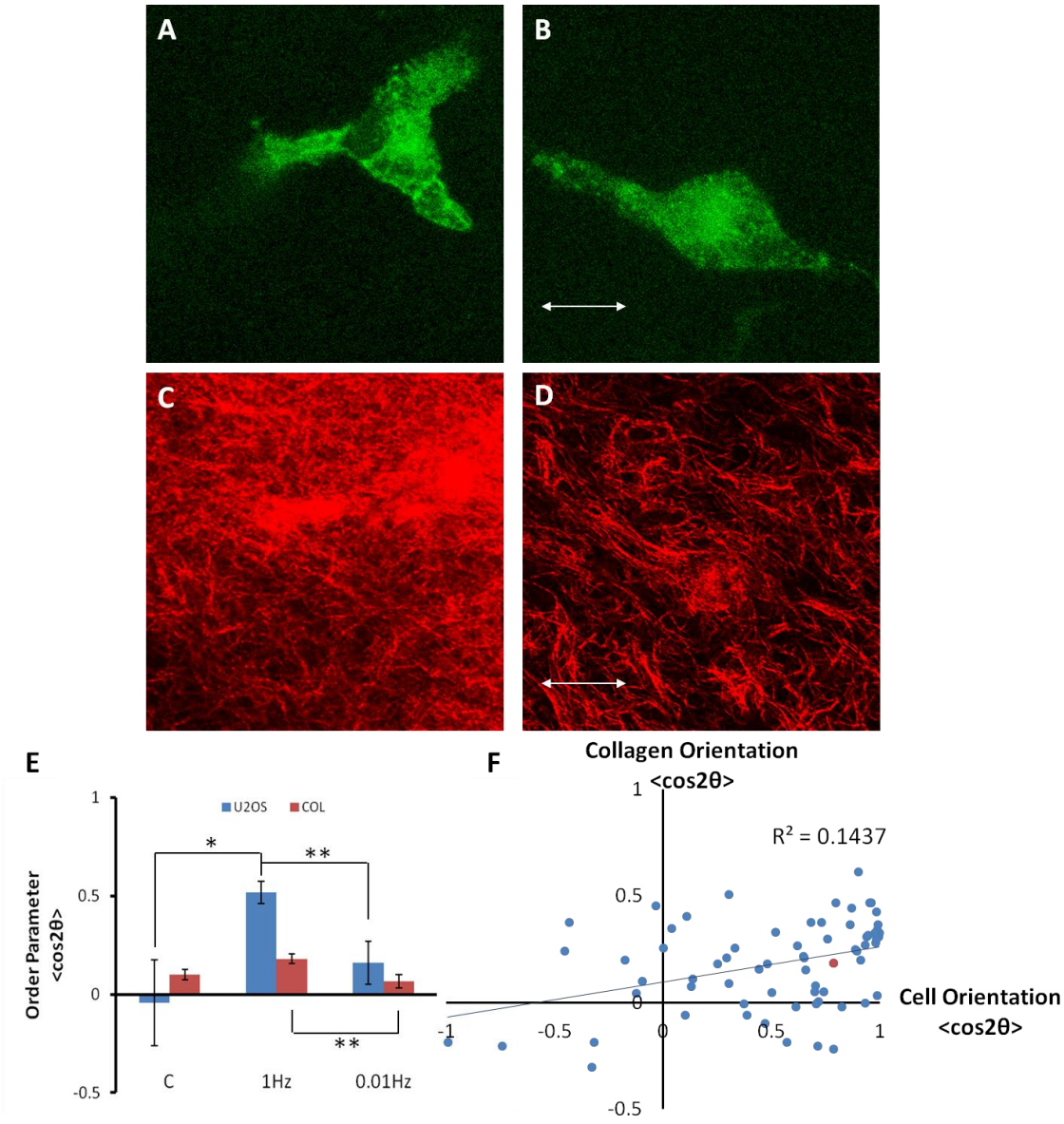

Figure 20. Cyclic stretch induced U2OS cells and collagen fibrils to align in the direction of stretch in collagen microspheres supported within PEGDA hydrogel. Representative images of U2OS cells (**A**, **B**) and collagen fibrils (**C**, **D**) subjected to 6 hours of 7.5% cyclic uniaxial stretch at a frequency 1 Hz in the direction indicated in (**B**) and (**D**) compared to static controls (**A**, **C**). (**E**) Order parameters were computed for each image to quantify the extent of cell (blue column) and collagen fibril (red column) alignment and the results were summarized (mean ± S.D.; n = 25). * and ** indicated significant difference from group (*P<0.05 and **P<0.01). (**F**) The orientations of cell and their surrounding collagen fibril in response to stretch were correlated for each image (R^2=0.1437). Red circle was the data point for the representative image (**B**) and (**D**).

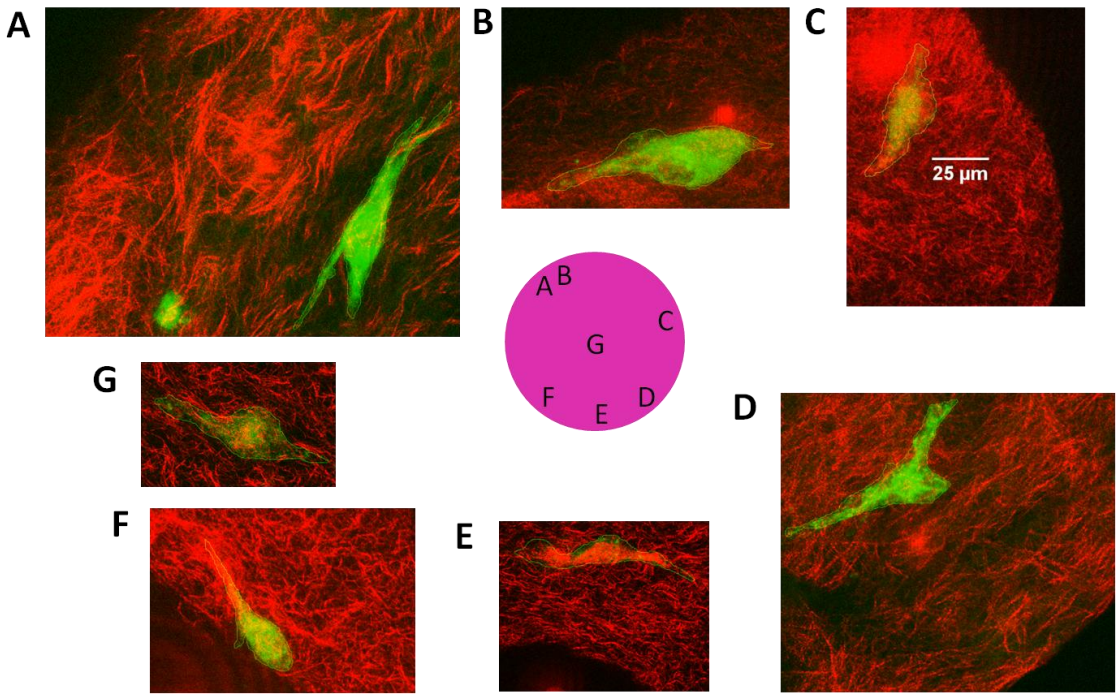

Figure 21. A montage of cell and collagen morphologies at various locations within a microsphere. After 6 hours of 7.5% cyclic uniaxial stretch at a frequency 1 Hz, cells (green) and collagen fibrils (red line) near the boundary were largely aligned to the tangential direction of collagen-PEGDA (black) interface (**A-F**). (**G**) Cells (green) in the center of the spheroidal collagen domains were significantly elongated to the directions of matrix stretch. In some cases, the cells were manually outlined with a thin green line.

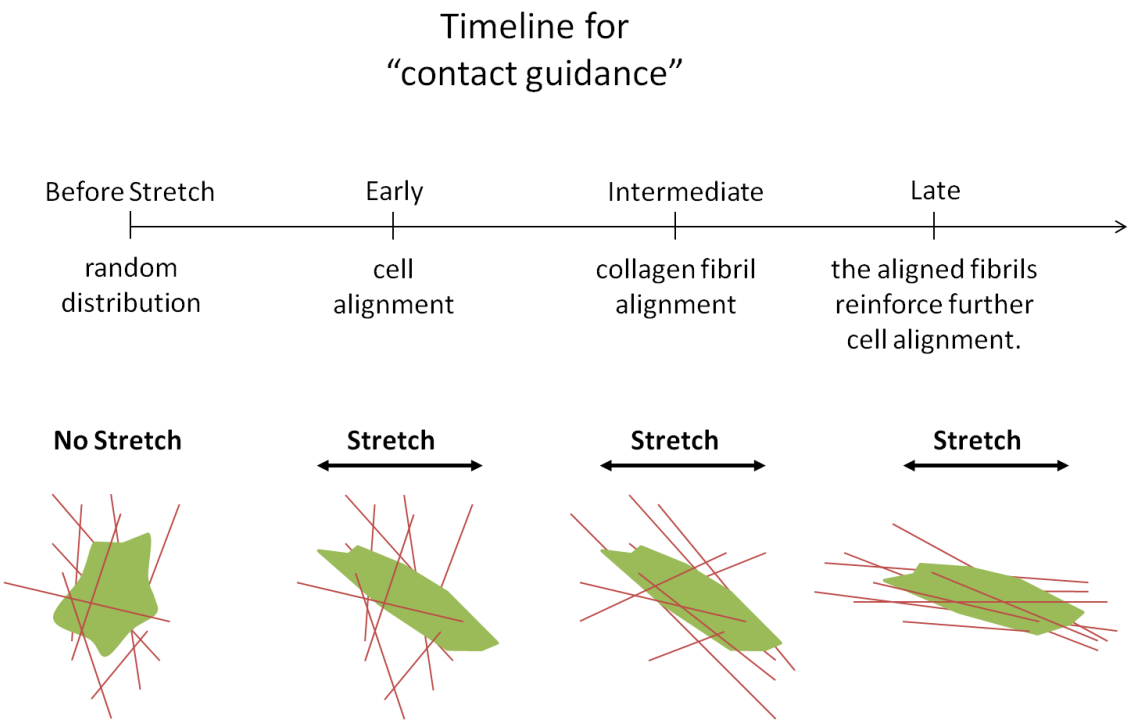

Figure 22. Timeline for contact guidance. Cyclic uniaxial stretch induced cells alignment first, then collagen fibrils, and finally the aligned fibrils help to reinforce further cell alignment.

APPENDIX B VISUAL C++ PROGRAM FOR THE SARCOMERIC MODEL

The program is edited in .cpp file which can be compiled and executed by Visual C++ compiler. The output data is saved in .txt file named 'file.txt' and 'histogram.txt'. The simulation results are recorded in 'file.txt' for every cycle in the order: time, the maximum and minimum value of fiber stretch, the maximum and minimum value of fiber tension, and the extent of stress fiber alignment, while 'histogram.txt' records the distribution of stress fibers at 0, 1, 4, 8 and 12 hr. The parameters we are interested in are Koff, k1, and freq, which are defined in the program. Since Visual C++ cannot generate real random numbers between 0 and 1, we employ 'rng_mt.cpp' which is a random number generator program.

```
// q is fiber stretch in each individual stress fibers
// x is the value of fiber stretch after the self-adjustment activity
// theta is the angle of stress fibers generated by rng_mt
// dfgrd is the deformation gradient (F)
// Histogram is the angle of stress fibers at 0, 1, 4, 8, and 12 hr
// SFangle is the distribution of stress fibers with 10 degree intervals from -π/2 to π/2
// MassTurnover is the summation of disassembled stress fibers for every 100 sec
// turnover_rate is the average turnover rate of stress fibers for every 100 sec
// CircularVariance: the extent of stress fiber alignment
// freq is frequency
// sr and srv are l and l_ref
// ASRmax and ASRmin are the maximum and minimum value of fiber stretch in each cycle
//FiberStrain and FiberTension are the strain and tension for each fiber
//FTmax and FTmin are the maximum and minimum value of fiber tension in each cycle
// p is random number
// probability: the probability that a particular stress fiber existing at time t disassemble at time t+dt
// str_inc is every small incremental magnitude of stretch λ
// srdep is the level of fiber stretch when stress fibers reassemble
// srop is the homeostatic level of fiber stretch ( )
// SFnum is the numbers of stress fibers in individual cells
// dt is a fixed increment time
// cyclenum is total cycle number for each simulation = duration * 3600 (sec) * frequency

#Program name: sarcomeric_FR_FS_SW_TW.cpp
#include<fstream>
#include<stdio.h>
#include<stdlib.h>
#include<math.h>
#include<ctime>
#include <cstdio>
#include <cmath>
```

```
#define PI 3.141592653589793
using namespace std;
void init_genrand(unsigned long s);
void init_by_array(unsigned long init_key[], unsigned long key_length);
unsigned long genrand_int32(void);
long genrand_int31(void);
double genrand_real1(void);
double genrand_real2(void);
double genrand_real3(void);
double genrand_res53(void);
long double square(long double x);
long double rvm (double mu,double kappa);
int main(int argc, char *argv[]){
    long double q[1000][2], x[2][1], theta[1][1000], srv[1000];
    long double dfgrd[2][2], Histogram[1][1000][5], h[5] = {0.0, 1.0, 4.0, 8.0, 12.0};
    int SFangle[18][5] = {0};
    int i, j, m, h1, n2, MassTurnover, cycle,;
    double turnover_rate[1], CircularVariance[1];
    long double freq = 1.0, Vel, Vel_0 = 0.03;
    long double sr, ASRmax, ASRmin, FiberStrain, FiberTension, FTmax, FTmin;
    long double k, p, probability, z;
    long double force_i, force_0 = 17.0, K = 170.0;
    long double Q1 = Vel_0/force_0, Q2 = Vel_0, f_B = 2.2;
    long double avg_force;
    long double str_inc, stretch = 1.1, srop = 1.1, srdep = 1.1, etacos, etasin;
    long double k1 = 0.00003, Koff = 0.000001, SFnum = 1000.0, poisson = 0.19;
    long double dt = 0.01, t, str_t1, str_t2, cyclenum = 12*3600*freq;
    //Fast Relaxation
    int Ssteps = 100/freq-5, Rsteps = 5;

    //Fast Stretch
    //int Ssteps = 5, Rsteps = 100/freq-5;

    ofstream outfile;
    outfile.open("file.txt");
    srand( (unsigned)time(0) );
    unsigned long init[4] = {0x123, 0x234, 0x345, 0x456}, length = 4;
    init_by_array(init, length);
    outfile<<"Koff="<<Koff<<" "<<"k1="<<k1<<" "<<"freqency="<<freq<<" "<<"Q2="<<Q2<<"
        "<<"Vel_0="<<Vel_0<<endl;

    // Simulations //
    for(j = 0; j < 1; j++){
        etacos = 0.0;
        etasin = 0.0;
        MassTurnover = 0.0;
        t = 0.0;
        sr = 0.0;
        FiberTension = 0.0;
        Vel = 0.0;
        avg_force = 0.0;
        for(i = 0; i < SFnum ; i++){
            theta[j][i] = PI * genrand_real1()-PI/2; // theta is a random function between -90 degree and
```

```
            90 degree //
        q[i][0] = srdep * cos(theta[j][i]);
        q[i][1] = srdep * sin(theta[j][i]);
        z = atan(q[i][1]/q[i][0]);
        etacos = etacos + cos(2.0*z);
        etasin = etasin + sin(2.0*z);
        sr = sqrt(square(q[i][0]) + square(q[i][1]));
        srv[i] = 1.0;
        force_i = K*(sr/srv[i] - 1.0);
        avg_force += force_i;
        FiberStrain = sqrt(square(q[i][0]) + square(q[i][1])) - 1;
        FiberTension = FiberTension + 20.5*square(FiberStrain) + 45.7*FiberStrain;
}
sr = 0.0;
for(i = 0; i < SFnum ; i++){
        z = atan(q[i][1]/q[i][0]);
        sr = sr + sqrt(square(q[i][0]) + square(q[i][1]));
}
sr = sr/SFnum;
FiberTension = FiberTension/SFnum;
ASRmax = sr;
ASRmin = sr;
FTmax = FiberTension;
FTmin = FiberTension;
CircularVariance[j] = 1.0 - sqrt(square(etacos)+square(etasin))/SFnum;
//turnover_rate[j] = MassTurnover * freq / cycleper100int / SFnum;
printf("cycle: %d, CircularVariance: %f \n",cycle, CircularVariance[j]);
outfile<<"time(sec)"<<" "<<"ASR(max)"<<" "<<"ASR(min)"<<"
        "<<"FiberTension(max)"<<" "<<"FiberTension(min)"<<"
        "<<"Circular_Variance"<<endl;
outfile<<t<<" "<<ASRmax<<" "<<ASRmin<<" "<<FTmax<<" "<<FTmin<<"
        "<<CircularVariance[j]<<endl; // write to file.txt //
for(cycle = 1; cycle <= cyclenum; cycle++){
        ASRmax = 0.0;
        ASRmin = stretch * srop;
        FTmax = 0.0;
        FTmin = 20.5*square(stretch*srop-1) + 45.7*(stretch*srop-1);
        // create n steps of stretch for Fast Relaxation or Fast Stretch //
        str_t1 = srdep;
        for(n2 = 1; n2 <= Ssteps; n2++){
                t = t + dt;
                //Fast Relaxation
                str_t2 = (srop*stretch-srop)/(1/freq-0.05)*(t-(cycle-1)/freq) + srop;

                //Fast Stretch
                //str_t2 = (srop*stretch-srop)/0.05*(t-(cycle-1)/freq) + srop;

                str_inc = str_t2 / str_t1;
                str_t1 = str_t2;
                // create greens deformation gradient tensor for step stretch //
                dfgrd[0][0] = str_inc;
                dfgrd[0][1] = 0.0;
                dfgrd[1][0] = 0.0;
```

```
dfgrd[1][1] = 1.0 - poisson*(str_inc-1.0);
avg_force = 0.0;
for(i = 0; i < SFnum; i++){
	// calculate axial strain ratio in stretched fibers
	x[0][0] = dfgrd[0][0]*q[i][0] + dfgrd[0][1]*q[i][1];
	x[1][0] = dfgrd[1][0]*q[i][0] + dfgrd[1][1]*q[i][1];
	sr = sqrt(square(x[0][0]) + square(x[1][0]));
	force_i = K * (sr/srv[i] - 1.0);
	Vel = Q1 * (force_0 - force_i);
	avg_force += force_i;
	srv[i] = srv[i] - 2*Vel*dt;
	probability = ( Koff*exp(force_i/f_B)*dt + k1*exp(-Q2/abs(Vel)) );
	q[i][0] = x[0][0];
	q[i][1] = x[1][0];
	p = genrand_res53();
	if (p <= probability) {
		// random distribution
		theta[j][i] = genrand_real1();
		theta[j][i] = PI*theta[j][i];

		q[i][0] = srdep * cos(theta[j][i]);
		q[i][1] = srdep * sin(theta[j][i]);
		srv[i] = 1.0;
		MassTurnover = MassTurnover + 1;
	}
	if (cycle == 12.0 * 3600 * freq){
		z = atan(q[i][1]/q[i][0]);
		Histogram[j][i][4] = z;
	}
	if (cycle == 8.0 * 3600 * freq){
		z = atan(q[i][1]/q[i][0]);
		Histogram[j][i][3] = z;
	}
	if (cycle == 4.0 * 3600 * freq){
		z = atan(q[i][1]/q[i][0]);
		Histogram[j][i][2] = z;
	}
	if (cycle == 1.0 * 3600 * freq){
		z = atan(q[i][1]/q[i][0]);
		Histogram[j][i][1] = z;
	}
	if (cycle == 1){
		z = atan(q[i][1]/q[i][0]);
		Histogram[j][i][0] = z;
	}

}
/*
if(cycle>0){
	outfile<<t<<" "<<avg_force/SFnum<<endl;
}
*/
sr = 0.0;
```

```
        FiberTension = 0.0;
        for(i = 0; i < SFnum; i++){
            sr = sr + sqrt(square(q[i][0]) + square(q[i][1]));
            FiberStrain = sqrt(square(q[i][0]) + square(q[i][1])) - 1;
            FiberTension = FiberTension + 20.5*square(FiberStrain) + 45.7*FiberStrain;
        }
        sr = sr/SFnum;
        if(sr > ASRmax){
            ASRmax = sr;
        }
        else{
            ASRmax = ASRmax;
        }
        if(sr < ASRmin){
            ASRmin = sr;
        }
        else{
            ASRmin = ASRmin;
        }
        FiberTension = FiberTension/SFnum;
        if(FiberTension > FTmax){
            FTmax = FiberTension;
        }
        else{
            FTmax = FTmax;
        }
        if(FiberTension < FTmin){
            FTmin = FiberTension;
        }
        else{
            FTmin = FTmin;
        }
}
// create n steps of release for Fast Relaxation or Fast Stretch //
str_t1 = srdep*stretch;
for(n2 = 1; n2 <= Rsteps; n2++){
        t = t + dt;
        //Fast Relaxation
        str_t2 = srop*stretch - (srop*stretch-srop)/0.05*(t-(cycle-1)/freq-(1/freq-0.05));

        //Fast Stretch
        //str_t2 = srop*stretch - (srop*stretch-srop)/(1/freq-0.05)*(t-(cycle-1)/freq-0.05);

        str_inc = str_t2/str_t1;
        str_t1 = str_t2;
        // create greens deformation gradient tensor for step release //
        dfgrd[0][0] = str_inc;
        dfgrd[0][1] = 0.0;
        dfgrd[1][0] = 0.0;
        dfgrd[1][1] = 1.0 - poisson*(str_inc-1.0);
        avg_force =0.0;
        // stretch all fibers one increment
        for(i = 0; i < SFnum; i++){
```

```
        // calculate axial strain ratio in stretched fibers
        x[0][0] = dfgrd[0][0]*q[i][0] + dfgrd[0][1]*q[i][1];
        x[1][0] = dfgrd[1][0]*q[i][0] + dfgrd[1][1]*q[i][1];
        sr = sqrt(square(x[0][0])+square(x[1][0]));
        force_i = K * (sr/srv[i] - 1.0);
        Vel = Q1 * (force_0 - force_i);
        avg_force += force_i;
        srv[i] = srv[i] - 2*Vel*dt;
        probability = ( Koff*exp(force_i/f_B)*dt + k1*exp(-Q2/abs(Vel)) );
        q[i][0] = x[0][0];
        q[i][1] = x[1][0];
        p = genrand_res53();
        if (p <= probability){
                // random distribution
                theta[j][i] = genrand_real1();
                theta[j][i] = PI*theta[j][i];

                q[i][0] = srdep*cos(theta[j][i]);
                q[i][1] = srdep*sin(theta[j][i]);
                srv[i] = 1.0;
                MassTurnover = MassTurnover + 1;
        }
        if (cycle == 12.0*3600*freq){
                z = atan(q[i][1]/q[i][0]);
                Histogram[j][i][4] = z;
        }
        if (cycle == 8.0*3600*freq){
                z = atan(q[i][1]/q[i][0]);
                Histogram[j][i][3] = z;
        }
        if (cycle == 4.0 * 3600 * freq){
                z = atan(q[i][1]/q[i][0]);
                Histogram[j][i][2] = z;
        }
        if (cycle == 1.0 * 3600 * freq){
                z = atan(q[i][1]/q[i][0]);
                Histogram[j][i][1] = z;
        }
        if (cycle == 1 ){
                z = atan(q[i][1]/q[i][0]);
                Histogram[j][i][0] = z;
        }
}
/*
if(cycle>0){
        outfile<<t<<" "<<avg_force/SFnum<<endl;

}
*/
sr = 0.0;
FiberTension = 0.0;
for(i = 0; i < SFnum; i++){
        sr = sr + sqrt(square(q[i][0]) + square(q[i][1]));
```

```
            FiberStrain = sqrt(square(q[i][0]) + square(q[i][1])) - 1;
            FiberTension = FiberTension + 20.5*square(FiberStrain) + 45.7*FiberStrain;
        }
        sr = sr/SFnum;
        if(sr > ASRmax){
            ASRmax = sr;
        }
        else{
            ASRmax = ASRmax;
        }
        if(sr < ASRmin){
            ASRmin = sr;
        }
        else{
            ASRmin = ASRmin;
        }
        FiberTension = FiberTension/SFnum;
        if(FiberTension > FTmax){
            FTmax = FiberTension;
        }
        else{
            FTmax = FTmax;
        }
        if(FiberTension < FTmin){
            FTmin = FiberTension;
        }
        else{
            FTmin = FTmin;
        }
}

//Square or Triangle Wave
/*
for(n2 = 1; n2 <= (100/freq); n2++){
    t = t + dt;

    //Square-Wave
    if(n2<=5){
        str_t1 = (srop*(stretch-1.0))/5*(n2-1) + srop;
        str_t2 = (srop*(stretch-1.0))/5*n2 + srop;
        str_inc = str_t2 / str_t1;
    }
    else if(n2>5 && n2<=(50/freq)){
        str_inc = 1.00;
    }
    else if(n2>(50/freq) && n2<=(50/freq+5)){
        str_t1 = srop*stretch - (srop*(stretch-1.0))/5*(n2-(50/freq+1));
        str_t2 = srop*stretch - (srop*(stretch-1.0))/5*(n2-50/freq);
        str_inc = str_t2 / str_t1;
    }
    else{
        str_inc = 1.00;
    }
```

```
// Triangle-Wave
if(n2<=(50/freq)){
	str_t1 = (srop*(stretch-1.0))/(50/freq)*(n2-1) + srop;
	str_t2 = (srop*(stretch-1.0))/(50/freq)*n2 + srop;
	str_inc = str_t2 / str_t1;
}
else{
	str_t1 = srop*stretch - (srop*(stretch-1.0))/(50/freq)*(n2-(50/freq+1));
	str_t2 = srop*stretch - (srop*(stretch-1.0))/(50/freq)*(n2-(50/freq));
	str_inc = str_t2 / str_t1;
}

dfgrd[0][0] = str_inc;
dfgrd[0][1] = 0.0;
dfgrd[1][0] = 0.0;
dfgrd[1][1] = 1.0 - poisson*(str_inc-1.0);
avg_force = 0.0;
for(i = 0; i < SFnum; i++){
	// calculate axial strain ratio in stretched fibers
	x[0][0] = dfgrd[0][0]*q[i][0] + dfgrd[0][1]*q[i][1];
	x[1][0] = dfgrd[1][0]*q[i][0] + dfgrd[1][1]*q[i][1];
	sr = sqrt(square(x[0][0]) + square(x[1][0]));
	force_i = K * (sr/srv[i] - 1.0);
	Vel = Q1 * (force_0 - force_i);
	avg_force += force_i;
	srv[i] = srv[i] - 2*Vel*dt;
	if(Vel==0.0){
		probability = ( Koff*exp(force_i/f_B)*dt + k1);
	}
	else{
		probability = ( Koff*exp(force_i/f_B)*dt + k1*exp(-Q2/abs(Vel)) );
	}
	q[i][0] = x[0][0];
	q[i][1] = x[1][0];
	p = genrand_res53();
	if (p <= probability) {

		// random distribution
		theta[j][i] = PI*genrand_real1()-PI/2.0;

		q[i][0] = srdep * cos(theta[j][i]);
		q[i][1] = srdep * sin(theta[j][i]);
		srv[i] = 1.0;
		MassTurnover = MassTurnover + 1;
	}
	if (cycle == 12.0 * 3600 * freq){
		z = atan(q[i][1]/q[i][0]);
		Histogram[j][i][4] = z;
	}
	if (cycle == 8.0 * 3600 * freq){
		z = atan(q[i][1]/q[i][0]);
		Histogram[j][i][3] = z;
```

```
                }
                if (cycle == 4.0 * 3600 * freq){
                        z = atan(q[i][1]/q[i][0]);
                        Histogram[j][i][2] = z;
                }
                if (cycle == 1.0 * 3600 * freq){
                        z = atan(q[i][1]/q[i][0]);
                        Histogram[j][i][1] = z;
                }
                if (cycle == 1){
                        z = atan(q[i][1]/q[i][0]);
                        Histogram[j][i][0] = z;
                }
        }
        if(cycle > 0){
                outfile<<t<<" "<<avg_force/SFnum<<endl;
        }
        sr = 0.0;
        FiberTension = 0.0;
        for(i = 0; i < SFnum; i++){
                sr = sr + sqrt(square(q[i][0]) + square(q[i][1]));
                FiberStrain = sqrt(square(q[i][0]) + square(q[i][1])) - 1;
                FiberTension = FiberTension + 20.5*square(FiberStrain) + 45.7*FiberStrain;
        }
        sr = sr/SFnum;
        if(sr > ASRmax){
                ASRmax = sr;
        }
        else{
                ASRmax = ASRmax;
        }
        if(sr < ASRmin){
                ASRmin = sr;
        }
        else{
                ASRmin = ASRmin;
        }
        FiberTension = FiberTension/SFnum;
        if(FiberTension > FTmax){
                FTmax = FiberTension;
        }
        else{
                FTmax = FTmax;
        }
        if(FiberTension < FTmin){
                FTmin = FiberTension;
        }
        else{
                FTmin = FTmin;
        }
}
*/
etacos = 0.0;
```

```
        etasin = 0.0;
        for(i = 0;i<SFnum;i++){
                z = atan(q[i][1]/q[i][0]);
                etacos = etacos + cos(2.0*z);
                etasin = etasin + sin(2.0*z);
                // record data for every cycle
                CircularVariance[j] = 1.0 - sqrt(square(etacos) + square(etasin))/SFnum;
                printf("cycle: %d, CircularVariance: %f \n",cycle, CircularVariance[j]);
                outfile<<"time(sec)"<<" "<<"ASR(max)"<<" "<<"ASR(min)"<<"
                        "<<"FiberTension(max)"<<" "<<"FiberTension(min)"<<"
                        "<<"Circular_Variance"<<endl;
                outfile<<t<<" "<<ASRmax<<" "<<ASRmin<<" "<<FTmax<<" "<<FTmin<<"
                        "<<CircularVariance[j]<<endl;
        }
}
outfile.close(); // close file.text //

// open histogram.txt file to record the orientation of stress fibers //
ofstream myfile("histogram.txt");
myfile.is_open();
for(j = 0; j<1; j++){
        myfile<<"Koff="<<Koff<<" "<<"k1="<<k1<<" "<<"freqency="<<freq<<endl; // write
                the header of histogram.txt //
        myfile<<"Repetation"<<" "<<"SFnum"<<" "<<"h"<<" "<<"angle"<<endl;
        for(i = 0; i < SFnum; i++){
                for (h1 = 0; h1 < 5; h1++){
                        myfile<<j<<" "<<i<<" "<<h[h1]<<" "<<Histogram[j][i][h1]<<endl; //
                                write to histogram.txt //
                        for(int num=1; num<18; num++){
                                if(Histogram[j][i][h1]*180/PI >= (-85.0+10*(num-1)) &&
                                Histogram[j][i][h1]*180/PI < (-85.0+10*num)){
                                        SFangle[num][h1]++;
                                }
                        }
                        if(Histogram[j][i][h1]*180/PI >= -90.0 && Histogram[j][i][h1]*180/PI
                        < -85.0){
                                SFangle[0][h1]++;
                        }
                        else if(Histogram[j][i][h1]*180/PI >= 85.0 &&
                        Histogram[j][i][h1]*180/PI<90.0){
                                SFangle[0][h1]++;
                        }
                }
        }
}
myfile<<"SFangle"<<" "<<h[0]<<"h"<<" "<<h[1]<<"h"<<" "<<h[2]<<"h"<<"
        "<<h[3]<<"h"<<" "<<h[4]<<"h"<<" "<<endl;
for(m = 0; m < 18; m++){
        myfile<<"angle"<<-90+10*m<<" "<<SFangle[m][0]<<" "<<SFangle[m][1]<<"
                "<<SFangle[m][2]<<" "<<SFangle[m][3]<<" "<<SFangle[m][4]<<endl; // write
                to histogram.txt //
}
myfile.close(); // close histogram.txt file //
```

```
        return EXIT_SUCCESS;
}
// create Square function //
long double square(long double x){
        long double y;
        y = (x)*(x);
        return y;
}
```

APPENDIX C VISUAL C++ PROGRAM FOR RANDOM NUMBER GENERATOR

The program is edited in .cpp file which should be put in the same directory as the stochastic model. The simulation generates a random number on [0,1) with 53-bit resolution.

```
#include <cstdio>
using namespace std;

/* Period parameters */
#define N 624
#define M 397
#define MATRIX_A 0x9908b0dfUL   /* constant vector a */
#define UPPER_MASK 0x80000000UL /* most significant w-r bits */
#define LOWER_MASK 0x7fffffffUL /* least significant r bits */

static unsigned long mt[N]; /* the array for the state vector  */
static int mti=N+1; /* mti==N+1 means mt[N] is not initialized */

/* initializes mt[N] with a seed */
void init_genrand(unsigned long s)
{
    mt[0]= s & 0xffffffffUL;
    for (mti=1; mti<N; mti++) {
        mt[mti] = (1812433253UL * (mt[mti-1] ^ (mt[mti-1] >> 30)) + mti);
        /* See Knuth TAOCP Vol2. 3rd Ed. P.106 for multiplier. */
        /* In the previous versions, MSBs of the seed affect   */
        /* only MSBs of the array mt[].                        */
        /* 2002/01/09 modified by Makoto Matsumoto             */
        mt[mti] &= 0xffffffffUL;
        /* for >32 bit machines */
    }
}

/* initialize by an array with array-length */
/* init_key is the array for initializing keys */
/* key_length is its length */
//void init_by_array(init_key, key_length)
//unsigned long init_key[], key_length;
void init_by_array(unsigned long init_key[], unsigned long key_length)
{
    int i, j, k;
    init_genrand(19650218UL);
    i=1; j=0;
    k = (N>key_length ? N : key_length);
    for (; k; k--) {
        mt[i] = (mt[i] ^ ((mt[i-1] ^ (mt[i-1] >> 30)) * 1664525UL))  + init_key[j] + j; /* non linear */
        mt[i] &= 0xffffffffUL; /* for WORDSIZE > 32 machines */
```

```
            i++; j++;
            if (i>=N) { mt[0] = mt[N-1]; i=1; }
            if (j>=key_length) j=0;
        }
        for (k=N-1; k; k--) {
            mt[i] = (mt[i] ^ ((mt[i-1] ^ (mt[i-1] >> 30)) * 1566083941UL)) - i; /* non linear */
            mt[i] &= 0xffffffffUL; /* for WORDSIZE > 32 machines */
            i++;
            if (i>=N) { mt[0] = mt[N-1]; i=1; }
        }

        mt[0] = 0x80000000UL; /* MSB is 1; assuring non-zero initial array */
}

/* generates a random number on [0,0xffffffff]-interval */
unsigned long genrand_int32(void)
{
    unsigned long y;
    static unsigned long mag01[2]={0x0UL, MATRIX_A};
     /* mag01[x] = x * MATRIX_A  for x=0,1 */

     if (mti >= N) { /* generate N words at one time */
     int kk;

            if (mti == N+1)   /* if init_genrand() has not been called, */
                init_genrand(5489UL); /* a default initial seed is used */

            for (kk=0;kk<N-M;kk++) {
                y = (mt[kk]&UPPER_MASK)|(mt[kk+1]&LOWER_MASK);
                mt[kk] = mt[kk+M] ^ (y >> 1) ^ mag01[y & 0x1UL];
            }
            for (;kk<N-1;kk++) {
                y = (mt[kk]&UPPER_MASK)|(mt[kk+1]&LOWER_MASK);
                mt[kk] = mt[kk+(M-N)] ^ (y >> 1) ^ mag01[y & 0x1UL];
            }
            y = (mt[N-1]&UPPER_MASK)|(mt[0]&LOWER_MASK);
            mt[N-1] = mt[M-1] ^ (y >> 1) ^ mag01[y & 0x1UL];

            mti = 0;
        }

    y = mt[mti++];

    /* Tempering */
     y ^= (y >> 11);
    y ^= (y << 7) & 0x9d2c5680UL;
     y ^= (y << 15) & 0xefc60000UL;
     y ^= (y >> 18);

     return y;
}

/* generates a random number on [0,0x7fffffff]-interval */
```

```
long genrand_int31(void)
{
    return (long)(genrand_int32()>>1);
}

/* generates a random number on [0,1]-real-interval */
double genrand_real1(void)
{
     return genrand_int32()*(1.0/4294967295.0);
     /* divided by 2^32-1 */
}

/* generates a random number on [0,1)-real-interval */
double genrand_real2(void)
{
     return genrand_int32()*(1.0/4294967296.0);
     /* divided by 2^32 */
}

/* generates a random number on (0,1)-real-interval */
double genrand_real3(void)
{
     return (((double)genrand_int32()) + 0.5)*(1.0/4294967296.0);
    /* divided by 2^32 */
}

/* generates a random number on [0,1) with 53-bit resolution*/
double genrand_res53(void)
{
    unsigned long a=genrand_int32()>>5, b=genrand_int32()>>6;
     return(a*67108864.0+b)*(1.0/9007199254740992.0);
}
/* These real versions are due to Isaku Wada, 2002/01/09 added */
```

APPENDIX D MATLAB PROGRAM FOR THE ORIENTATION OF STRESS FIBERS

The program is edited in .m file which can be compiled and executed by Matlab. Before starting the computation, put images in C:\images\ directory. Type imagename = 'filename' where filename is the name of the image file in the commend window. The file must be TIFF format, but do not include the '.tif' at the end of the filename. Run the program by typing CELL. There will be two output files named 'output.dat' and 'histogram.dat'. In the 'output.dat' file, the simulation results are recorded for the total numbers of orientation vector components (N) in the order: angle, covariance, x-position, y-position, sin(2θ)/N, cos(2θ)/N and use Eq. (7) to calculate the circular variance for each image. The plot generated by the program is the original image added with colored lines which matches the apparent orientation of fibers in each subregion. The distribution of stress fibers are saved as 'histogram.dat' and plotted as the circular histograms by Oriana 2 circular statistics software (Rockware).

```
% Variable list
% ---------------
% ARE is the side length of an interrogation box
% BUFF is the buffer around the edge of the images needed for the masks
% origI is the original image
% MX, MY are the masks in the x- and y-directions
% filtIX, filtIY are the images that was convolved with MX, MY
% X, Y are the sizes of filtIX and filtIY
% G is the size of the correlation for a pixel
% Angle is the angle of lowest gradient


namex = strcat('C:\images\',imagename,'.tif');
outname = strcat('C:\images\',imagename,'.dat');
histname = strcat('C:\images\',imagename,'HIST.dat');

clear angles;
clear image;
clear origI;
clear filtIX;
clear filtIY;
clear G;
clear Angle;
clear mean_int;

ARE=10;
BUFF=4;
limit = 0.7;
% read in image. If image is indexed then convert to greyscale
[image, map] = imread(namex);
if (map)
```

```
    bwimage = ind2gray(image,map);
    origI=double(bwimage);
else
    origI=double(image);
end;
X = size(origI,2);
Y = size(origI,1);

% make masks
for i=-BUFF:BUFF
    for j=-BUFF:BUFF
        MX(i+1+BUFF,j+1+BUFF)= j/2*exp(-(i^2+j^2)/4);
        % MY(i+1+BUFF,j+1+BUFF)= i/2*exp(-(i^2+j^2)/4);
    end;
end;

% convolve image with masks. filtIX measures gradients in the x-direction,
% while filtIY measures gradients in the y-direction. Thus vertical lines
% give high values in filtIX, while horizontal lines give high values in
% filtIY.
filtIX=double(imfilter(origI,MX,'conv'));
filtIY=double(imfilter(origI,MX','conv'));
%filtIX=filtIX(:,:,3);
%filtIY=filtIY(:,:,3);

for i=1:BUFF
    filtIX(:,X-BUFF+1)=[];
    filtIY(:,X-BUFF+1)=[];
    filtIX(Y-BUFF+1,:)=[];
    filtIY(Y-BUFF+1,:)=[];
end;
for i=1:BUFF
    filtIX(:,1)=[];
    filtIY(:,1)=[];
    filtIX(1,:)=[];
    filtIY(1,:)=[];
end;
% compute metrics for convolved matrices
G=(filtIX.^2+filtIY.^2).^0.5;
filtIX=filtIX+0.0000001;
Angle=atan(filtIY./filtIX);
meanG=mean(mean(G,2));
meanAngle=mean(mean(Angle,2));
fprintf('avg. G: %6.2f \n',meanG);
fprintf('avg. angle: %6.2f \n',meanAngle*180/pi);

% compute metrics for individual features
threshold = mean(mean(origI,2))/limit;
features=1;
%step through image for each feature
for k = (1+ARE):(2*ARE):(Y-ARE-1-2*BUFF)
    for l = (1+ARE):(2*ARE):(X-ARE-1-2*BUFF)
```

```
      AMAX=90;
      ACMAX=0;
      AChold=0;
      CORATMX=0;

      % feature mean intensity and continue if it is higher then
      % threshold
      meanint = sum(sum(origI(k-ARE:k+ARE,l-ARE:l+ARE)))/(4*ARE*ARE);
      mean_int(features) = meanint;

      if (mean_int(features) > threshold)
        angles(features,3) = l;
        angles(features,4) = k;
        for m = 0:179
          aval = (m-90)*pi/180;
          AA = 0;
          CORATIO = 0;
          for i = -ARE:ARE
            for j = -ARE:ARE
              cang = Angle(k+i,l+j);
              cosval1 = exp(2*cos(2*(cang-aval)))/exp(2);
              AA = AA + G(k+i,l+j)*cosval1;
              CORATIO = CORATIO + cosval1;
            end;
          end;
          AChold = AChold + AA;
          if (AA > ACMAX)
            AMAX = m;
            ACMAX = AA;
          end;
          if (CORATIO > CORATMX)
            CORATMX = CORATIO;
          end;
        end;
      end;

      % store avg. coratio for feature with largest coratio
      angles(features,2)  = CORATMX/(4*ARE*ARE);
      % loc_dev(features) = 180/pi*(0.5-(ssin^2+scos^2)^0.5/(8*ARE*ARE))^0.5;

      % only keep this feature if the weight is high enough */
      if (mean_int(features) > threshold) && (angles(features,2) > 0.1)
        % store histogram contribution */
        angles(features,5) = angles(features,1);
        angles(features,1) = AMAX;
        fprintf('\n %d  x=%d y=%d angle=%d coratio=%6.2lf \n',...
        features,angles(features,3),angles(features,4),AMAX,angles(features,2));
        features = features + 1;
      end;
    end;
  end;
```

```
features = features-1;
% save histogram and "angles" matrix to files
angleadj = angles(:,1)+2.5;
for i=1:features
   if (angleadj(i) > 180)
      angleadj(i) = angleadj(i) - 180;
   end;
end;
histo = hist(angleadj,36);

angles(:,5)=sin(angles(:,1)*2*pi/180)/features;
angles(:,6)=cos(angles(:,1)*2*pi/180)/features;

% angles stores the values for each interrogation box in a row with
%column 1 = angle, 2= covariance, 3=x-position, 4=y-position, 5=sin(2@)/N,
%column 6 = cos(2@)/N

save c:\histogram.dat histo -ASCII;
save c:\output.dat angles -ASCII;

ssin=0;
scos=0;
for i=1:features
   ssin = ssin + sin(2*angles(i,1)*pi/180);
   scos = scos + cos(2*angles(i,1)*pi/180);
end;
cmean = 0.5*atan(ssin/scos);
% adjust cmean to be in range [-pi/2,pi/2]
if (ssin > 0) && (scos < 0)
   cmean = cmean + pi/2;
end;
if (ssin < 0) && (scos < 0)
   cmean = cmean - pi/2;
end;

fprintf('\n N: %d  mean: %6.2f  SD: %6.2f \n',features, cmean*180/pi);

imshow(image);
for i=1:features-1
   if (angles(i,1)<22.5)
      line([angles(i,3)-5 angles(i,3)+5],[angles(i,4) angles(i,4)],...
         'Color',[1 0 0],'Marker','none','LineStyle','-');
   end;
   if ((angles(i,1)>22.5) && (angles(i,1)<67.5))
      line([angles(i,3)-5 angles(i,3)+5],[angles(i,4)-5 angles(i,4)+5],...
         'Color',[0 1 0],'Marker','none','LineStyle','-');
   end;
   if ((angles(i,1)>67.5) && (angles(i,1)<112.5))
      line([angles(i,3) angles(i,3)],[angles(i,4)-5 angles(i,4)+5],...
         'Color',[0 0 1],'Marker','none','LineStyle','-');
   end;
   if ((angles(i,1)>112.5) && (angles(i,1)<157.5))
```

```
        line([angles(i,3)-5 angles(i,3)+5],[angles(i,4)+5 angles(i,4)-5],...
            'Color',[1 1 0],'Marker','none','LineStyle','-');
    end;
    if (angles(i,1)>157.5)
        line([angles(i,3)-5 angles(i,3)+5],[angles(i,4) angles(i,4)],...
            'Color',[1 0 0],'Marker','none','LineStyle','-');
    end;
end;
```

APPENDIX E MATLAB PROGRAM FOR THREE-POINT STRAIN ANALYSIS

The program is edited in .m file which can be compiled and executed by Matlab. Before starting the computation, create an Excel file in C:\strain analysis\ directory. Save any three sets of maker point from experimental data in the Excel file. After executing the program, there will be an output file named 'test.dat' in which the principal strains and Poisson ratio are recorded using the method listed in **Section II**.

```
clc
clear

%take info for experimental data
exceln = input(' Enter the file name for data: ');
np = input(' Enter the number of the maker points: ');
nm = input(' Enter the number of the conditions: ');

%input data from file
namex = strcat('C:\strain analysis\',exceln,'.xlsx');
num = xlsread(namex);

for p = 1:nm-1

   for i = 1:1

      % enter the original coordinates here
      a=[num(3*i-2,2) num(3*i-2,3)];
      b=[num(3*i-1,2) num(3*i-1,3)];
      c=[num(3*i,2) num(3*i,3)];

      % enter the final coordinates here
      A=[num(3*i-2,2*p+2) num(3*i-2,2*p+3)];
      B=[num(3*i-1,2*p+2) num(3*i-1,2*p+3)];
      C=[num(3*i,2*p+2) num(3*i,2*p+3)];

      s(1)=(B-A)*(B-A)'-(b-a)*(b-a)';
      s(2)=(C-A)*(C-A)'-(c-a)*(c-a)';
      s(3)=(C-B)*(C-B)'-(c-b)*(c-b)';
      x(1,:)=b-a;
      x(2,:)=c-a;
      x(3,:)=c-b;
      M(:,1)=2*x(:,1).^2;
      M(:,2)=4*x(:,1).*x(:,2);
      M(:,3)=2*x(:,2).^2;
      E=s/M';
      E(1)=sqrt(1+2*E(1))-1;
      E(3)=sqrt(1+2*E(3))-1;
      e1=[E(1) E(2);E(2) E(3)];
```

```
        % The output gives the principal strains
        strains = eig(e1);
        Poisson = -strains(1)/strains(2);

        j=p-1;
        output(j*3+1,i)=strains(1);
        output(j*3+2,i)=strains(2);
        output(j*3+3,i)=Poisson;

    end

end

%average 3 set of data for each condition
%output(:,4)=(1/3)*[output(:,1)+output(:,2)+output(:,3)];
output

%save to file
save R:\test.dat output -ASCII;
```

VITA

Name: Hui-Ju Hsu

Address: Biomedical Engineering
c/o Dr. Roland Kaunas
Texas A&M University
College Station, TX 77843-3120

Email Address: emmeline0814@gmail.com

Education: B.S., National Cheng Kung University, Taiwan, 2004

M.S., National Cheng Kung University, Taiwan, 2006

M.S., Texas A&M, USA, 2009

Ph.D., Texas A&M, USA, 2012